

# STUDY OF THE HOYLE STATE

*By*

**TAPAN KUMAR RANA**

Enrolment No PHYS04200904009

**Variable Energy Cyclotron Centre, Kolkata**

*A thesis submitted to the  
Board of Studies in Physical Sciences*

*In partial fulfillment of requirements  
for the Degree of*

**DOCTOR OF PHILOSOPHY**

*of*

**HOMI BHABHA NATIONAL INSTITUTE**



**December, 2014**



# Homi Bhabha National Institute

## Recommendations of the Viva Voce Board

As members of the Viva Voce committee, we certify that we have read the dissertation prepared by **Tapan Kumar Rana** entitled “**STUDY OF THE HOYLE STATE**” and recommend that it may be accepted as fulfilling the thesis requirement for the award of Degree of Doctor of Philosophy.

.....**Date:**  
Chairman - Dr. Sudhee Ranjan Banerjee

.....**Date:**  
Guide / Convener - Dr. Chandana Bhattacharya

.....**Date:**  
Member 1 - Dr. Subinit Roy

.....**Date:**  
Member 2 - Dr. Vijay Shankar Pandit

.....**Date:**  
Member 3 - Shri Amitava Roy

.....**Date:**  
Member 4 - Dr. Surjit Mukherjee

Final approval and acceptance of this dissertation is contingent upon the candidate's submission of the final copies of the thesis to HBNI.

I hereby certify that I have read this dissertation prepared under my direction and recommend that it may be accepted as fulfilling the thesis requirement.

**Date:**

**Place:**

**Signature of Guide**

**Dr. Chandana Bhattacharya**



## **STATEMENT BY AUTHOR**

This dissertation has been submitted in partial fulfillment of requirements for an advanced degree at Homi Bhabha National Institute (HBNI) and is deposited in the Library to be made available to borrowers under rules of the HBNI.

Brief quotations from this dissertation are allowable without special permission, provided that accurate acknowledgement of source is made. Requests for permission for extended quotation from or reproduction of this manuscript in whole or in part may be granted by the Competent Authority of HBNI when in his or her judgement the proposed use of the material is in the interests of scholarship. In all other instances, however, permission must be obtained from the author.



Tapan Kumar Rana



## DECLARATION

I, hereby declare that the investigation presented in the thesis has been carried out by me. The work is original and has not been submitted earlier as a whole or in part for a degree/diploma at this or any other Institution / University.



Tapan Kumar Rana



# List of Publications

## Publications relevant to the thesis:

### Referred Journals:

1. “Consistency of nuclear thermometric measurements at moderate excitation”, **T. K. Rana**, C. Bhattacharya, S. Kundu, K. Banerjee, S. Bhattacharya, A. Dey, T. K. Ghosh, G. Mukherjee, J. K. Meena, D. Gupta, S. Mukhopadhyay, D. Pandit, S. R. Banerjee, A. Roy and P. Dhara, Phys. Rev. C **78**, 027602 (2008).
2. “Cluster emission in  $^{13}\text{C} + ^{12}\text{C}$  and  $^{12}\text{C} + ^{12}\text{C}$  reaction at 6 MeV/nucleon”, **T. K. Rana**, C. Bhattacharya, S. Kundu, K. Banerjee, S. Bhattacharya, G. Mukherjee, T. K. Ghosh, J. K. Meena, P. Dhara, M. Biswas, H. Pai, K. Mahata, S. Kumar, K. Ramachandran, P. C. Rout, S. K. Pandit, V. Nalal and R. G. Pillay, International Journals of Modern Phys E **20**, 789 (2011).
3. “Estimation of direct components of the decay of the Hoyle state”, **T. K. Rana**, S. Bhattacharya, C. Bhattacharya, S. Kundu, K. Banerjee, T. K. Ghosh, G. Mukherjee, R. Pandey, P. Roy, V. Srivastava, M. Gohil, J. K. Meena, H. Pai, A. K. Saha, J. K. Sahoo and R. M. Saha, Phys. Rev. C **88**, 021601(R) (2013).
4. “Further limit on  $3\alpha$  decay of the Hoyle state”, **T. K. Rana**, C. Bhattacharya, S. Bhattacharya, S. Kundu, K. Banerjee, T. K. Ghosh, G. Mukherjee, R. Pandey, P. Roy, V. Srivastava, M. Gohil, J. K. Meena, H. Pai, A. K. Saha, J. K. Sahoo and R. M. Saha, EPJ Web of Conferences, **66**, 03072 (2014).
5. “Decay of the Hoyle state”, S. Bhattacharya, **T. K. Rana**, C. Bhattacharya, S. Kundu, K. Banerjee, T. K. Ghosh, G. Mukherjee, R. Pandey, P. Roy, V. Srivastava, M. Gohil, J. K. Meena, H. Pai, A. K. Saha, J. K. Sahoo and R. M. Saha, Pramana journal of Physics, **83**, 673 (2014).

## Conference Proceedings:

1. “*Structure and decay mechanism of the Hoyle state*”, **T. K. Rana**, S. Bhattacharya, C. Bhattacharya, S. Kundu, K. Banerjee, G. Mukherjee, J. K. Meena, R. Pandey, M. Gohil, H. Pai, A. Dey, T. K. Ghosh, M. Biswas, G. Prajapati, Proc. of DAE-BRNS Symp. on Nucl. Phys. **56**, 492 (2011).
2. “*Three  $\alpha$  - decays of the Hoyle state of  $^{12}\text{C}$  in  $^{12}\text{C} + ^{12}\text{C}$  reaction*”, **T. K. Rana**, C. Bhattacharya, S. Kundu, K. Banerjee, S. Bhattacharya, G. Mukherjee, T. K. Ghosh, J. K. Meena, P. Dhara, M. Biswas, H. Pai, K. Mahata, S. Kumar, K. Ramachandran, P. C. Rout, S. K. Pandit, V. Nalal and R. G. Pillay, Proc. of DAE- BRNS Symp. on Nucl. Phys. **55**, 230 (2010).
3. “*Simulations for the charged particle detector array at VECC*”, D. Gupta, S. Bhattacharya, G. Mukherjee, C. Bhattacharya, K. Banerjee, A. Dey, T. K. Ghosh, S. Kundu, J. K. Meena, **T. K. Rana**, Proc. of DAE- BRNS symp. on Nucl. Phys. **53**, 701 (2008).
4. “*Simulations for VECC charged particle detector array*”, D. Gupta, S. Bhattacharya, G. Mukherjee, C. Bhattacharya, K. Banerjee, A. Dey, T. K. Ghosh, S. Kundu, J. K. Meena, **T. K. Rana**, Proc. of International Workshop on multifragmentation and related topics, Caen(France), **95**, 321 (2007).
5. “*Two particle correlation studies and measurement of temperature*”, **T. K. Rana**, C. Bhattacharya, S. Kundu, K. Banerjee, A. Dey, T. K. Ghosh, G. Mukherjee, D. Gupta, J. K. Meena, A. Roy, P. Dhara, S. R. Banerjee, S. Bhattacharya, Proc. of DAE-BRNS Symp. on Nucl. Phys. **52**, 299 (2007).
6. “*Event reconstruction techniques for Si (strip)-CsI(Tl) Telescope for VECC Charged Particle Array*”, **T. K. Rana**, K. Banerjee, S. Kundu, A. Dey, C. Bhattacharya, S. Bhattacharya, J. K. Meena, G. Mukherjee, T. K. Ghosh, D. Gupta, Proc. of DAE-BRNS Symp. on Nucl. Phys. **51**, 600 (2006).

7. “Testing of CsI(Tl) Detectors”, **T. K. Rana**, K. Banerjee, S. Kundu, C. Bhattacharya, S. Bhattacharya, A. Dey, Proc. of DAE-BRNS Symp. on Nucl. Phys. **50**, 448 (2005).

### Other publications:

#### Referred Journals:

1. “Experimental study of  $^{26}\text{Al}$  through the In pick-up reaction  $^{27}\text{Al}(d, t)$ ”, Vishal Srivastava, C. Bhattacharya, **T. K. Rana**, S. Manna, S. Kundu, S. Bhattacharya, K. Banerjee, P. Roy, R. Pandey, G. Mukherjee, T. K. Ghosh, J. K. Meena, T. Roy, A. Chaudhuri, M. Sinha, A. Saha, Md. A. Asgar, A. Dey, Subinit Roy, and Md. M. Shaik, Phys. Rev. C **91**, 054611 (2015).
2. “Direct evidence of “washing out” of nuclear shell effects”, A. Chaudhuri, T. K. Ghosh, K. Banerjee, S. Bhattacharya, Jhilm Sadhukhan, C. Bhattacharya, S. Kundu, J. K. Meena, G. Mukherjee, R. Pandey, **T. K. Rana**, P. Roy, T. Roy, V. Srivastava, and P. Bhattacharya, Phys. Rev. C **91**, 044620 (2015)..
3. “Angular momentum dependence of the nuclear level density in the  $A \approx 170-200$  region” M. Gohil, Pratap Roy, K. Banerjee, C. Bhattacharya, S. Kundu, **T. K. Rana**, T. K. Ghosh, G. Mukherjee, R. Pandey, H. Pai, V. Srivastava, J. K. Meena, S. R. Banerjee, S. Mukhopadhyay, D. Pandit, S. Pal, and S. Bhattacharya, Phys. Rev. C **91**, 014609 (2015).
4. “Fragment emission studies in low energy light ion reactions”, **T. K. Rana**, C. Bhattacharya, S. Manna, V. Srivastava, K. Banerjee, S. Kundu, P. Roy, R. Pandey, A. Chaudhuri, T. Roy, T. K. Ghosh, G. Mukherjee, S. Bhattacharya, J. K. Meena, S. K. Pandit, K. Mahata, P. Patale, A. Shrivastava, and V. Nanal, EPJ Web of Conferences, **86**, 00036 (2015).
5. “Structure of  $^{26}\text{Al}$  studied by one-nucleon transfer reaction  $^{27}\text{Al}(d, t)$ ”, Vishal Srivastava, C. Bhattacharya, **T. K. Rana**, S. Manna, S. Kundu, S. Bhattacharya,

- K. Banerjee, P. Roy, R. Pandey, G. Mukherjee, T. K. Ghosh, J. K. Meena, T. Roy, A. Chaudhuri, M. Sinha, A. Saha, J. Sahoo, R. Saha Mondal, Md. A. Asgar, Subinit Roy and Md. Moin Shaikh, EPJ Web of Conferences, **86**, 00055 (2015).
6. “*Fusion - fission dynamics: fragment mass distribution studies*”, S. Bhattacharya, A. Chaudhuri, T. K. Ghosh, K. Banerjee, C. Bhattacharya, S. Kundu, G. Mukherjee, **T. K. Rana**, P. Roy, R. Pandey, P. Bhattacharya, EPJ Web of Conferences, **86**, 00004 (2015).
  7. “*Search for rotational state of the Hoyle state in complete kinematic experiment  $^{12}\text{C}(\alpha, \alpha') 3\alpha$* ”, **T. K. Rana**, C. Bhattacharya, S. Bhattacharya, S. Kundu, K. Banerjee, T. K. Ghosh, G. Mukherjee, R. Pandey, M. Gohil, A. Dey, J. K. Meena, G. Prajapati, P. Roy, H. Pai, M. Biswas, EPJ Web of Conferences, **66**, 03010 (2014).
  8. “*Angular momentum dependence of the nuclear level density parameter*”, M. Gohil, Pratap Roy, K. Banerjee, S. Bhattacharya, C. Bhattacharya, S. Kundu, **T. K. Rana**, T. K. Ghosh, G. Mukherjee, R. Pandey, J. K. Meena, H. Pai, V. Srivastava, A. Dey, D. Pandit, S. Mukhopadhyay, S. Pal and S. R. Banerjee, EPJ Web of Conferences, **66**, 03073 (2014).
  9. “*Identification of intruder  $\pi_{13/2}$  state in  $^{197}\text{Tl}$* ”, H. Pai, G. Mukherjee, S. Bhattacharya, C. Bhattacharya, S. Bhattacharyya, T. Bhattacharjee, S. Chanda, S. Rajbanshi, A. Goswami, M. R. Gohil, S. Kundu, T. K. Ghosh, K. Banerjee, **T. K. Rana**, R. Pandey, G. K. Prajapati, S. R. Banerjee, S. Mukhopadhyay, D. Pandit, S. Pal, J. K. Meena, P. Mukhopadhyay and A. Choudhury, EPJ Web of Conferences **66**, 02079 (2014).
  10. “*Crossing of large multiquasiparticle magnetic-rotation bands in  $\text{Bi } 198$* ”, H. Pai, G. Mukherjee, S. Bhattacharyya, C. Bhattacharya, S. Bhattacharya, T. Bhattacharjee, S. K. Basu, S. Kundu, T. K. Ghosh, K. Banerjee, **T. K. Rana**, J. K.

- Meena, R. K. Bhowmik, R. P. Singh, S. Muralithar, S. Chanda, R. Garg, B. Maheshwari, D. Choudhury, A. K. Jain, *Phys. Rev. C* **90**, 064314 (2014).
11. “*MONSTER: a TOF Spectrometer for  $\beta$ -delayed Neutron Spectroscopy*”, T. Martínez, D. Cano-Ott, J. Castilla, A. R. Garcia, J. Marin, G. Martinez, E. Mendoza, C. Santos, F. J. Tera, D. Villamarin, J. Agramunt, A. Algora, C. Domingo, M. D. Jordan, B. Rubio, J. L. Taín, C. Bhattacharya, K. Banerjee, S. Bhattacharya, P. Roy, J. K. Meena, S. Kundu, G. Mukherjee, T. K. Ghosh, **T. K. Rana**, R. Pandey, A. Saxena, B. Behera, H. Penttilä, A. Jokinen, S. Rinta-Antila, C. Guerrero, M. C. Ovejero, *Nuclear Data Sheets* **120**, 78 (2014).
  12. “*Deformation in  $^{28}\text{Si}^*$  produced via  $^{16}\text{O} + ^{12}\text{C}$  reaction*”, S. Kundu, C. Bhattacharya, S. Bhattacharya, **T. K. Rana**, K. Banerjee, S. Mukhopadhyay, D. Gupta, A. Dey, R. Saha, *Phys. Rev. C* **87**, 024602 (2013).
  13. “*Effect of collectivity on the nuclear level density*”, Pratap Roy, K. Banerjee, M. Gohil, C. Bhattacharya, S. Kundu, **T. K. Rana**, T. K. Ghosh, G. Mukherjee, R. Pandey, H. Pai, V. Srivastava, J. K. Meena, S. R. Banerjee, S. Mukhopadhyay, D. Pandit, S. Pal and S. Bhattacharya, *Phys. Rev. C* **88**, 031601(R) (2013).
  14. “*Band structures and intruder  $\pi i_{13/2}$  state in  $^{197}\text{Tl}$* ”, H. Pai, G. Mukherjee, S. Bhattacharya, C. Bhattacharya, S. Bhattacharyya, T. Bhattacharjee, S. Chanda, S. Rajbanshi, A. Goswami, M. R. Gohil, S. Kundu, T. K. Ghosh, K. Banerjee, **T. K. Rana**, R. Pandey, G. K. Prajapati, S. R. Banerjee, S. Mukhopadhyay, D. Pandit, S. Pal, J. K. Meena, P. Mukhopadhyay and A. Choudhury, *Phys. Rev. C* **88**, 064302 (2013).
  15. “*Complex-fragment emission in low-energy light-ion reactions*”, S. Kundu, C. Bhattacharya, K. Banerjee, **T. K. Rana**, S. Bhattacharya, A. Dey, T. K. Ghosh, G. Mukherjee, J. K. Meena, P. Mali, S. Mukhopadhyay, D. Pandit, H. Pai, S. R. Banerjee, D. Gupta, P. Banerjee, Suresh Kumar, A. Shrivastava, A. Chatterjee, K. Ramachandran, K. Mahata, S. K. Pandit and S. Santra, *Phys. Rev. C* **85**, 064607 (2012).

16. “*A Large High Vacuum Reaction Chamber for Nuclear Physics Research at VECC, Kolkata*”, S. Kundu, S. Bhattacharya, J. K. Meena, T. K. Ghosh, T. Bhattacharjee, P. Mukhopadhyay, C. Bhattacharya, **T. K. Rana**, K. Banerjee, G. Mukherjee, S. R. Banerjee, D. L. Bandyopadhyay, M. Ahammed and P. Bhattacharya, J. Phys. Conf. Ser. **390**, 012075 (2012).
17. “*Measurement and simulation of neutron response function of organic liquid scintillator detector*”, M. Gohil, K. Banerjee, S. Bhattacharya, C. Bhattacharya, S. Kundu, **T. K. Rana**, G. Mukherjee, J. K. Meena, R. Pandey, H. Pai, T. K. Ghosh, A. Dey, S. Mukhopadhyay, D. Pandit, S. Pal, S. R. Banerjee, T. Bandyopadhyay, Nucl. Instrum. Methods A **664**, 304 (2012).
18. “*Angular-momentum-gated light-particle evaporation spectra from  $^{97}\text{Tc}^*$  and  $^{62}\text{Zn}^*$  systems*”, Pratap Roy, K. Banerjee, S. Bhattacharya, C. Bhattacharya, S. Kundu, **T. K. Rana**, T. K. Ghosh, G. Mukherjee, R. Pandey, J. K. Meena, M. Gohil, H. Pai, V. Srivastava, A. Dey, Deepak Pandit, S. Mukhopadhyay, S. Pal and S. R. Banerjee, Phys. Rev. C **86**, 044622 (2012).
19. “*Variation of nuclear level density with angular momentum*”, K. Banerjee, S. Bhattacharya, C. Bhattacharya, M. Gohil, S. Kundu, **T. K. Rana**, G. Mukherjee, R. Pandey, P. Roy, H. Pai, A. Dey, T. K. Ghosh, J. K. Meena, S. Mukhopadhyay, D. Pandit, S. Pal and S. R. Banerjee Phys. Rev. C **85**, 064310 (2012).
20. “*Study of the  $1p$  transfer channel in the  $^{12}\text{C} + ^{27}\text{Al}$  reaction at 6 - 7 MeV per nucleon*”, Aparajita Dey, S. Kundu, **T. K. Rana**, K. Banerjee, C. Bhattacharya, M. Biswas, T. K. Ghosh, H. Pai, G. Mukherjee, J. K. Meena, D. Gupta, S. Bhattacharya, S. Mukhopadhyay, D. Pandit, S. R. Banerjee, Suresh Kumar, A. Chatterjee, K. Ramachandran, K. Mahata, S. Santra and S. Pandit, Phys. Scr. **2012**, 014011 (2012).
21. “*Measurement of Giant Dipole Resonance width at low temperature: A new experimental perspective*”, S. Mukhopadhyay, Deepak Pandit, Surajit Pal, Srijit

- Bhattacharya, A. De, S. Bhattacharya, C. Bhattacharya, K. Banerjee, S. Kundu, **T. K. Rana**, G. Mukherjee, R. Pandey, M. Gohil, H. Pai, J. K. Meena and S. R. Banerjee, Phys. Lett. B **709**, 9 (2012).
22. “*Onset of deformation at  $N = 112$  in Bi nuclei*”, H. Pai, G. Mukherjee, R. Raut, S. K. Basu, A. Goswami, S. Chanda, T. Bhattacharjee, S. Bhattacharyya, C. Bhattacharya, S. Bhattacharya, S. R. Banerjee, S. Kundu, K. Banerjee, A. Dey, **T. K. Rana**, J. K. Meena, D. Gupta, S. Mukhopadhyay, Srijit Bhattacharya, Sudeb Bhattacharya, S. Ganguly, R. Kshetri and M. K. Pradhan, Phys. Rev. C **85**, 064317 (2012).
23. “*Properties of the alpha cluster states of  $^{212}\text{Po}$  from elastic scattering of alpha particles from  $^{208}\text{Pb}$* ”, C. Basu, S. Adhikari, S. Bhattacharya, C. Bhattacharya, T. K. Ghosh, K. Banerjee, **T. K. Rana**, S. Ray, R. Pandey, G. Prajapati, A. Dey, A. K. Mitra, J. K. Meena, American Institute of Phys. Conf. Series **1491**, 321 (2012).
24. “*Evidence of quasi fission in  $^{16}\text{O} + ^{238}\text{U}$  reaction at sub barrier energies*”, K. Banerjee, T. K. Ghosh, S. Bhattacharya, C. Bhattacharya, S. Kundu, **T. K. Rana**, G. Mukherjee, J. K. Meena, J. Sadhukhan, S. Pal, P. Bhattacharya, K. S. Golda, P. Sugathan, R. P. Singh Phys. Rev. C **83**, 024605 (2011).
25. “*Change over from compound nuclear fission to quasi-fission*”, T. K. Ghosh, K. Banerjee, C. Bhattacharya, S. Bhattacharya, S. Kundu, P. Mali, J. K. Meena, G. Mukherjee, S. Mukhopadhyay and **T. K. Rana**, EPJ Web of Conference **2**, 10003 (2010).
26. “*Extreme nuclear shapes examined via giant dipole resonance lineshapes in hot light-mass systems*”, Deepak Pandit, S. Mukhopadhyay, Srijit Bhattacharya, Surajit Pal, A. De, S. Bhattacharya, C. Bhattacharya, K. Banerjee, S. Kundu, **T. K. Rana**, A. Dey, G. Mukherjee, T. K. Ghosh, D. Gupta and S. R. Banerjee, Phys. Rev. C **81**, 061302(R) (2010).

27. “Variation of neutron detection characteristics with dimension of BC501A neutron detector”, K. Banerjee, T. K. Ghosh, S. Kundu, **T. K. Rana**, C. Bhattacharya, J. K. Meena, G. Mukherjee, P. Mali, D. Gupta, S. Mukhopadhyay, D. Pandit, S. R. Banerjee, S. Bhattacharya, T. Bandyopadhyay, S. Chatterjee, Nucl. Instrum. Methods A **608**, 440 (2009).
28. “Light charged-particle emission from hot  $^{32}\text{S}^*$  formed in  $^{20}\text{Ne} + ^{12}\text{C}$  reaction”, Aparajita Dey, S. Bhattacharya, C. Bhattacharya, K. Banerjee, **T. K. Rana**, S. Kundu, S. R. Banerjee, S. Mukhopadhyay, D. Gupta and R. Saha, Eur. Phys. J. A **41**, 39 (2009).
29. “Sharp change-over from compound nuclear fission to quasifission”, T. K. Ghosh, K. Banerjee, C. Bhattacharya, S. Bhattacharya, S. Kundu, P. Mali, J. K. Meena, G. Mukherjee, S. Mukhopadhyay and **T. K. Rana**, Phys. Rev. C **79**, 054607 (2009).
30. “Fragment emission studies of the  $^{16}\text{O} + ^{12}\text{C}$  reaction”, S. Kundu, A. Dey, K. Banerjee, **T. K. Rana**, S. Mukhopadhyay, D. Gupta, R. Saha, S. Bhattacharya and C. Bhattacharya, Phys. Rev. C **77**, 024318 (2008).
31. “Giant dipole resonance width in nuclei near Sn at low temperature and high angular momentum”, Srijit Bhattacharya, S. Mukhopadhyay, Deepak Pandit, Surajit Pal, A. De, S. Bhattacharya, C. Bhattacharya, K. Banerjee, S. Kundu, **T. K. Rana**, A. Dey, G. Mukherjee, T. K. Ghosh, D. Gupta and S. R. Banerjee, Phys. Rev. C **77**, 024318 (2008).
32. “Study of dissipative collisions of  $^{20}\text{Ne}$  ( $\approx 7\text{-}11$  MeV/nucleon) +  $^{27}\text{Al}$ ”, Aparajita Dey, C. Bhattacharya, S. Bhattacharya, **T. K. Rana**, S. Kundu, K. Banerjee, S. Mukhopadhyay, S. R. Banerjee, D. Gupta and R. Saha, Phys. Rev. C **75**, 064606 (2007).
33. “Characteristics of Gd-loaded liquid scintillators BC521 and BC525”, K. Banerjee, S. Kundu, S. Mukhopadhyay, **T. K. Rana**, S. Bhattacharya, C. Bhat-

- tacharya, S. R. Banerjee, T. K. Ghosh, G. Mukherjee, T. Bandyopadhyay, A. Dey, J. K. Meena, P. Mukhopadhyay, D. Gupta, S. Pal, D. Pandit, S. Bhattacharya, Nucl. Instrum. Methods A **580**, 1383 (2007).
34. “*LAMBDA: Large Area Modular BaF<sub>2</sub> Detector Array for the measurement of high energy gamma rays*”, S. Mukhopadhyay, Srijit Bhattacharya, Deepak Pandit, A. Ray, Surajit Pal, K. Banerjee, S. Kundu, **T. K. Rana**, S. Bhattacharya, C. Bhattacharya, A. De, S. R. Banerjee, Nucl. Instrum. Methods A **582**, 603 (2007).
35. “*Characterization of fragment emission in <sup>20</sup>Ne ( $\approx 7-11$  MeV/nucleon) + <sup>12</sup>C reactions*”, Aparajita Dey, C. Bhattacharya, S. Bhattacharya, S. Kundu, K. Banerjee, S. Mukhopadhyay, D. Gupta, T. Bhattacharjee, S. R. Banerjee, S. Bhattacharyya, **T. K. Rana**, S. K. Basu, R. Saha, K. Krishan, A. Mukherjee, D. Bandopadhyay and C. Beck, Phys. Rev. C **76**, 034608 (2007).
36. “*Evidence of large nuclear deformation of <sup>32</sup>S\* formed in the <sup>20</sup>Ne + <sup>12</sup>C reaction*”, Aparajita Dey, S. Bhattacharya, C. Bhattacharya, K. Banerjee, **T. K. Rana**, S. Kundu, S. Mukhopadhyay, D. Gupta and R. Saha, Phys. Rev. C **74**, 044605 (2006).
37. “*Survival of orbiting in <sup>20</sup>Ne (7- 10 MeV/nucleon) + <sup>12</sup>C reactions*”, C. Bhattacharya, A. Dey, S. Kundu, K. Banerjee, S. Bhattacharya, S. Mukhopadhyay, D. Gupta, T. Bhattacharjee, S. R. Banerjee, S. Bhattacharya, **T. K. Rana**, S. K. Basu, R. Saha, S. Bhattacharjee, K. Krishan, A. Mukherjee and D. Bandopadhyay Phys. Rev. C **72**, 021601(R) (2005).

#### Conference Proceedings (selected):

1. “*Isotopic effects in fragment emission studies in low energy light ion reactions*”, C. Bhattacharya, **T. K. Rana**, Santu Manna, V. Srivastava, K. Banerjee, S. Kundu, P. Roy, R. Pandey, A. Chaudhuri, T. Roy, T. K. Ghosh, G. Mukherjee, S.

- Bhattacharya, J. K. Meena, S. K. Pandit, K. Mahata, P. Patale, A. Shrivastava, V. Nanal, Proc. of the Int. Symp. on Nucl. Phys. **58**, 530 (2013).
2. “*Signature of collective enhancement in nuclear level density*”, Pratap Roy, K. Banerjee, M. Gohil, C. Bhattacharya, S. Kundu, **T. K. Rana**, T. K. Ghosh, G. Mukherjee, R. Pandey, H. Pai, V. Srivastava, J. K. Meena, S. R. Banerjee, S. Mukhopadhyay, D. Pandit, S. Pal, S. Bhattacharya, Proc. of the Int. Symp. on Nucl. Phys. **58**, 378 (2013).
  3. “*Study of ( $^4\text{He}, t$ ) reaction on  $^{27}\text{Al}$  target at 50 MeV*”, Aparajita Dey, Vishal Srivastava, C. Bhattacharya, S. Ganguly, **T. K. Rana**, S. Kundu, T. K. Ghosh, K. Banerjee, P. Roy, R. Pandey, H. Pai, G. Mukherjee, M. R. Gohil, J. K. Meena, S. Bhattacharya, Proc. of the Int. Symp. on Nucl. Phys. **58**, 594 (2013).
  4. “*Development of proto-type neutron detector for MONSTER*”, K. Banerjee, Pratap Roy, C. Bhattacharya, J. K. Meena, R. Pandey, T. K. Ghosh, S. Kundu, **T. K. Rana**, G. Mukherjee, A. K. Saha, A. K. Sahoo, R. Mandal Saha, S. Bhattacharya, A. Saxena, B. Behera, T. Martinez, D. Cano ott, J. Castilla, A. R. Garcia, J. Marin, C. Santos, G. Martinez, E. Mendoza, C. Santos, F. J. Tera, D. Villamarin, J. Agramunt, A. Algora, C. Domingo, M. D. Jordan, B. Rubio, J. L. Tain, H. Penttila, A. Jokinen, S. Rinta Antila, C. Guerrero, M. C. Ovejero, Proc. of the Int. Symp. on Nucl. Phys. **58**, 886 (2013).
  5. “*Measurement of efficiency and time resolution of PPAC*”, R. Pandey, T. K. Ghosh, K. Banerjee, P. Roy, C. Bhattacharya, A. Chaudhuri, S. Kundu, **T. K. Rana**, G. Mukherjee, J. K. Meena, V. Srivastava, A. K. Saha, J. K. Sahoo, S. Bhattacharya, Proc. of the Int. Symp. on Nucl. Phys. **58**, 982 (2013).
  6. “*Search of  $2_2^+$  state of the Hoyle state of  $^{12}\text{C}$* ”, **T. K. Rana**, S. Bhattacharya, C. Bhattacharya, S. Kundu, K. Banerjee, T. K. Ghosh, G. Mukherjee, R. Pandey, M. Gohil, A. Dey, J. K. Meena, G. Prajapati, P. Roy, H. Pai, M. Biswas, Proc. of DAE- BRNS Symp. on Nucl. Phys. **57**, 422 (2012).

7. “*Charged particle detector array  $45^0 - 175^0$* ”, S. Kundu, C. Bhattacharya, **T. K. Rana**, K. Banerjee, S. Bhattacharya, J. K. Meena, R. Saha, G. Mukherjee, T. K. Ghosh, R. Pandey, P. Roy, M. Gohil, V. Srivastava, A. Dey, G. Pal, S. Roy, S. R. Bajirao, C. Nandi , Proc. of DAE Symp. On Nucl. Phys. Vol. **57**, 864 (2012).
8. “*Isoscaling in  $^{13}\text{C} + ^{12}\text{C}$  and  $^{12}\text{C} + ^{12}\text{C}$  reactions at  $\sim 6 \text{ MeV/u}$* ”, **T. K. Rana**, C. Bhattacharya, S. Kundu, K. Banerjee, S. Bhattacharya, G. Mukherjee, T. K. Ghosh, J. K. Meena, P. Dhara, M. Biswas, H. Pai, K. Mahata, Suresh Kumar, K. Ramachandran, P. C. Rout, S. K. Pandit, V. Nanal and R. G. Pillay, Proc. of DAE- BRNS Symp. on Nucl. Phys. **54**, 388 (2009).
9. “*Study of light particle emission in  $\alpha$  like and non- $\alpha$  like nuclei*”, **T. K. Rana**, S. Kundu, K. Banerjee, C. Bhattacharya, A. Dey, T. K. Ghosh, G. Mukherjee, D. Gupta, S. Bhattacharya, J. K. Meena, S. R. Banerjee, S. Mukhopadyay , D. Pandit, P. Mali, A. Srivastava, Suresh Kumar, A. Chatterjee, K. Ramachandran, Proc. of DAE- BRNS Symp. on Nucl. Phys. **53**, 501 (2008).
10. “*Testing of a CsI(Tl) detector and its energy calibration*”, S. Kundu, K. Banerjee, T. K. Rana, C. Bhattacharya, P. C. Rout, A. Mitra, E. T. Mirgule, V. Nanal, Suresh Kumar, V. M. Datar, D. R. Chakrabarty, S. Bhattacharya, A. Dey, G. Mukherjee, T. K. Ghosh, D. Gupta, J.K. Meena Proc. of DAE- BRNS Symp. on Nucl. Phys. **51**, 618 (2006).



Tapan Kumar Rana



*To*  
*My loving parents*



## Acknowledgements

First and foremost, I would like to express my deep gratitude and thanks to my PhD thesis supervisor, Dr. Chandana Bhattacharya for her valuable guidance, constant support, encouragement, motivation and sincere interest throughout my entire PhD program. I am really very proud to get an opportunity to work with her to complete this work. Apart from her, I would like to thank to the members of my PhD advisory committee: Prof. S. R. Banerjee, Prof. Subinit Roy, Prof. U. S. Pandit and Shri. Amitava Roy, for their valuable suggestions and comments.

I am extremely thankful and grateful to Prof. Sailajananda Bhattacharya for his continuous encouragement and open hearted support to complete this thesis work. I have learned a lot of physics from him, which is far more than one can learn by reading any textbook. I also thank him for proofreading of various drafts of this thesis and synopsis which helped me to present my research work in an effective manner. Thank you so much Sir!

I would like to acknowledge my sincere thanks to my colleagues who directly or indirectly helped me to perform experimental and developmental activities, which have been included in the present thesis. As they are too many to mention everyone by name, I would like to thank a few individuals in particular who have helped in their own different ways to complete this work. I would like to thank to my colleague Dr. Samir Kundu for his support, particularly in the developmental activities included in this thesis. I am also thankful to my other colleagues, Dr. Kaushik Banerjee, Jaikiran Meena, Dr. C. K. Ghosh, Dr. G. mukherjee, R. Pandey, P. Roy, S. Manna, Dr. A. Dey, Dr. H. Pai, Dr. M. Gohil, U. Srivastava, A. Chaudury, R. Saha Modak, A. K. Saha

and Jayanta Sahu for their helpful and freehearted support. I would also like to thank to my other collaborators Prof. S. R. Banerjee, Dr. S. Mukhopadhyay, Dr. D. Pandit, Dr. D. Gupta, R. Saha of VEC, Kolkata, Prof. S. Kumar, Dr. K. Mahata, S. K. Pandit, Dr. P. C. Raut, Dr. K. Ramachandran of BARRC, Mumbai and Prof. U. Nandal, Prof. R. G. Pillay of CTR, Mumbai for their help.

I extremely grateful to Prof. D. K. Srivastava, Director, VEC, for providing a favourable environment for nuclear physics research in the institute, which is indirectly help me to achieve this goal.

I would also like to thank Amitava Roy and Partha Dhara for providing the data acquisition software for on line as well as off line, and giving continuous support which helped me to collect and analyze the experimental data.

The experiments included in the present thesis have been performed using K130 Cyclotron, VEC at Kolkata and BARRC-CTR Pelletron facility at Mumbai. I would like to express my special gratitude to the operating staff of these accelerators to provide us smooth and uninterrupted beams.

I would also like to express my special thanks to the target making laboratories at VEC and CTR for providing the good quality of targets for performing the experiments, the results of which have been included in this thesis.

I am grateful to all of my friends and seniors who have supported and inspired me during many difficulties in my life. Immediately I remember Dr. Jajati Kesari Nayak, Prafulla Kr Behera, Subas Jena, Pradeep Kumar, R. Mahanto, Hemendra Pandey, Vineet Kr Bakesh and Waseem Siddqui for their support and help.

Finally, I would like to thank my wife, Reeta, for the support and care she had taken during this work, that allowed me to finish this journey. My loving thanks are also due to my two sons, Deeshan and Shreyan, who have been my constant source of energy and I thank them for providing cheerful atmosphere at home. It is my duty of course, to acknowledge my parents, whose encouragement, and loving support brought me to where I am today. I also like to thank to my younger brother Rajesh, my sister Bijaylaxmi and their families for their loving support. I would like to thank my maternal uncles and all my relatives for their sympathy during this work.

*Tapan Kumar Rana*

Tapan Kumar Rana



# Contents

<b>SYNOPSIS</b>	<b>xxxi</b>
<b>List of Figures</b>	<b>xliii</b>
<b>List of Tables</b>	<b>xliv</b>
<b>1 Introduction</b>	<b>1</b>
1.1 The Hoyle state . . . . .	3
1.1.1 Role of the Hoyle state in nucleosynthesis . . . . .	3
1.1.2 Present status on structure of the Hoyle state . . . . .	6
1.1.3 The triple $\alpha$ reaction rate . . . . .	8
1.2 Motivation . . . . .	11
<b>2 Development of high resolution charged particle detector array</b>	<b>15</b>
2.1 Introduction . . . . .	15
2.2 Design and simulation of the high resolution charged particle detector array . . . . .	19
2.2.1 Design of individual telescope . . . . .	23
2.2.2 Silicon Detectors . . . . .	23
2.2.2.1 Single-sided Silicon Strip Detector (SSSD) . . . . .	24
2.2.2.2 Double-sided Silicon Strip Detector (DSSD) . . . . .	24

2.2.2.3	Design of the detector frame . . . . .	25
2.2.2.4	Characterisation of silicon strip detectors . . . . .	26
2.2.3	CsI(Tl) detector . . . . .	29
2.2.3.1	Design of CsI(Tl) detector . . . . .	30
2.2.3.2	Characterisation of CsI(Tl) detector . . . . .	31
2.3	Development of event reconstruction technique . . . . .	32
2.3.1	Event selection . . . . .	33
2.3.2	Position identification in DSSD . . . . .	34
2.3.3	Particle Identification by $\Delta E - E$ method . . . . .	36
2.4	In beam performance test of a prototype telescope . . . . .	38
2.4.1	Experimental details . . . . .	38
2.4.2	Performance Testing of event reconstruction technique . . . . .	40
2.4.3	Physics extraction from the prototype telescope testing . . . . .	42
2.4.4	Performance test of final telescopes . . . . .	46
2.5	Design and development of mechanical structure of detector array . . . . .	49
2.5.1	Single telescope housing . . . . .	49
2.5.2	Support structure of detector array . . . . .	50
2.5.3	Readout electronics and data acquisition system . . . . .	51
2.5.4	Status of the high resolution array . . . . .	53
<b>3</b>	<b>Study of decay mechanism of the Hoyle state</b> . . . . .	<b>55</b>
3.1	Introduction . . . . .	55
3.2	Experiment for study of the Hoyle state . . . . .	56
3.2.1	Accelerator used: Variable energy cyclotron . . . . .	56
3.2.2	Experimental setup . . . . .	59
3.2.3	Readout electronics and data acquisition system . . . . .	60
3.3	Data Analysis procedure . . . . .	61
3.3.1	Energy calibrations . . . . .	63

3.3.2	Position identification in DSSD . . . . .	66
3.3.3	Particle Identification technique . . . . .	67
3.3.4	Target thickness measurement . . . . .	68
3.3.5	Energy loss corrections . . . . .	69
3.3.6	Event reconstruction . . . . .	70
3.3.7	Kinematical cuts for filtering of events . . . . .	71
3.3.8	Monte Carlo simulation . . . . .	73
3.3.9	Dalitz Plot technique . . . . .	77
3.4	Techniques used for estimation of decay mechanism . . . . .	81
3.4.1	The relative energy distribution of $^8\text{Be}$ like pairs . . . . .	82
3.4.2	The distribution of root mean square energy deviation: . . . . .	83
3.4.3	The distribution of radial projection of the Dalitz plot: . . . . .	84
3.5	Estimation of decay components of the Hoyle state . . . . .	87
3.6	Results and discussions . . . . .	90

**4 Summary and Conclusions 93**



# SYNOPSIS

In nuclear physics, clustering plays an important role in determining the structure of light nuclei. Moreover the study of these nuclei is crucial for various astrophysical scenarios. The study of  $\alpha$ -cluster emission is one of the most important ways to investigate the structure of  $N = Z$  nuclei. It is important to extract maximum possible information on these emitted cluster particles using the sophisticated detector system to understand their emission mechanism and ultimately to know the underlying nuclear structure of the decaying nuclei. In particular, the study of  ${}^8\text{Be}$ ,  ${}^{12}\text{C}$ ,  ${}^{16}\text{O}$  as two, three and four  $\alpha$ -cluster structures, respectively, is important to estimate elemental abundances in universe through stellar-nucleosynthesis process. In recent years, there has been lot of interest in the study of cluster states using resonance particle spectroscopy with special emphasis on the structure of second  $0^+$  excited state of  ${}^{12}\text{C}$  at 7.65 MeV, the famous Hoyle state, which is believed to play a key role in the synthesis of  ${}^{12}\text{C}$  and the other heavy elements in the Universe. Though a few attempts have been made in the past to understand the nature of this Hoyle state, the study of structure of this state is still a subject of great interest. From nuclear structure point of view too, the Hoyle state presents many unique features which are yet to be understood properly. The standard shell-model approaches as well as no-core shell model (NCSM1) calculations failed to reproduce the state; however, recent calculations within no core shell model framework with no effective limitation on the number of harmonic oscillators in the model space (NCSM2) have been able to demonstrate the existence of low lying cluster structures in  ${}^{12}\text{C}$  ( $0_2^+$  Hoyle state and its excited  $2_2^+$  state). The *ab – initio* calculation using lattice chiral effective field theory (LEFT) has been able to identify a resonance in  ${}^{12}\text{C}$  having the characteristics of the Hoyle state. Besides, this state has long been considered as a classic example of  $\alpha$ -cluster nuclear states in light nuclei as well as a candidate for exotic  $3\alpha$  linear chain configuration. At the same time, this state is known to possess a relatively large radius compared to that of the ground state. So, it may be conjectured that the  $\alpha$ -clusters in the Hoyle state remain in quasi-free gas like state. This observation, together with the bosonic nature of  $\alpha$ -particles and the fact

all three  $\alpha$ -particles are in the same state ( $0^+$ ), has led to the speculation that the state may be interpreted in terms of a nuclear Bose-Einstein condensation (BEC). Because of the gas like structure of the condensate, the relative positions of the  $\alpha$ -particles in the Hoyle state should be uncorrelated. However, recent fermionic molecular dynamics (FMD) calculations indicate that the relative positions of the  $\alpha$ -particles are correlated mostly resembling  ${}^8\text{Be}$  plus  $\alpha$  configurations. The predominance of this ( ${}^8\text{Be} + \alpha$ ) structure has been observed experimentally in the sequential nature of decay of the Hoyle state. However, the predominance of one type of configuration (say  ${}^8\text{Be} + \alpha$ ) does not rule out the possibility of existence of other configurations (*i.e.*, BEC) in isolated situations. Similar interesting features may also exist for other higher unbound resonances which are yet to be explored. Understanding the origin and structure of the Hoyle state continues to remain a strong challenge to theory and attracts considerable experimental efforts. The information about the structure of  $\alpha$ -cluster resonances are usually extracted from the particle decay studies. Thus precise studies of decay mechanism of the states play an important role in deciphering the structure information of these exotic states. Moreover, the break-up of a physical system into a three-body continuum with Coulomb interaction is not yet a well-understood problem of few-body physics, although it is being studied over many years. The study of these processes will help to improve our understanding of the inverse triple- $\alpha$  process and to probe to what extent the three particles of the final state may be present as a cluster structure in the many-body initial state. To study the above mentioned phenomena, a sophisticated detector system with high granularity and high resolution needed. In the present thesis, a high resolution charged particle detector array has been developed and use it (partially) to study the particle unstable states, particularly the Hoyle state, formed in low energy ( $\lesssim 15$  MeV/A) light heavy-ion reactions. The thesis mainly consists of two parts. The first part is related to the development of high granular-high resolution charged particle detector array and its event reconstruction technique. The second part of the thesis dedicated to the study of the decay mechanism of Hoyle state of  ${}^{12}\text{C}$  in inelastic scattering of  $\alpha$  on  ${}^{12}\text{C}$  at 15 MeV/A energy.

The first part of the thesis is related to the development of detector array and its data reduction technique. We have been developing a high resolution charged particle detector array, which would ultimately be used for nuclear physics experiments with K500 super-conducting cyclotron at VECC. The main objective of high resolution charged particle detector array is to study the hot nuclei produced in intermediate energy heavy ion collision by calorimetric as well as spectroscopic techniques. This array will cover the angular range (laboratory) of  $7^{\circ}$  to  $45^{\circ}$  (most of the intermediate mass fragments will be emitted within this zone), and it is needed to identify them in energy, mass and charge for physics extraction. Therefore, the detector should have high energy resolution, high granularity, low detection threshold and good isotopic identification capacity. Keeping all these in mind, the detector array has been developed. It consists of 24 telescopes, each telescope is made up of three elements; first element is a  $50 \mu\text{m}$ ,  $\Delta E$ , Single-sided Silicon Strip Detector (SSSD : 16 strips, each of dimension  $50 \text{ mm} \times 3 \text{ mm}$ ), second element is a  $500/1000 \mu\text{m}$ ,  $E/\Delta E$ , Double-sided Silicon Strip Detector (DSSD : 16 strips (each  $50 \text{ mm} \times 3 \text{ mm}$ ) per side in mutually orthogonal directions) and third element is CsI(Tl) detector (4 nos.), each of thickness 6 cm. The complete mechanical structure is such that the array, after complete assembly, form a surface of a sphere of radius 20 cm. Development of data analysis procedure of the this array is quite complex as it consist of multiple channels in each telescope (52 channels per telescope, total of 1248 channels for the whole array). Event reconstruction technique for the analysis of the data from multiple telescopes has been developed in ROOT platform under the present thesis program. Characterisation (mainly energy resolution and uniformity) of Si-strip detectors and CsI(Tl) detectors for each telescope has been performed. Design and development of whole mechanical support structure of array as well as each housing of telescope have been performed. Initially, a prototype telescope has been developed, which consisted of  $65 \mu\text{m}$ ,  $\Delta E$ , SSSD,  $300 \mu\text{m}$ ,  $E/\Delta E$ , DSSD and backed by four CsI(Tl) detectors of thickness 4 cm; the performance of the prototype has been tested experimentally using  $145 \text{ MeV } ^{20}\text{Ne}$  beam from the room temperature cyclotron, VECC, Kolkata, on the  $^{12}\text{C}$  target. Emitted particles have

been measured using this telescope in the angular range  $27^{\circ}$  to  $40^{\circ}$  in laboratory. Multi-particle correlation has been studied (such as  $2\alpha$ ,  $d-\alpha$ , which correspond to  ${}^8\text{Be}$ ,  ${}^6\text{Li}$  particle unstable states). From the above correlation study, nuclear source temperature has been extracted using three different methods (slope thermometer, excited state thermometer and double isotope thermometer methods). The estimated temperature using three different methods have been found to be consistent at this excitation energy. Second performance testing of final design of telescope has been performed at BARC-TIFR Pelletron, Mumbai, to measure the particle unstable states formation in  ${}^{12,13}\text{C} + {}^{12}\text{C}$  reactions. Performance test of all elements of the detector array have been completed. The complete detector array with all the elements as well as the electronics have been tested and the array (full or part of it) is being used for physics experiment.

Second part of the present thesis is related to the study of Hoyle state of  ${}^{12}\text{C}$  in a complete kinematics experiment. The experiment has been performed at the Variable Energy Cyclotron Centre, Kolkata, using 60 MeV  ${}^4\text{He}$  ion beam from the K130 cyclotron on  ${}^{12}\text{C}$  target (self-supported with a thickness  $\sim 90 \mu\text{g}/\text{cm}^2$ ). Typical beam current used for the experiment was  $\sim 2.5$  pA. Different excited states in  ${}^{12}\text{C}$  nuclei were produced through inelastic scattering of  ${}^4\text{He}$  from  ${}^{12}\text{C}$ . Two DSSD detectors, each of  $500 \mu\text{m}$  thickness, have been used in forward direction to detect  $3\alpha$  decay from  ${}^{12}\text{C}^*$  and one telescope consisting of a  $50 \mu\text{m}$  SSSD, as  $\Delta E$ , and  $500 \mu\text{m}$  DSSD as E, in backward direction to detect and identify the inelastic  $\alpha$ -particles. The two DSSD detectors and strip detector telescope were placed at kinematically correlated angles for coincident detection of inelastically scattered  ${}^4\text{He}$  in the backward angle telescope (covering the angular range approximately  $88^{\circ} - 132^{\circ}$ ) and the three  $\alpha$ -particles, originating from the decay of the states of the recoiling  ${}^{12}\text{C}^*$ , at the forward angle detectors (covering the angular range approximately  $20^{\circ} - 92^{\circ}$ ). All strips of the detectors were read out individually using standard readout electronics.

The study of break up (direct versus sequential break up) of Hoyle state of  ${}^{12}\text{C}$  into its constituent  $\alpha$ -particles is still of great interest and is very important also from the structural and astrophysical point of view. The triple- $\alpha$  reaction is fully dominated by

the s-wave resonances in the temperature range ( $T = 10^8 \text{ K} - 10^9 \text{ K}$ ) in which stellar helium burning takes place. The astrophysical reaction rate calculations are based on the assumption that triple- $\alpha$  capture process proceeds exclusively via sequential two-step process ( $\alpha + \alpha \rightarrow {}^8\text{Be}$ ;  ${}^8\text{Be} + \alpha \rightarrow {}^{12}\text{C}^*$ ). Calculations indicate that even minor change of the process (from sequential to direct) may modify the triple- $\alpha$  capture rate [C. Angulo *et al.*, Nucl. Phys. A **656**, 3 (1999)], and thus the relative abundance of  ${}^{12}\text{C}$ , which, in turn, would affect the stellar evolution process [C. Tur *et al.*, Astrophys. J. **718**, 357 (2010)]. So, precise quantitative measurement of all direct processes (deviation from sequential) in Hoyle state decay is crucially important from nuclear structure as well as astrophysics points of view. In recent times, several experiments have been performed to investigate and quantify the roles of various decay modes of Hoyle state. In addition, attempts have also been made to identify and differentiate among various types of direct decays, such as decay into equal energies (DDE), decay into a linear chain (DDL) and decay in phase space (DD $\Phi$ ), and to quantify their contributions, which are supposed to throw new lights on the exotic structure of the Hoyle state. The first experimental estimate of direct  $3\alpha$  decay of the Hoyle state was made by Freer *et al.* [Phys. Rev. C **49**, 1751(R) (1994)], who, using a Dalitz plot and its projection in terms of  ${}^8\text{Be}$  like pairs, estimated an upper limit of 4% on direct  $3\alpha$  decay in phase space branches bypassing the ground state of  ${}^8\text{Be}$ . In a recent work, Raduta *et al.* [Phys. Lett. B **705**, 65 (2011)] identified two direct decay branches, DDE and DDL, with a combined branching percentage of 17(5) %, and argued that the DDE branch corresponds to the signature of an  $\alpha$  condensate structure. This 17 % direct decay implies a same amount of reduction in the reaction rate calculation in the temperature range of  $3\alpha$  fusion ( $10^8 - 10^9 \text{ K}$ ), which is larger than the current estimate of uncertainty on the reaction rate; this is a serious issue that needs to be cross-checked by independent, precise, higher statistics experiment. More recently, Manfredi *et al.* [Phys. Rev. C **85**, 037603 (2012)] have estimated, using optimizations of the distribution of  ${}^8\text{Be}$  like pairs as well as the distribution of root mean square energy deviation, the upper limit for contributions of DD $\Phi$  and DDE to be 3.9 % and 0.45 %, respectively, at 99.75 % confidence level .

In another recent work, Kirsebom *et al.* [Phys. Rev. Lett. **108**, 202501 (2012)] have estimated, using the optimization of symmetric Dalitz plot and its radial projection, the upper limits for DDE, DDL and DD $\Phi$  components to be 0.09%, 0.09% and 0.5%, respectively, at 95% confidence level.

It is clear from above that there is a discrepancy among different measurements; in particular, all measurements except that of Raduta *et al.* indicate that the direct decay modes are very small fractions (upper limit  $\sim 5\%$  or less). Therefore, exclusive experiments with higher statistics of Hoyle events are needed to verify and cross check the recent experimental results and to reach a consensus on this issue. This is important because, apart from crucial astrophysical significance (triple- $\alpha$  reaction rate and consequently the abundance of carbon), various DD modes, though small, are considered to be manifestations of new and exotic structures (linear chain, nuclear Bose-Einstein condensate, etc.) which are special for the Hoyle state. In this thesis, different decay mechanism of Hoyle state has been estimated in a high resolution and high statistics experimental measurement. It has been performed in a complete kinematical experiment of inelastic scattering of  $\alpha$  (60 MeV) on  $^{12}\text{C}$ . Only fully detected ( $4\alpha$  in exit channel) events were considered for the present analysis to avoid any possible propagation of error originating from the uncertainty in the determination of the momentum of the fourth particle escaping detection in otherwise kinematically complete,  $3\alpha$  events. The number of fully detected ( $4\alpha$ ) Hoyle state events in the present data was around 20,000, which is nearly 4-10 times higher than the number of events considered in any earlier experiment.

For quantitative estimation of the individual contributions of the three direct decay modes (DDL, DDE, and, DD $\Phi$ ), of the Hoyle state, an event-by-event Monte Carlo simulation program has been developed using CERN library in ROOT platform to take into account the geometrical efficiencies of the setup. In the simulation, all experimental effects have been properly considered. Simultaneous optimization of three different distributions (the relative energy of  $^8\text{Be}$  like pairs, the root mean square energy deviation, and the radial projection of symmetric Dalitz plot) derived from the

experimental data with those generated from a simulated event set has been performed to arrive at a consistent estimate of the contributions of various direct decay modes. The optimization procedure was further repeated numerous times with different sets of simulated data sampled randomly from a much larger pool of simulated events to extract the distribution of the best-fit values and determine the contribution for each mode; if the contribution for some mode was not statistically significant, the upper limit of the contribution has been extracted at 99.75 % confidence limit (CL). Simultaneous optimization of three different distributions using  $\chi^2$  minimization technique has led to the determination of non-zero branching ratios for direct decay in phase space (DD $\Phi$  :  $0.60 \pm 0.09$  %), and direct decay with equal energy (DDE :  $0.30 \pm 0.1$  %). The present study has also led to the estimation of upper limit for direct decay of linear chain (DDL : 0.1%) at 99.75 % confidence level. This is the first time in a complete kinematics experiment, the quantitative contributions of different direct components of Hoyle state decay have been extracted.



# List of Figures

1.1	<i>The Ikeda threshold diagram for <math>N\alpha</math> nuclei.</i>	2
1.2	<i>Schematic view of level diagram of <math>^{12}\text{C}</math>. The Hoyle state is produced through fusion of triple-<math>\alpha</math> process. Ground state of <math>^{12}\text{C}</math> is produced through the decay of the Hoyle state (7.65 MeV) by cascade <math>\gamma</math>-decay or by internal pair production.</i>	4
2.1	<i>Schematic view of the full <math>4\pi</math> charged particle detector array.</i>	18
2.2	<i>The detected LCP multiplicity events in percentage (mother event LCP multiplicities of 2, 8, 14, 20, 26, 32) for <math>^{40}\text{Ca} + ^{40}\text{Ca}</math> reaction at 50 MeV/A. The solid lines are guides to the eyes while the dotted lines are reduced multiplicities. The inset shows distribution of 1 million HIPSE events with lines as guides to the eyes.</i>	20
2.3	<i>The percentage of particles (a,b,c) and multiple hits (d,e,f) for <math>^{40}\text{Ca} + ^{40}\text{Ca}</math> reaction at different detector elements of the telescope of array. The solid (open) circles correspond to multiplicity events for all (light) charged particles while open triangles are fragments other than LCP. The lines are the guides to the eyes. The inset in (f) shows the type of particles with atomic number <math>Z</math> at CsI(Tl) detectors of the array.</i>	21
2.4	<i>The schematic design and arrangement of high resolution Si-strips-CsI(Tl) detector array.</i>	22
2.5	<i>The schematic view of different elements of a telescope.</i>	22
2.6	<i>Design of the DSSD frame.</i>	27
2.7	<i>Strip detectors with kaptons.</i>	28
2.8	<i>The energy spectrum of <math>\alpha</math>-particles emitted from <math>^{241}\text{Am}</math> source for a particular strip.</i>	29
2.9	<i>Non-uniformity in thickness along the strip in 16 different positions of all strips of 50 <math>\mu\text{m}</math> SSSD.</i>	29

2.10	(A) Design of one CsI(Tl) detector and (B) assembly of four CsI(Tl) crystals as used in the telescope. . . . .	31
2.11	Single CsI(Tl) detector with photodiode and pre-amplifier. . . . .	32
2.12	Close pack of four CsI(Tl) detectors. . . . .	32
2.13	Non-uniformity in the light output. Numbers are the peak position of the $\alpha$ -spectrum in terms of channel number. . . . .	33
2.14	Spectrum of $\alpha$ -particle emitted from $^{241}\text{Am}$ measured using a CsI(Tl) detector. . . . .	33
2.15	Schematic diagram for hit position generation using DSSD. Two particles are incident (as shown by two arrows) on the DSSD and their positions are defined by the corresponding front and back strips (shown in different colours). . . . .	34
2.16	Two-dimensional scattered plot of position identification threshold given in DSSD for $^{229}\text{Th}$ - $\alpha$ source. Five different blocks of energies (as shown) correspond to the five different groups of energies of the source. . . . .	35
2.17	Three-dimensional scattered plot of position identification in DSSD using the same data as in Fig. 2.16. . . . .	36
2.18	Two dimensional spectrum between $\Delta E$ , 65 $\mu\text{m}$ strip, versus $E$ , 300 $\mu\text{m}$ strip. Charged particles are emitted in the reaction 145 MeV $^{20}\text{Ne}$ on $^{12}\text{C}$ obtained by the prototype telescope. . . . .	39
2.19	Two dimensional spectrum between 300 $\mu\text{m}$ strip versus CsI(Tl) detector. Light charged particles emitted in the reaction 145MeV $^{20}\text{Ne}$ on $^{12}\text{C}$ obtained by the prototype telescope. . . . .	40
2.20	(a) $\alpha$ - $\alpha$ and (b) $d$ - $\alpha$ correlation functions plotted as a function of the relative momentum, $q$ , for the reaction $^{20}\text{Ne} + ^{12}\text{C}$ at 145 MeV. Filled circles are the experimental data and the dotted line is the background (see text). . . . .	41
2.21	Typical energy spectrum of protons in the c.m, for the reaction $^{20}\text{Ne} + ^{12}\text{C}$ . Filled circles are the experimental data and the solid line represents the fitted curve to extract the slope. . . . .	43
2.22	Same as Fig. 2.21 for $\alpha$ particles. . . . .	43
2.23	Comparison of temperatures obtained from different "thermometers". The solid line is the weighted average. . . . .	46
2.24	Particle identification spectra obtained in $^{13}\text{C} + ^{12}\text{C}$ reaction using the final telescope. . . . .	47

2.25	<i>Excitation energy of <math>^8\text{Be}</math> reconstructed from <math>2\alpha</math> coincidence in both <math>^{12}\text{C} + ^{12}\text{C}</math> (solid circle) and <math>^{13}\text{C} + ^{12}\text{C}</math> (solid triangle) reactions. Normalized cross sections along the Y-axis. . . . .</i>	48
2.26	<i>Excitation energy of <math>^{12}\text{C}</math> reconstructed from <math>3\alpha</math> coincidence in both <math>^{12}\text{C} + ^{12}\text{C}</math> (solid circle) and <math>^{13}\text{C} + ^{12}\text{C}</math> (solid triangle) reactions. Normalized cross sections along the Y-axis. . . . .</i>	49
2.27	<i>(A) Design of a telescope, and (B) photograph of the telescope with strip detectors and CsI(Tl) detectors. . . . .</i>	51
2.28	<i>Complete high resolution charged particle detector array with support structure. . . . .</i>	52
2.29	<i>Block diagram of electronics used for individual channel. . . . .</i>	52
2.30	<i>Block diagram of electronics for 24 telescopes. . . . .</i>	54
2.31	<i>Detector array with complete electronics and data acquisition system (DAQ). . . . .</i>	54
3.1	<i>K130 Variable energy cyclotron with switching magnet and various beam lines. . . . .</i>	57
3.2	<i>Layout of different beam lines of K130-cyclotron. . . . .</i>	57
3.3	<i>Experimental setup used in the experiment inside the scattering chamber of third beam line. . . . .</i>	60
3.4	<i>Schematic of the experimental setup as used in the experiment. . . . .</i>	61
3.5	<i>Block diagram of electronic setup. . . . .</i>	62
3.6	<i>Electronic setup used in the experiment. . . . .</i>	63
3.7	<i>Spectrum of <math>^{229}\text{Th}</math>-<math>\alpha</math> source in Si-strip detector. The energy calibration before experiment started is shown in black histogram and the same after experiment was over is shown in red histogram. . . . .</i>	64
3.8	<i>Calibration curve for a typical strip of <math>50\mu\text{m}</math>, <math>\Delta E</math>-detector of the backward telescope. . . . .</i>	65
3.9	<i>Calibration curve for a typical strip of <math>500\mu\text{m}</math>, E-detector. . . . .</i>	65
3.10	<i>Two-dimensional scattered plot between energy obtained in front strip (EF) versus back strip (EB) in DSSD. . . . .</i>	66
3.11	<i>Position identification in DSSD. . . . .</i>	67
3.12	<i>Two-dimensional scattered plot between <math>\Delta E - E</math> for the backward telescope strip at <math>105^\circ</math>. . . . .</i>	68

3.13	<i>The effect of energy loss correction in total energy spectrum of four <math>\alpha</math>. The total energy spectrum, where no corrections have been taken into account, only the measured sum energies of four <math>\alpha</math>'s is shown in black line and the other one (red line) is the corresponding spectrum after incorporated all energy corrections. . . . .</i>	70
3.14	<i>(a, b, c, d) Illustration of the use of different gates in filtering the data. The excitation energy of the recoiling <math>^{12}\text{C}</math> obtained from the inelastic <math>\alpha</math> has been plotted against the excitation energy reconstructed from the three decay <math>\alpha</math> particles (see text for details). . . . .</i>	73
3.15	<i>TDC time gate (see text). . . . .</i>	74
3.16	<i>Momentum conservation gate (see text). . . . .</i>	74
3.17	<i>Total energy gate (see text). . . . .</i>	75
3.18	<i>Schematic diagram of Dalitz plot. . . . .</i>	78
3.19	<i>Relative energy spectra for the Hoyle state decay three <math>\alpha</math>-particles. The histograms in (a), (b),(c) and solid circles in (d) are the experimental data (red line/solid circle) and the histograms in black color are the results of Monte Carlo calculations. . . . .</i>	80
3.20	<i>Monte Carlo simulation for different types of the Hoyle state decay; (a) SD, (b) DDE, (c) DD<math>\Phi</math>, (d) DDL (see text for details). . . . .</i>	80
3.21	<i>Experimental Dalitz plot for fully detected Hoyle events for the reaction <math>\alpha + ^{12}\text{C}</math>. . . . .</i>	81
3.22	<i>Schematic representation of the contributions of SD, DDE, DDL and DD<math>\Phi</math> processes as a function of the relative energy of <math>^8\text{Be}</math> like pairs (see text). Solid circles are experimental data and solid line (red), dotted line (red), dash line (blue), dash-dot line (green) curves are simulation results for SD, DDE, DDL and DD<math>\Phi</math>, respectively. . . . .</i>	82
3.23	<i>The distribution of root mean square energy deviation, symbols/lines are same as in Fig. 3.22. . . . .</i>	83
3.24	<i>The Dalitz plot and associated projections, <math>\rho</math> and <math>\Phi</math>, here <math>\varepsilon_i</math> denotes the normalized energy of the <math>i^{\text{th}}</math> <math>\alpha</math>-particle. . . . .</i>	84
3.25	<i>Symmetric Dalitz plots for (a) SD, (b) DDL, (c) DDE (d) DD<math>\Phi</math>. . . . .</i>	85
3.26	<i>Measured Dalitz plot distribution without any kinematic fitting. . . . .</i>	85
3.27	<i>The distribution of the radial projection of the symmetric Dalitz plot, symbols/lines are same as in Fig. 3.22. . . . .</i>	86

3.28	<i>The distribution of <math>^8\text{Be}</math> like pairs of each event of the Hoyle state decay of <math>^{12}\text{C}^*</math> (filled circle). Filled circles correspond to the experimental data and the lines correspond to various simulation results; only sequential decay (dotted line), total decay (including SD, DDE, DDL and <math>DD\Phi</math>)- best fit (red line), total decay - with 99.75 % upper confidence limit (blue dash line)(see text).</i>	87
3.29	<i>The distribution of root mean square energy deviation of the <math>\alpha</math>-particles from the Hoyle state decay events. The symbols are explained in Fig. 3.28.</i>	89
3.30	<i>The distribution of the radial projection of the symmetric Dalitz plot of each event of the Hoyle state decay in the <math>^{12}\text{C}</math> frame (filled circle). The symbols are explained in Fig. 3.28.</i>	89



# List of Tables

3.1	<i>Technical specifications of K130 cyclotron.</i>	58
3.2	<i>Comparison of different experimental estimates of direct decay modes of the Hoyle state.</i>	91



# Chapter 1

## Introduction

Nuclear physics is the branch of physics which deals with the study of fundamental properties of atomic nuclei theoretically as well as experimentally and reveals their underlying structures and reaction dynamics. The basic building blocks of the atomic nucleus are protons and neutrons, known as nucleons. The observed properties of the nucleus are in fact the reflection of the properties and the mutual interaction of these nucleons. It has been conjectured that the nucleons are inside the nucleus may also exist in the form of compact close-packed cluster of four nucleons (two-neutrons and two protons, *i.e.*,  ${}^4\text{He}$  nucleus) as a sub-unit of the nucleus. The  ${}^4\text{He}$  nucleus possesses a significantly higher binding energy compared to its nearest neighbours and its first excited state is lying at much higher excitation energy (20.2 MeV) above the ground state. These properties of  ${}^4\text{He}$  nucleus make it a candidate as a sub-unit ingredient of nuclei. Clustering, particularly in the form of  $\alpha$ -cluster, is well established both in heavy as well as light nuclei [1, 2, 3, 4].

Investigation on the structure of nuclei with  $N = Z$ , particularly even  $Z$  and  $N$  nuclei, is very interesting and important from nuclear structure as well as astrophysical points of view [5, 6, 7, 8]. The  $\alpha$ -clustering plays an important role in determining the structure of these  $N = Z$  nuclei. In 1938, Hafstad and Teller conjectured that the ground state of nuclei with  $N = Z$  could be described in terms of geometric arrangements of

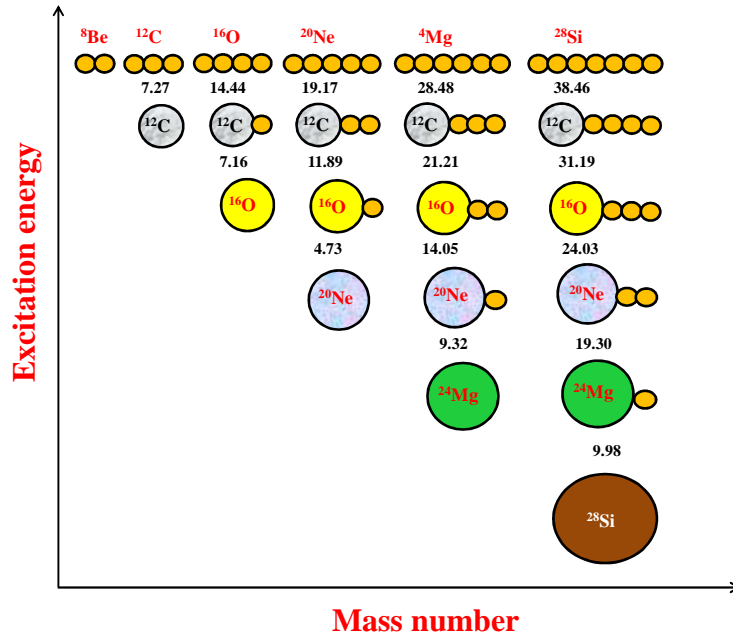


Figure 1.1: The Ikeda threshold diagram for  $N\alpha$  nuclei.

$\alpha$ -particles known as  $\alpha$ -clusters [9]. In 1960, this idea of cluster structure near the decay threshold has been developed by Ikeda and his co-workers [10]. The Ikeda diagram (as shown in Fig. 1.1) predicts widespread clustering structure, and in particular  $\alpha$ -cluster structure in nuclei for the states at energies near the cluster separation thresholds. The simplest case of two  $\alpha$ -clustered system is  ${}^8\text{Be}$ , which possesses a dumbbell like structure with axial deformation of 2:1. The nuclei  ${}^{12}\text{C}$ ,  ${}^{16}\text{O}$  and  ${}^{20}\text{Ne}$  are well known examples of three, four and five  $\alpha$ -clustered nuclei, respectively. These nuclei are unstable against breakup into its particular clusters at excitation energy close to the corresponding particle decay thresholds. Each of the threshold value for the decay into the corresponding cluster nucleus is mentioned in Fig. 1.1. Most of the states are particle unbound above this threshold. So, studying these particle/cluster decays, one can extract valuable information about the structure of these nuclei, which are believed to play vital role in understanding several stellar processes.

In recent years, the study of cluster states using resonance particle spectroscopy with special emphasis on the structure of second  $0^+$  excited state of  $^{12}\text{C}$  at 7.65 MeV, known as the famous Hoyle state, has evoked a lot of interest, as the state is believed to play a key role in the synthesis of  $^{12}\text{C}$  and the other heavy elements in the Universe [11]. Aim of the present thesis is to study the Hoyle state, particularly its decay mechanism, using high precision, high resolution, kinematically complete measurement of the decay products.

## 1.1 The Hoyle state

Synthesis of  $^{12}\text{C}$  and other heavy chemical elements are quite essential for the existence of life and everything on Earth. The formation of  $^{12}\text{C}$  is the main key behind the synthesis of all heavy elements that proceed through  $^{12}\text{C}$ . But carbon itself would not have existed in sufficient amount to form life, if there did not exist one excited state in proper position (just above the particle decay threshold) in  $^{12}\text{C}$ . This unusual excited state is the second excited state of  $^{12}\text{C}$ , which is the famous Hoyle state. Though quite a few attempts have been made in the past to understand the nature of the Hoyle state, the study of the structure of this state is still a subject of great interest in recent time. The  $^{12}\text{C}$  isotope of carbon is the most abundance among its available stable isotopes and is the fourth most abundant on earth. Although  $^{12}\text{C}$  is one of the most well studied nucleus, surprisingly many aspects about the excited states of the nucleus are still unknown. In the following section we will discuss how the Hoyle state plays a crucial role in the formation of elements found in the Universe, commonly termed as nucleosynthesis process.

### 1.1.1 Role of the Hoyle state in nucleosynthesis

All elements, that we observe in the solar system or in Universe, are believed to be formed through multi-step fusion process generally termed as nucleosynthesis. The

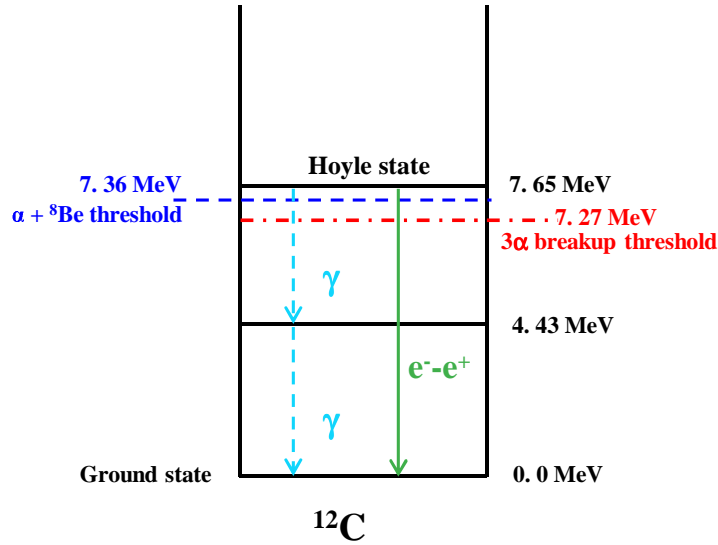


**Figure 1.2:** Schematic view of level diagram of  $^{12}\text{C}$ . The Hoyle state is produced through fusion of triple- $\alpha$  process. Ground state of  $^{12}\text{C}$  is produced through the decay of the Hoyle state (7.65 MeV) by cascade  $\gamma$ -decay or by internal pair production.

nucleosynthesis first initiated during ‘Big Bang’ is called primordial nucleosynthesis, which lasted for a few minutes ( $\sim 3$  minutes) after the ‘Big Bang’, till the temperature fell below the temperature necessary for fusion. This initial ‘Big Bang’ has been responsible for the creation of most of the mass of the Universe as we see today, predominantly in the form of hydrogen and helium. Synthesis of heavier elements (carbon and beyond) is believed to have taken place later in the heart of stars formed by hydrogen and helium through a number of nuclear reactions, termed as stellar nucleosynthesis process. In stars like Sun, the main process of energy production is ‘hydrogen burning’ through proton-proton (pp) chain reaction, by which protons fuse to form nuclei upto helium. The cores of these stars are comprised mainly of helium, and Bethe [12] conjectured that no significant amount of any element heavier than helium can be produced by stellar thermonuclear reactions due to the lack of stable nuclear isotopes with mass numbers 5 and 8. So, the question arises; how the elements like  $^{12}\text{C}$  and  $^{16}\text{O}$  were formed. To circumvent this problem, it was first proposed independently by Estonian-Irish astronomer E. J. Öpik [13] and an Austrian theoretician, E. E. Salpeter [14] that the synthesis of carbon might have taken place through a successive  $3\alpha$  cap-

ture process, since the direct formation is inhibited by the negligible probability that three  $\alpha$ -particles simultaneously collide and fuse in the stellar medium. In this successive  $3\alpha$  capture process, two  $\alpha$ -particles in the first step fuse to form the unstable  ${}^8\text{Be}$ . As the decay life time of  ${}^8\text{Be}$  is approximately few orders of magnitude longer than the interaction time between the two  $\alpha$ -particles, there will be build up of only a small concentration of  ${}^8\text{Be}$  in equilibrium with  $\alpha$  particles (one ground state  ${}^8\text{Be}$  nucleus for every  $10^9$   $\alpha$ 's). In second step, it ( ${}^8\text{Be}$ ) then combines with the third  $\alpha$ -particle by a non-resonant process to form  ${}^{12}\text{C}$  as



Since the density of  ${}^8\text{Be}$  in the stellar plasma is very low, because of its short lifetime of  $\sim 10^{-16}$  s, this non-resonant process was considered to be slow enough to explain the observed abundance of carbon. Energetically, the  ${}^{12}\text{C}$  produced in this way will be unbound, as its excitation energy ( $E_x$ ) will be above the  $3\alpha$  decay threshold. In order to explain this mystery, in 1953, the British astronomer Fred Hoyle suggested that this small probability of  $\alpha$ -capture by short lived  ${}^8\text{Be}$  would be greatly enhanced if the carbon nucleus had an energy level close to the combined energies of the reacting  ${}^8\text{Be}$  and  $\alpha$  nuclei [15]. Then, the reaction would be a faster ‘resonant’ reaction to explain the observed abundance of  ${}^{12}\text{C}$  in Universe. With the new hypothesized resonance the carbon yield would increase by a factor of about  $10^7$  to  $10^8$  compared to the non resonant process given by Öpik and Salpeter [13, 14]. The existence of such a  $0_2^+$  state at  $E_x \sim 7.654$  MeV, known as the Hoyle state, was experimentally confirmed soon afterwards [16], and its properties were established on the basis of a measurement of  $\alpha$ -particles emitted in the  $\beta$ -decay of  ${}^{12}\text{B}$  [17]. This triggered vigorous theoretical and experimental activities in the next few decades, as the Hoyle state is considered to hold the key to understand a variety of problems of nuclear astrophysics like elemental abundance in the Universe as well as the stellar nucleosynthesis process as a whole [18]. The energy level diagram of  ${}^{12}\text{C}$  is shown in Fig. 1.2. The formation of stable

carbon takes place only through the radiative transition to the ground state, *i.e.*, either through cascade gamma transitions or through invisible gamma ( $e^- - e^+$ ) transition (as shown in Fig. 1.2). After the formation of  $^{12}\text{C}$  through triple  $\alpha$  fusion, the reaction  $^{12}\text{C}(\alpha, \gamma)^{16}\text{O}$  would convert part of the  $^{12}\text{C}$  into  $^{16}\text{O}$ . The rate of conversion highly depends on the relative rates of these two reactions [triple  $\alpha$  fusion and the  $^{12}\text{C}(\alpha, \gamma)^{16}\text{O}$  reactions]. The subsequent evolution of star greatly depends on the ratio of  $^{12}\text{C}$  and  $^{16}\text{O}$ , which in turn depend on the rate of triple  $\alpha$  reaction and the  $^{12}\text{C}(\alpha, \gamma)^{16}\text{O}$  reaction. The location of the energy level of the Hoyle state in  $^{12}\text{C}$  is exactly at the required position for the production of  $^{12}\text{C}$  in Universe and consequently for formation of carbon-based life in earth [19]. If the energy level of the Hoyle state would be little bit higher, essentially all  $^{12}\text{C}$  would be converted into  $^{16}\text{O}$ , on the opposite, if the energy level would be little bit lower, then the stars start  $^{12}\text{C}$  burning early, so no  $^{16}\text{O}$  could be created [20]. Nature's fine tuning of the energy level of the Hoyle state at appropriate position with right properties, the location of the resonant level of the Hoyle state is such that the level of  $^{16}\text{O}$  at 7.1187 MeV is non-resonant, slightly less than the combined masses of  $^{12}\text{C}$  and the  $\alpha$  particle. This ensures that a significant fraction of the  $^{12}\text{C}$  created will not be destroyed by  $\alpha$  capture. Any small change in position of the energy level (within 100 keV) of the Hoyle state, it is impossible or very difficult to form the carbon as well as the other heavy elements [20].

### 1.1.2 Present status on structure of the Hoyle state

The prediction of the 7.65 MeV resonance, the second excited state of  $^{12}\text{C}$ , by Fred Hoyle was a remarkable inference from astrophysics to nuclear structure point of view and it had a dramatic effect on the subsequent development of stellar nucleosynthesis and other branches of astrophysics. The existence of the Hoyle state has been predicted and experimentally observed six decades ago, but nevertheless the structure of the state is still not known properly. The structure of the Hoyle state is a matter of great interest and is a longstanding problem in nuclear physics, which has received

much theoretical attention recently, like, lattice effective field theory [21, 22], no-core shell model [23, 24], fermionic molecular dynamics [25] and  $\alpha$ -cluster models [26, 27]. The present status of experimental as well as theoretical studies on the Hoyle state has recently been well described in a review by Freer *et.al.* [11]. From the nuclear structure point of view, the Hoyle state presents many unique features which are yet to be understood properly. The Hoyle state cannot be described easily by any known models of atomic nuclei. The standard shell-model approaches as well as *ab-initio* calculation using no-core shell model (NCSM1) failed to reproduce the state [23]; however, recent calculations within no core shell model framework with no effective limitation on the number of harmonic oscillators in the model space (NCSM2) have been able to demonstrate the existence of low lying cluster structures in  $^{12}\text{C}$  (the second  $0_2^+$  state, known as the Hoyle state and its excited  $2_2^+$  state) [24]. The *ab-initio* calculation using lattice chiral effective field theory (LEFT) has been able to identify a resonance in  $^{12}\text{C}$  having the characteristics of the Hoyle state [21]. Besides, this state has long been considered as a classic example of  $\alpha$ -cluster nuclear states in light nuclei [25, 26, 27] as well as a candidate for exotic  $3\alpha$  linear chain configuration [26, 28]. Recently, it has been demonstrated from first principle that the structure of the Hoyle state is almost like a linear chain arrangement of three  $\alpha$  [22]; however, more recently it has been claimed experimentally that the structure of the state is like a triangular structure with  $\alpha$ -particles in three vertices of the triangle [29]. As this state is also known to possess a relatively large radius compared to that in the ground state [30, 31], it was further conjectured that the  $\alpha$ -clusters in the Hoyle state may remain in quasi-free gas like state [32, 33]. Considering the bosonic nature of  $\alpha$ -particles and the fact that the initial states of all three  $\alpha$ -particles, as well as the final (Hoyle) state are in the same ( $0^+$ ) state, it was tempting to speculate that the state may be interpreted in terms of a nuclear Bose-Einstein condensate (BEC) [34, 35, 36]. However, recent fermionic molecular dynamics (FMD) calculations have indicated that the  $\alpha$ -cluster structure of the Hoyle state was mostly resembling  $^8\text{Be}$  plus  $\alpha$  configuration [25], which has been verified in the observed sequential nature of its decay [37]. The predominance of this

correlated ( ${}^8\text{Be} + \alpha$ ) structure, as well as the prediction that antisymmetrisation is not negligible [25], do not go well with the naive BEC scenario. Regarding the shape of the Hoyle state also, there is discrepancy between various model predictions [38]; whereas FMD predicts a oblate equilateral triangle shape and LEFT predicts a bent arm chain (obtuse triangular) structure, deformed prolate shape, BEC model predicts the Hoyle state to be spherically symmetric. Moreover, the rms radii of the Hoyle state, predicted by the above models, are also different from each other [38]. However, it is likely that the above-mentioned unusual structure of this state may modify the decay mode of  ${}^{12}\text{C}$ , thereby affecting the reaction rate of  ${}^{12}\text{C}$  as well as that of other heavy elements [39, 40].

In nucleosynthesis reaction rate calculations, it is implicitly assumed that the decay of the Hoyle state proceeds exclusively via a sequential two-step process, i.e, via the ground state of  ${}^8\text{Be}$  [41]. Deviations from the two step process have been predicted to modify the relative abundance of  ${}^{12}\text{C}$ , and thereby affect the future evolution of stars in the Universe [42, 43, 44]. So, it is crucial to determine the quantitative contributions of all direct processes other than sequential decay to get a clear picture of the Hoyle state decay.

### 1.1.3 The triple $\alpha$ reaction rate

The triple  $\alpha$  reaction, *i.e.* the fusion of three  $\alpha$  to form  ${}^{12}\text{C}$  nucleus, plays an important role in the stellar nucleosynthesis. It is the main process behind the synthesis of carbon in star which bridged the mass gaps (mass  $A = 5$  and  $A = 8$  nuclei) and allowed nucleosynthesis to proceed further. It is the main mechanism by which early generation of stars evolved from the hydrogen and helium formed after the Big Bang. Furthermore, this triple- $\alpha$  reaction plays an important catalytic role in various explosive burning phases of star in which the stellar temperature exceeds  $2 \times 10^9$  K. At low temperatures below  $10^8$  K, triple- $\alpha$  process no longer proceed via sequential process (through  ${}^8\text{Be}$ ) because of too small thermal energy, where the reactions pro-

ceed directly via other three body mechanism. The rate of the triple- $\alpha$  reaction at low temperature is also very important for evolution of the first generation of stars (see for more discussion in [45]). The triple- $\alpha$  reaction is fully dominated by the s-wave resonances in the intermediate temperature range (from  $T = 10^8$  K to  $T = 10^9$  K) at which stellar helium burning takes place and is fully determined by the properties of the Hoyle state, which one can measure experimentally. For this reason the reaction rate is known rather accurately even though it cannot be measured directly in the laboratory. Currently, the rate is known with 10% precision, but efforts are underway to reduce this to 5% [46]. The reaction rate calculations are far more complicated in low and high temperature domains. At high temperature domain ( $> 10^9$  K) contributions of several other high lying states of  $^{12}\text{C}$  take place which are not well established. This is specially true for the excited state of the Hoyle state, which has been experimentally observed recently [38, 47, 48]. In the low temperature region ( $< 10^8$  K) sophisticated three body models are necessary to calculate the rate [49]. The astrophysical reaction rate ( $R$ ) calculations are based on the assumption that triple- $\alpha$  capture process proceeds exclusively via the sequential two-step process ( $\alpha + \alpha \rightarrow {}^8\text{Be}$ ;  ${}^8\text{Be} + \alpha \rightarrow {}^{12}\text{C}^*$ ), which may be expressed as,

$$R \propto T^{-\frac{3}{2}} \frac{\Gamma_{\alpha 0} \Gamma_{rad}}{\Gamma} \exp\left(-\frac{E}{kT}\right), \quad (1.3)$$

where,  $E$  is the energy of the Hoyle state relative to the  $3\alpha$  decay threshold,  $T$  is the temperature,  $\Gamma (= \Gamma_{\alpha} + \Gamma_{rad})$ ,  $\Gamma_{\alpha}$ ,  $\Gamma_{rad}$  correspond to total, total- $\alpha$  decay and total radiative decay widths of the Hoyle state, respectively. Total radiative decay width ( $\Gamma_{rad}$ ) is the combined electromagnetic widths for the decay of the excited state to the  $^{12}\text{C}$  ground state via sequential  $\gamma$  emission ( $\Gamma_{\gamma}$ ) and internal pair conversion ( $\Gamma_{\pi}$ ). Total- $\alpha$  decay width is  $\Gamma_{\alpha} = \Gamma_{\alpha 0} + \Gamma_{3\alpha}$ , where,  $\Gamma_{\alpha 0}$  and  $\Gamma_{3\alpha}$  are the partial decay widths for sequential ( ${}^{12}\text{C}^* \rightarrow {}^8\text{Be} + \alpha \rightarrow \alpha + \alpha + \alpha$ ) and direct ( ${}^{12}\text{C}^* \rightarrow \alpha + \alpha + \alpha$ ) decays, respectively.

In the above description of the reaction rate calculation, there is an implicit assumption that the total  $\alpha$  decay width is from sequential decay only, *i.e.*,  $\Gamma_{\alpha} = \Gamma_{\alpha 0}$ . Now, we know that  $\Gamma_{rad} \ll \Gamma_{\alpha}$  ( $\frac{\Gamma_{rad}}{\Gamma_{\alpha}} = 4.12(11) \times 10^{-4}$ ) [50]; therefore,  $\Gamma \simeq \Gamma_{\alpha} \equiv \Gamma_{\alpha 0}$ , if

there is no direct decay. Under this condition the expression for reaction rate becomes,

$$R \equiv R_{seq} \propto T^{-\frac{3}{2}} \Gamma_{rad} \exp\left(-\frac{E}{kT}\right). \quad (1.4)$$

showing that the rate depends on two components only,  $E$  and  $\Gamma_{rad}$ . The latter is very important from astrophysics and is determined from the measurement of three quantities

$$\Gamma_{rad} = \Gamma_{\pi} + \Gamma_{\gamma} = \frac{\Gamma_{\pi} + \Gamma_{\gamma}}{\Gamma} \frac{\Gamma}{\Gamma_{\pi}} \Gamma_{\pi} \quad (1.5)$$

The current recommended [11] values are

$$E = 379.38 \pm 0.20 \text{ keV} \quad (1.6)$$

$$\frac{\Gamma_{\pi} + \Gamma_{\gamma}}{\Gamma} = (4.03 \pm 0.10) \times 10^{-4} \quad (1.7)$$

$$\frac{\Gamma_{\pi}}{\Gamma} = (6.7 \pm 0.6) \times 10^{-6} \quad (1.8)$$

$$\Gamma_{\pi} = 62.0 \pm 2.0 \text{ } \mu\text{eV} \quad (1.9)$$

However, if  $\Gamma_{3\alpha} \neq 0$ , then  $\Gamma_{\alpha 0}/\Gamma < 1$ , and therefore,  $R \equiv R_{seq+dir} < R_{seq}$ . Calculations indicate that even minor change of the process (from sequential to direct) may modify the triple- $\alpha$  capture rate [41], and thus the relative abundance of  $^{12}\text{C}$ , which, in turn, would affect the stellar evolution process [43]. Hence, precise quantitative measurements of all direct processes (deviation from sequential) in the Hoyle state decay is crucially important from nuclear structure as well as astrophysics points of view. So, identification and quantification of these decay modes are crucial to probe deeply into the structure of the Hoyle state. Presently, there are three direct decay modes, *i.e.*, decay in linear chain (DDL), decay into equal energies (DDE), and direct decay in phase space (DD $\Phi$ ), which correspond to linear  $3\alpha$  chain, Bose-Einstein condensate of  $3\alpha$  particles, and dilute Bose gas structures, respectively, have been identified. The DDL decay mode corresponds to the breaking of  $3\alpha$  linear chain, where two  $\alpha$ -particles on two sides will move with equal and opposite velocities, whereas the one at the centre will remain static. The DDE decay mode is intended to focus on the BEC-type decay;

in this case the three  $\alpha$ -particles will have equal energies (decay from same condensed state); finally, the  $DD\Phi$  type decay, where the kinetic energies of the  $\alpha$ -particles will uniformly fill up the available phase space, corresponds to the gas-like configuration of the Hoyle state. In the present thesis, it has been planned to estimate the contributions of different decay mechanisms of the Hoyle state through precision, high statistics measurements.

## 1.2 Motivation

The existence of non-sequential decay component of the Hoyle state implies a modification in the reaction rate calculation for carbon formation inside star, which in turn directly affects the formation of heavier elements and also the future generation of star in the Universe. From nuclear structure point of view too, the Hoyle state is unique on several aspects as discussed earlier. So, precise measurement of different components of decay mechanism is very crucial from nuclear structure as well as astrophysical, points of view. In recent years, quite a few experiments have been performed to investigate and quantify the roles of various decay modes *i.e.* sequential decay (SD) and direct  $3\alpha$  decay (DD) of the Hoyle state. In addition, attempts have also been made to identify and differentiate among various types of direct decays, such as decay into equal energies, decay in linear chain and direct decay in phase space, and quantify their contributions, which are supposed to throw new lights on the exotic structure of the Hoyle state. First experimental estimation of direct  $3\alpha$  decay of the Hoyle state was made by Freer *et al.* [37], who, using Dalitz plot and its projection in terms of  ${}^8\text{Be}$  like pairs, estimated an upper limit of 4% on direct  $3\alpha$  decay in phase space branches bypassing the ground state of  ${}^8\text{Be}$ . In a recent work, Raduta *et al.* [51] identified two direct decay branches, DDE and DDL, with a combined branching percentage of 17(5) %, and argued that the DDE branch corresponds to the signature of  $\alpha$  condensate structure. If this is correct, the equation 1.3 implies  $\sim 17$  (5) % reduction in the reaction rate calculation in the temperature range of triple alpha fusion

( $10^8 - 10^9$  K). This reduction in the reaction rate is larger than the current estimate of uncertainty on it and the consequences would be far more dramatically change in the low temperature ( $< 10^8$  K) region; this is a serious issue that needs to be verified by independent, precise, higher statistics experiment. More recently, J. Manfredi *et al.* [52] have estimated, using optimisations of the distribution of  $^8\text{Be}$  like pairs as well as the distribution of root mean square energy deviation, the upper limit for contributions of  $\text{DD}\Phi$  and  $\text{DDE}$  to be 3.9 % and 0.45 %, respectively, with a upper confidence limit of 99.75 %. In another recent work, Kirsebom *et al.* [53] have estimated, using the optimisation of symmetric Dalitz plot and its radial projection, the upper limits for  $\text{DDE}$ ,  $\text{DDL}$  and  $\text{DD}\Phi$  components to be 0.09%, 0.09% and 0.5%, respectively, at 95% confidence limit. This is a complete kinematic experiment  $^{11}\text{B}(^3\text{He},\text{d})3\alpha$  and total of 5,000 events of the Hoyle state has been analysed to study the decay structure of the Hoyle state. It has been found from the above discussion that there is a discrepancy among various measurements. However, all measurements except that of Raduta *et al.* [51] indicate that the direct decay modes are very small fractions (upper limit  $\sim 5$  % or less); therefore, exclusive experiments with higher statistics of Hoyle events (HE) are needed to verify and cross check the recent experimental results and to reach a consensus on this issue. This is important because, apart from crucial astrophysical significance (triple  $\alpha$  reaction rate and consequently the abundance of carbon), various  $\text{DD}$  modes, though small, are considered to be manifestations of new and exotic structures (linear chain, nuclear Bose-Einstein condensate, etc.) which are special for the Hoyle state.

High resolution, high granularity, large solid angle coverage detector array is an essential tool for precise and complete kinematical experiments of the kind discussed above. Moreover, such an array is extremely useful for detailed charged particle spectroscopy experiments in medium (Fermi) energy domain. In order to perform such high resolution, high multiplicity kinematically complete experiments, an array of Si-strip detector telescope has been developed. The details of the high resolution charged particle detector array will be discussed in the next chapter. Hence, the main motiva-

tion behind the present thesis is to develop a highly granular, high resolution charged particle detector array and use the whole or part of the array elements to study the Hoyle state of  $^{12}\text{C}$  by a complete kinematics measurement of its decay. The thesis mainly consists of two parts. First part (Chapter 2) is devoted to the development and testing of high resolution charged particle detector array and its software analysis tools for physics extraction. The second part (Chapter 3) is devoted to the study of the decay mechanism of particle unstable states of  $^{12}\text{C}$  (the Hoyle state decay in particular with high statistics) in inelastic scattering of  $\alpha$  on  $^{12}\text{C}$  target at 60 MeV.



# Chapter 2

## Development of high resolution charged particle detector array

### 2.1 Introduction

The experimental study of nucleus-nucleus collision is essential to probe the properties of nuclei at extreme conditions of spin and temperature. Such study provides information about the reaction dynamics and the thermal properties of the nuclei under extreme condition, which includes the complete spectrum of mechanisms ranging from the compound nucleus formation, deep inelastic collision, projectile breakup to multi fragmentation of the colliding particles, depending on the collision energy. In order to disentangle these complex mechanisms or processes, simultaneous detection of all or as many as possible reaction products is very much essential. In the case of energetic heavy-ion collision, it is well known that multi detector arrays are very essential and important tools to investigate the dynamical properties of the reaction process. However, in the case of low energy ( $E \leq 10$  MeV/A) nucleus-nucleus collision, the interaction between the projectile and the target is dominated by mean field and the exit channel is mostly binary in nature. Therefore, one can extract the thermal or the

dynamical information of the reaction by detecting any one of the reaction product with the help of small number detectors. However, larger array of detectors is always desirable for more effective utilisation of beam time. At higher beam energy, *i.e.* for more energetic nuclear collisions ( $E \geq 30\text{-}40$  MeV/A), the reaction dynamics changes from mean field dominated regime to individual nucleon-nucleon collision. The transition is indicated by gradual change in observed reaction processes also; for example, mean field process like binary fission is gradually replaced by multi fragmentation; non-central, peripheral reactions like binary dissipative collisions change over to projectile fragmentation. In order to study these processes around the Fermi energy ( $\sim 37$  MeV/nucleon) domain, one needs powerful experimental equipments (detector arrays) for detecting as many of the reaction products as possible with best possible energy and spatial resolutions. The detector array should be designed in such a way that it should have large angular coverage with high granularity, capability of isotopic as well as mass identification of the fragments, and, as low as possible detection threshold.

The design consideration of the detector array in different energy regime is different and it also depends upon the physics motivation. For example, at low projectile energy, there is less kinematic focusing, array elements may be uniform in size and should cover a large solid angle in the laboratory. On the other hand, at high projectile energy, because of the strong kinematical focusing, it is required that the detector array should be high granular in forward hemisphere, as it covers the major part of the total ( $4\pi$ ) solid angle subtended at the center of mass. Several such large detector arrays in different laboratory around the world are currently in operation [54]. For example, INDRA [55], is a  $4\pi$  detector array which has been extensively used for multi-fragmentation study. It mostly consists of ionisation chamber plus Si- CsI(Tl) telescopes and covered 90 % of  $4\pi$ . The array CHIMERA [56], is also a large  $4\pi$  charged particle detector array, made up of Si-CsI(Tl) telescopes with time of flight measurement. Large Area Silicon Strip Array (LASSA) [57] is another auxiliary detector array made up of nine high resolution telescopes, each telescope consisting of one  $65 \mu\text{m}$  single sided Si-strip detector, one  $500\text{-}1500 \mu\text{m}$  double sided Si-strip detec-

tor backed by four CsI(Tl) detectors of thickness 4-6 cm. The High Resolution Array (HiRA) [58], at National Superconducting Cyclotron Laboratory (NSCL), MSU, is a large solid-angle array of silicon strip-detectors that has been developed for the study of variety of nuclear structure, nuclear astrophysics and nuclear reaction experiments using heavy ion beam. It consists of 20 telescopes, each of which is constructed from a 65  $\mu\text{m}$  Si-strip detector, 1.5 mm Si-strip detector and four CsI(Tl) detectors. The 65  $\mu\text{m}$  Si-strip detector is single sided (32 strips on the junction (front) side only, while the 1.5 mm detector is segmented into 32 strips per side in front and back, mutually orthogonal to each other. Individual active surface areas of Si-strip detector is of 64 mm x 64 mm.

A  $4\pi$  charged particle detector array (CPDA) facility is being developed at Variable Energy Cyclotron Centre (VECC), Kolkata, for nuclear physics experiment using the upcoming K500 superconducting cyclotron. Motivation behind the development of the array is to study the properties of the hot nuclei produced in energetic heavy ion collision at around Fermi energy domain. The K500 superconducting cyclotron at VECC will provide energetic ion beams (typically, 10 - 80 MeV/A for  $A_{proj} < 100$  and 5 - 20 MeV/A for heaviest ions) for nuclear physics research. So the array being developed should be capable to detect all types of emitted charged particles ranging from light charged particles to fragments upto  $Z \approx 40$ . Depending upon the kinematics, relative yield of different kinds of particles will vary at different angular region around the beam direction. So, the requirement of detectors are different in different angular range, which in turn depends upon the type and energy of the reaction products. Based on these considerations, it was decided that the  $4\pi$  CPDA would consist of three different arrays, (i) forward array (angular coverage  $\theta \sim 7^\circ$  to  $45^\circ$ ), (ii) backward array (angular coverage  $\theta \sim 45^\circ$  to  $175^\circ$ ) and (iii) extreme forward array (angular coverage  $\theta \sim 3^\circ$  to  $7^\circ$ ). A schematic view of the charged particle detector array being developed at VECC is displayed in Fig. 2.1. The backward array of CPDA will consists of only CsI(Tl) detectors of varying dimensions (thickness  $\sim 2 - 4$  cm). This part of the array will be kept at 15 cm from the target in backward direction and has been designed in

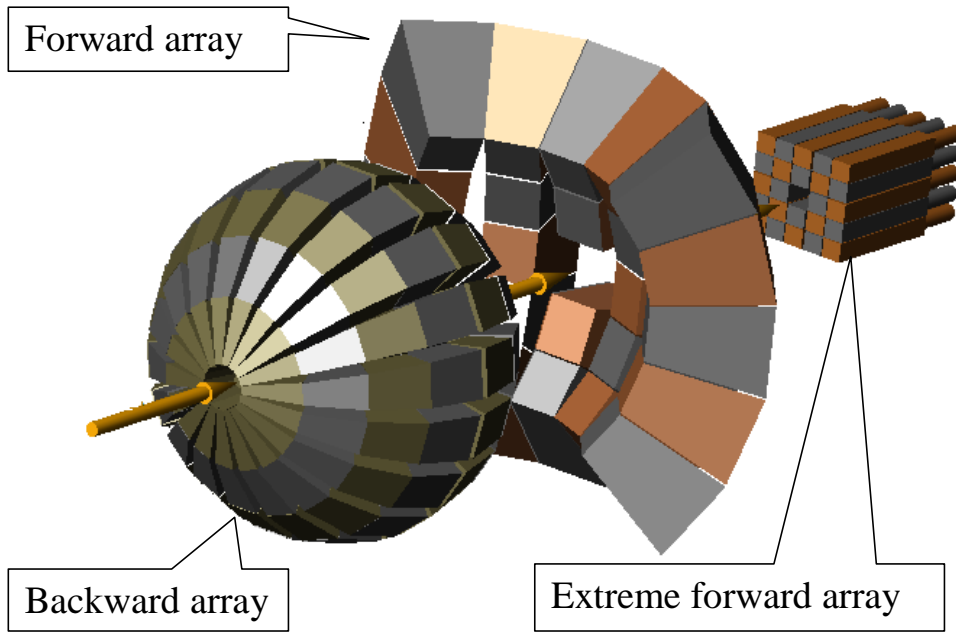


*Figure 2.1: Schematic view of the full  $4\pi$  charged particle detector array.*

such a fashion that the detectors after complete assembly will form a spherical surface of radius 15 cm. The extreme forward array will be made up of 32 plastic phoswitch detectors (each will consist of a combination of one fast and one slow plastic scintillators). This part of the array will be kept at 40 cm from the target in forward direction and the face of the detector would form a wall. Development of the forward array, the high resolution Si(strip) - Si(strip) - CsI(Tl) charged particle detector array, contributes a part of the present thesis; therefore, the design and fabrication of forward part of the array has been described in details.

In the following sections the development of the high resolution forward array will be described. The design and simulation of the array as well as performance test of prototype elements will be described in section 2.2. The event identification and reconstruction techniques will be described in section 2.3 and in-beam performance test of the array elements will be given in section 2.4. Finally, the mechanical design and fabrication of whole mechanical structure of the array and the installation of detectors with complete electronics will be described in section 2.5.

## 2.2 Design and simulation of the high resolution charged particle detector array

Study of thermodynamical properties of nuclei requires precise information about the yields of charge as well as mass identified fragments emitted in the reaction. Due to wide variety of fragment type and energy, we need to build detectors that can simultaneously identify both heavy fragments as well as light charged particles and measure their energies over a wide angular range. To optimise the design of the high resolution array, detailed Monte Carlo simulation has been performed, which is described below. From the simulation study, it has been found that the emission of complex fragments is restricted to forward hemisphere only due to Lorentz boost. At these energies,  $45^\circ$  in the laboratory system typically covered  $> 90^\circ$  in center of mass. Therefore, the forward array was designed to cover the angular range of  $7^\circ$  to  $45^\circ$ , as most of the intermediate mass fragments are likely to be emitted within this zone. It has also been observed that multiple hit probability are less at 20 cm from the target at this energy. It is needed to identify all these fragments in charge as well as mass (as far as possible). Therefore, the detector array should have good energy resolution, high granularity, low detection threshold and capability of good elemental as well as isotopic identification.

Monte Carlo simulation has been carried out to study the response of the high resolution array. Typical simulation using the phenomenological event generator HIPSE (heavy ion phase space exploration) [59] for the reactions  $^{40}\text{Ca} + ^{40}\text{Ca}$  and  $^{40}\text{Ca} + ^{197}\text{Au}$  (50 MeV/nucleon) have been studied (each reaction of 1 million events) [60, 61]. The events are macroscopic/microscopic representations of heavy ion collisions at energies around Fermi energy. The events span all possible impact parameters, maximum of touching radius of projectile and target, *i.e.*, from central collision (higher multiplicity events) to elastic scattering (lower multiplicity events) events. The light charged particle (LCP) multiplicity events detected within the active geometrical acceptance of the high resolution array in percentage for different LCP multiplicities in the mother events of  $^{40}\text{Ca} + ^{40}\text{Ca}$  at 50 MeV/A are shown in Fig. 2.2. The inset of Fig. 2.2 shows mother

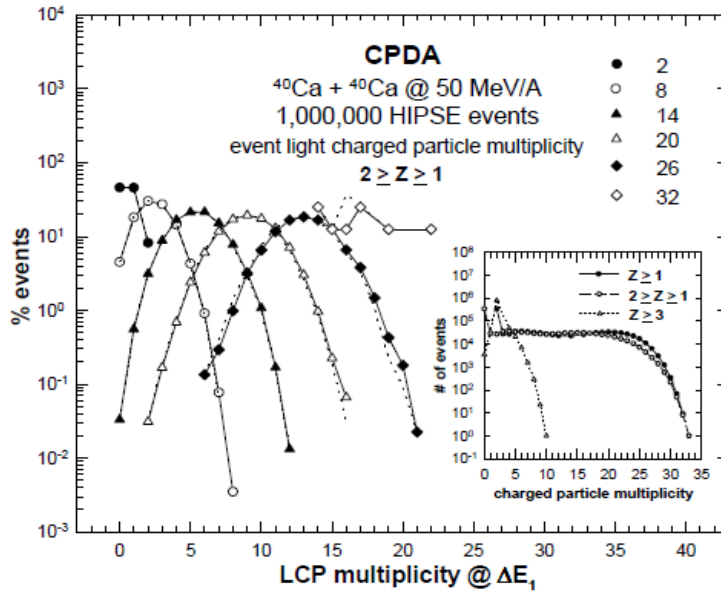


**Figure 2.2:** The detected LCP multiplicity events in percentage (mother event LCP multiplicities of 2, 8, 14, 20, 26, 32) for  $^{40}\text{Ca} + ^{40}\text{Ca}$  reaction at 50 MeV/A. The solid lines are guides to the eyes while the dotted lines are reduced multiplicities. The inset shows distribution of 1 million HIPSE events with lines as guides to the eyes.

event distribution for the reaction. The hollow circles/triangles imply multiplicities of LCP ( $1 \leq Z \leq 2$ )/fragments ( $Z \geq 3$ ) while the solid circles are multiplicities of all charged particles ( $Z \geq 1$ ). The fragment multiplicities are quite low and fall sharply while the majority are LCP. If the event LCP multiplicity is 26 (solid diamond), the most probable detected multiplicity is 13 and such events are about 18% of all LCP multiplicity 26 events. For  $^{40}\text{Ca} + ^{197}\text{Au}$  the corresponding values are 4 and 22%. The dotted lines in Fig. 2.2 are reduced multiplicities due to multiple hits on same strips of the thin ( $\Delta E$ ) detector of the telescopes. The multiple hit probability in different detector elements of the telescope are shown in Fig. 2.3. The total charged particle multiplicity 26 events contain about 78% charged particles (Fig. 2.3a) and 22% neutrons (Fig. 2.3b) in an event. About 40% of the charged particles impinge on  $\Delta E$  (Fig. 2.3c), most of which are LCP in this case. The charged particle multiple hit probability (for multiplicity 26 events) is about 0.7% at  $\Delta E$  (Fig. 2.3d), 0.05% at  $\Delta E/E$  (Fig. 2.3e)

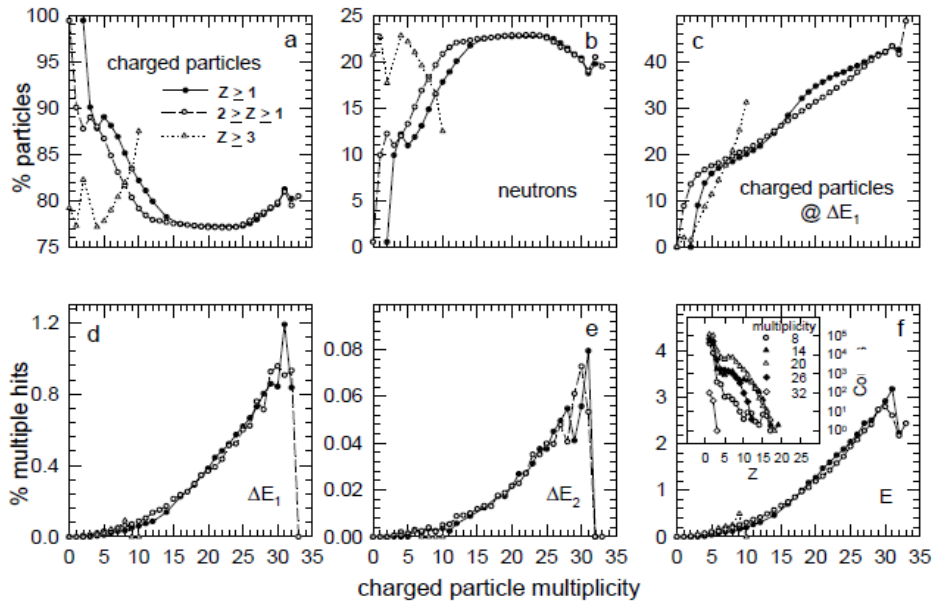


**Figure 2.3:** The percentage of particles (a,b,c) and multiple hits (d,e,f) for  $^{40}\text{Ca} + ^{40}\text{Ca}$  reaction at different detector elements of the telescope of array. The solid (open) circles correspond to multiplicity events for all (light) charged particles while open triangles are fragments other than LCP. The lines are the guides to the eyes. The inset in (f) shows the type of particles with atomic number  $Z$  at CsI(Tl) detectors of the array.

and 2% at CsI(Tl) (Fig. 2.3f) for  $^{40}\text{Ca} + ^{40}\text{Ca}$  reaction and 0.04% at  $\Delta E$ , 0.002% at  $\Delta E/E$  and 0.1% at CsI(Tl) for  $^{40}\text{Ca} + ^{197}\text{Au}$  reaction.

The forward array has been designed and constructed to fulfill the above requirements. It consists of 24 identical telescopes. Each telescope consists of three elements [Si(strip)  $\Delta E$ , Si(strip)  $E/\Delta E$ , 4 CsI(Tl) detectors] and has an active area of  $50 \times 50 \text{ mm}^2$ . The complete mechanical structure of this 24 telescope array is such that, after complete assembly, the detector faces will form a surface of a sphere of radius 20 cm. The schematic diagram for the arrangement of 24 telescopes is shown in Fig. 2.4. In the next section, the details of different elements of the telescope have been described.

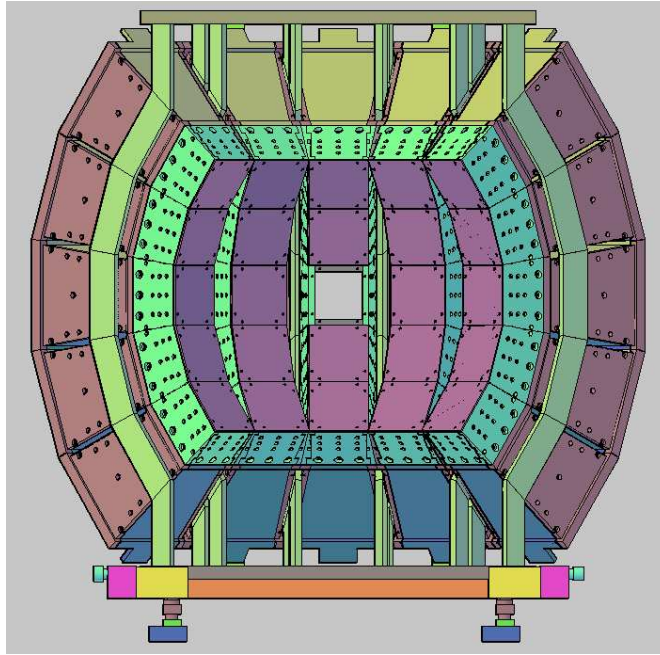


**Figure 2.4:** The schematic design and arrangement of high resolution Si-strips-CsI(Tl) detector array.

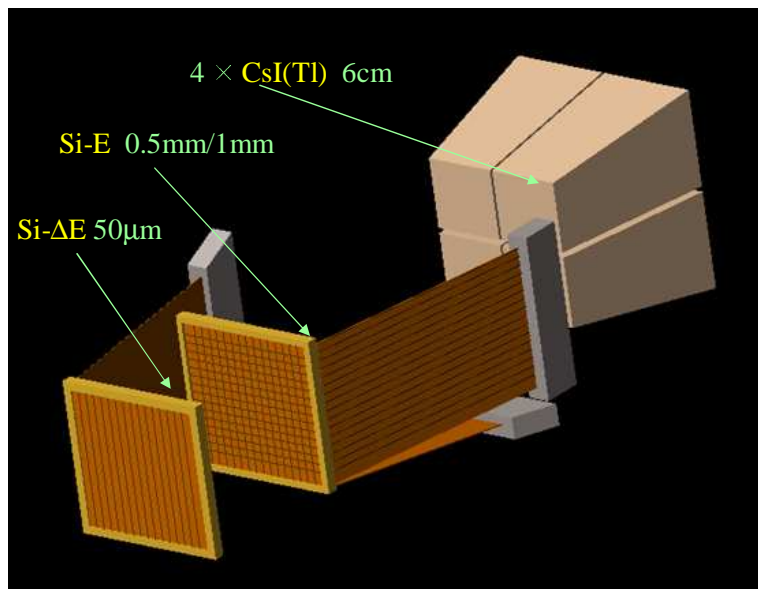


**Figure 2.5:** The schematic view of different elements of a telescope.

## 2.2.1 Design of individual telescope

A schematic configuration of the telescope used in the forward array is shown in Fig. 2.5. In order to detect light charged particles as well as heavy fragments emitted in the reaction, each telescope is composed of a ( $\Delta E$ ) Single-sided Silicon Strip Detector (SSSD) of  $\sim 50 \mu\text{m}$  thickness, ( $\Delta E/E$ ) Double-sided Silicon Strip Detectors (DSSD) of  $\sim 500/1000 \mu\text{m}$  thickness and four  $\sim 6 \text{ cm}$  thickness CsI(Tl) detectors (E) (four crystal because to have fast response and to make the telescope more granular). First-second layers ( $\sim 50 \mu\text{m}$  and  $\sim 500/1000 \mu\text{m}$  Si-strips) are for heavy fragments and second-third layers ( $\sim 500/1000 \mu\text{m}$  Si-strip and CsI(Tl) detectors) are for light particles detection. The thicknesses were chosen to have good isotopic identification for the fragments with ( $Z < 10$ ) produced in low and intermediate energy heavy-ion reactions. In addition to good isotopic resolution, it will also provide a low energy threshold for particle identification. The detailed design and characteristics of each element are described in next few subsections.

## 2.2.2 Silicon Detectors

Silicon detector is very powerful device for detecting charged particles produced in energetic nucleus-nucleus collisions. Advantage of this detector is that it has a very good energy resolution with linear response over a wide range of energy. Because of the availability of large area silicon wafer, one can use single detector as a multi-detector by segmenting the contacts of the main detector volume into different section called strips. With this, one can achieve good position resolution and the corresponding detectors are referred as silicon strip detectors. Although silicon detectors are very good for charged particle detection, they have few drawbacks. These are very fragile (particularly the thinner ones) and are prone to radiation damage. The Silicon strip detectors (SSSD and DSSD) used in the present array are ion-implanted, passivated

devices obtained from M/s. Micron Semiconductors Ltd., UK [62] details of which will be described as below.

### 2.2.2.1 Single-sided Silicon Strip Detector (SSSD)

The first element of the telescope has been chosen as  $\sim 50 \mu\text{m}$  SSSD, so as to have low energy threshold for highly ionizing particles; the threshold for  $\alpha \sim 2 \text{ MeV/A}$ , and that for  $^{40}\text{Ca}$  is  $\sim 5.5 \text{ MeV/A}$ . It is made up of a single silicon wafer having an active surface area of  $50 \times 50 \text{ mm}^2$ . It consists of 16 vertical strips in front side (each of dimension  $50 \text{ mm} \times 3 \text{ mm}$  and in between two consecutive strips  $50 \text{ mm} \times 0.13 \text{ mm}$  separation gap) which are read out individually and back side is grounded. This detector is used as transmission type ( $\Delta E$ ) detector in telescopic mode. Typical full depletion voltage (FD) for these detectors ranges from 4 V to 8 V, and can be operated up to 2FD; total leakage current at 2FD is  $\sim 20 \text{ nA}$  (typical) at  $25^\circ\text{C}$  with max. leakage current  $100 \text{ nA}$ . The intrinsic resolution of the SSSD is  $< 70 \text{ keV}$  (specified) for  $5 \text{ MeV}$   $\alpha$  - particle.

### 2.2.2.2 Double-sided Silicon Strip Detector (DSSD)

This detector is also made up of a single silicon wafer and has an active surface area of  $50 \times 50 \text{ mm}^2$ . Each detector consists of 16 strips (each  $50 \text{ mm} \times 3 \text{ mm}$ ) per side in mutually orthogonal directions (front side vertical and back side horizontal). Front and back strips together form  $16 \times 16 = 256$  pixels, each of active area of  $3 \times 3 \text{ mm}^2$ . The position of the detected particle is assigned to the middle point of the pixel, which basically leads to an uncertainty of  $1.5 \text{ mm}$  in each one of the two dimensions. Two different thicknesses of DSSD, one  $\sim 500 \mu\text{m}$  and another  $\sim 1000 \mu\text{m}$  have been used in two different angular zones. The  $1000 \mu\text{m}$  detector have been used in the more forward angles (inner nine telescopes), because fragments in this zone have more energy. The thickness of these detectors have been chosen to stop upto  $\sim 42 \text{ MeV/A}$   $^{40}\text{Ca}$ . Full depletion voltages (FD) for these detectors are typically 30 - 35 V for  $500 \mu\text{m}$  and 120

- 130 V for 1000  $\mu\text{m}$ . The 500  $\mu\text{m}$  DSSD can be operated up to 2FD; total leakage current at 2FD V is 300 nA (typical at 25  $^{\circ}\text{C}$ ) with max. leakage current 1  $\mu\text{A}$ . The 1000  $\mu\text{m}$  DSSD can be operated up to FD + 30 V; total leakage current at FD + 30 V is  $\sim$  600 nA (at 25 $^{\circ}\text{C}$ ) with max. leakage current is 3  $\mu\text{A}$ . The intrinsic resolution of the DSSD, for 500  $\mu\text{m}$ , it is < 30 keV (specified) and for 1000  $\mu\text{m}$ , it is < 25 keV for 5 MeV  $\alpha$ -particle.

### 2.2.2.3 Design of the detector frame

The frames and the readout cables with connectors have been specifically designed by optimizing physical strength and dead area. The design of all Si-strip detectors has been performed in close association with the manufacturer, M/s. Micron Semiconductors Ltd., UK [62]. As the silicon strip detectors are very fragile, the holding frame of the silicon wafer should be strong enough. On the other hand, the close-packed design of the telescopes in the array require the minimum dead area (frame size) surrounding each Si wafer. The commercially available detector frame did not allow close packing of the telescope. Hence, by optimizing fragility and compactness, a new frame (as shown in Fig. 2.6) has been designed for the present array. The frame is made from glass epoxy with total outer dimension 60 mm  $\times$  60 mm [Fig. 2.6(a), (c)]. There is a slot of width 1.75 mm and depth 2.25 mm in the inner (top) sides of the frame [Fig. 2.6(c)]. These were kept to glue the silicon wafer and also to protect the wafer from other detector when the detectors will be placed in the telescopic mode. The outer ridge has four through holes, one in each corner which may be used to align the frame by dowel pins. Two slots are there in side 4 [Fig. 2.6(a), (d)], one in the top side of depth 1.5 mm and other on the outer side of depth 1 mm to placed the front side kapton. Top side depth has been kept 1.5 mm to ensure that wire bonding of the front side strip will be safely positioned and the outer side slot is to pass the kapton of  $\Delta\text{E}$  Si-strip detector through in between E detectors's frame and housing wall. In side 3, a slot of depth 3.25 mm and width of 4 mm is there in rear and inner side to keep the

kapton connected to backside strip. Three holes (M2) are there in each side which may be used to fix the detector with the housing. The frame of the SSSD detector is exactly same as DSSD. Only difference is, no kapton is there in side 3 and the outer side depth (side 4) is 0.5 mm.

Signals from the strips are taken out by cables made of kapton, a flexible polyimide as shown in Fig. 2.7. At the detector end, the kapton is bent perpendicular to the detector frame which helps to put the detectors in compact shape when they are used as a telescope with other detector. At this end 18 soft gold pads are there with each electrical tracking to connect with the strips using wire bonding of 3 aluminium wires each of  $\sim 25 \mu\text{m}$  thickness. At the other end of the cable, there is female flat ribbon connector (FRC) (SAMTEC SSQ-22-G-D-RA) with  $2 \times 10$  connectors with spacing 2.54 mm (0.1") through a printed circuit board. Out of these 20 connectors, 16 in the middle are connected to 16 strips in each side. Two are connected to the guard ring (G/R). Rest two have no connections in DSSD and connected with the back side (grounded) in SSSD as shown in Fig. 2.7.

Both types of detectors are made of bulk n-type silicon with  $p^+$  implantation to form a junction near the front. A G/R is there in the front side only. Further, onto the strips a  $\sim 0.20 \mu\text{m}$  aluminium layer is evaporated for conducting the signal. Total dead layer in the DSSD detector is  $\sim 0.6 \mu\text{m}$  including the implantation depth of about  $\sim 0.40 \mu\text{m}$ . It is very important to take this into account during the analysis, since different particle will loose different amount of energy in the dead layer.

#### 2.2.2.4 Characterisation of silicon strip detectors

After physical checking, the strip detectors have been tested offline using  $\alpha$ -source. First, the detector characteristics were checked using a  $^{241}\text{Am}$   $\alpha$ -source. Energy resolution of individual strip has been measured for both thin/thick Si-strip detectors and found to be  $< 70/40$  keV for 5.486 MeV  $\alpha$ -particles as shown in Fig. 2.8. Thickness variation along a strip of the detector, particularly in  $50 \mu\text{m}$  SSSD's, which are very





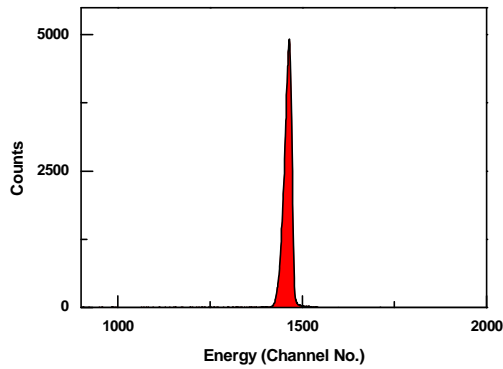


**Figure 2.8:** The energy spectrum of  $\alpha$ -particles emitted from  $^{241}\text{Am}$  source for a particular strip.

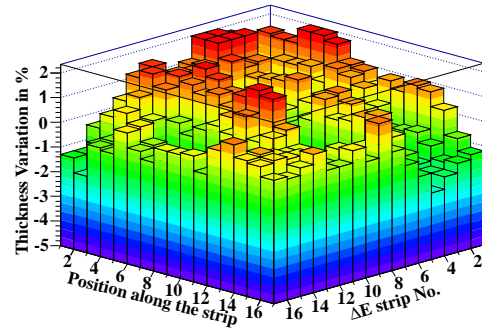


**Figure 2.9:** Non-uniformity in thickness along the strip in 16 different positions of all strips of  $50\ \mu\text{m}$  SSSD.

prone to thickness non-uniformity, will result in poor isotopic identification. So, it is very crucial to measure the thickness non-uniformity, particularly for thin detectors. Typical thickness non-uniformity of a thin ( $50\ \mu\text{m}$  SSSD) detector has been estimated using in-beam test and shown in Fig. 2.9. It has been found that the variation of thickness along a strip is within our acceptance limit (found to be  $< 3\%$ ).

### 2.2.3 CsI(Tl) detector

Thallium activated cesium iodide [CsI(Tl)] is used widely to detect energetic charged particles because of its high stopping power for charged particles and cost effectiveness. The crystal is easily machinable to give required shape, less hygroscopic than NaI(Tl), has very good performance at room temperature, and produces light in a frequency range which is well detectable by the available photodiodes or photomultiplier tubes. CsI(Tl) is used as a charged particle detector in two ways; (I) as a stop (E) detector in  $\Delta E$ -E telescopic mode, or, (II) as a single detector using its particle discrimination property to detect light charged particles. In the present array of the telescopes, CsI(Tl) is used as a stop (E) detector for the energetic particles.

### 2.2.3.1 Design of CsI(Tl) detector

All the custom made CsI(Tl) detectors have been procured from M/s. Scionix Holland Bv, The Netherland [63], as a complete assembly of CsI(Tl) crystal and photo diode with an integrated low noise charge sensitive preamplifier. Final design of the detectors have been done in association with the manufacturer. As per design of the array of the telescopes, the front face of the first strip detector will form the part of a sphere of radius of  $\sim 20$  cm. Accordingly, the shape of the CsI(Tl) crystal has been designed so as to ensure close pack geometry of the telescope; in addition, detectors have been slightly wedge shaped to ensure that the particle incident obliquely also get stopped in the crystal. The design of the typical detector is shown in Fig. 2.10(A); front and back faces are square shaped of dimension  $2.5 \text{ cm} \times 2.5 \text{ cm}$ , and  $3.5 \text{ cm} \times 3.5 \text{ cm}$ , respectively. The thickness of the detector is 6 cm, which can stop proton with energy upto  $\sim 140 \text{ MeV}$  and  $^{16}\text{O}$  with energy  $\sim 330 \text{ MeV/A}$ . A stack of four such detectors has been used as final stopping detector in the third layer of the telescope. The segmentation helps in improving the multi-hit probability and better energy resolution of CsI(Tl) detector. Further reduction in size of the crystal for the CsI(Tl) detector of the telescope would certainly be best for granularity but the effective cost would also increase proportionally; so we have restricted it to four detectors. The assembly of four of such CsI(Tl) will form a truncated pyramid with base area of  $7 \text{ cm} \times 7 \text{ cm}$  and front face will have same area as the active area ( $5 \text{ cm} \times 5 \text{ cm}$ ) of the strip detectors as shown in Fig. 2.10(B). Each crystal is wrapped on all sides except the front face in a special reflecting material covered with aluminized mylar of thickness  $\sim 50 \mu\text{m}$  and the front face ( $2.5 \text{ cm} \times 2.5 \text{ cm}$ ) is covered with a  $\sim 1 - 2 \mu\text{m}$  micron thick aluminized Mylar, which acts as entrance window. All these have been done to prevent scintillation light leaking through the crystal sides. Each crystal is coupled with a photodiode of active area  $18 \text{ mm} \times 18 \text{ mm}$  (Hamamatsu S3204-08). The total dimension of the photo diode is  $25.5 \text{ mm} \times 25.5 \text{ mm}$  with thickness  $2.54 \pm 0.2 \text{ mm}$  and it is coupled with crystal by special optical cement. The maximum reverse bias voltage that can be applied to photodiode is 100 V and the corresponding power dissipation is  $\sim 100 \text{ mW}$ . It can be

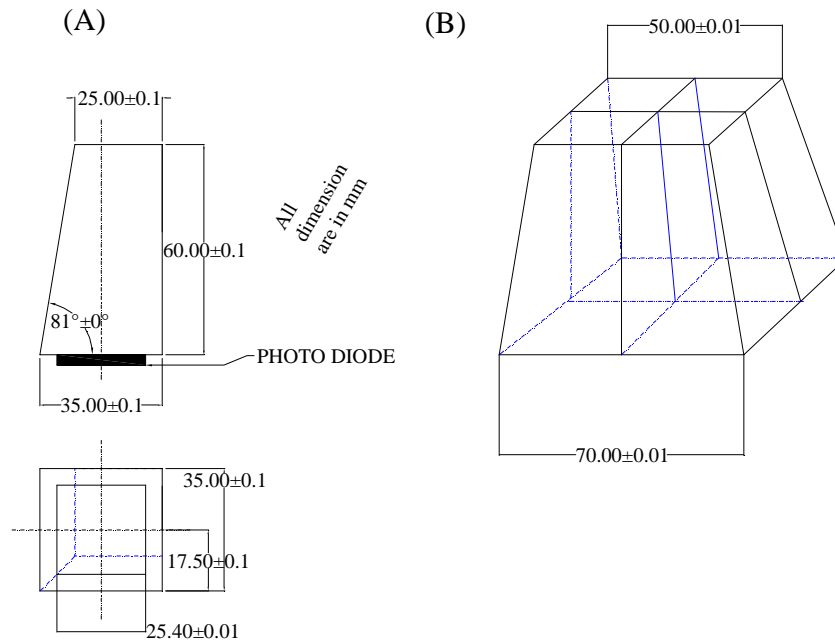


**Figure 2.10:** (A) Design of one CsI(Tl) detector and (B) assembly of four CsI(Tl) crystals as used in the telescope.

operated in the temperature range  $-20^{\circ}$  to  $60^{\circ}$  C. The spectral response is 321 - 1100 nm whereas the photo peak of CsI(Tl) is 550 nm. A charge sensitive preamplifier with gain of  $\sim 5$  mV/MeV is directly coupled with the crystal. The power dissipation in the preamplifier is 50 mW and it can be operated in vacuum. Single detector with complete assembly (photo diode and charged sensitive preamplifier) is shown in Fig. 2.11 and stack of four such detector are shown in Fig. 2.12

### 2.2.3.2 Characterisation of CsI(Tl) detector

The detail characterisation of all CsI(Tl) detectors have been carried out using  $^{241}\text{Am}$   $\alpha$ -source. Standard electronics have been used for testing purpose. The energy resolutions of all CsI(Tl) detectors are found to be less than 5 % at 5.486 MeV  $\alpha$  energy. Depending upon the uniformity of the thallium doping and the geometry of the detector, there may be some spatial non-uniformity in the light output of CsI(Tl) crystal. To measure the non-uniformity, a specially designed pin  $\alpha$ -source,  $^{241}\text{Am}$

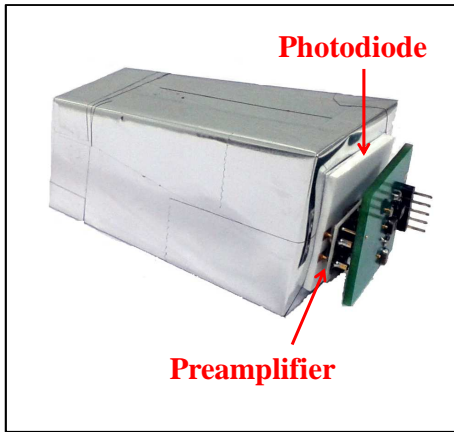


**Figure 2.11:** Single CsI(Tl) detector with photodiode and pre-amplifier.

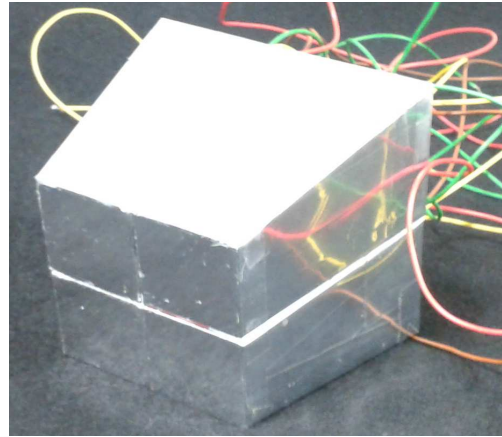


**Figure 2.12:** Close pack of four CsI(Tl) detectors.

(5.486 MeV) has been put at different position of the front face of the detector. The source was collimated (diameter 1 mm & length 5 mm) and kept very close (2 mm) to the detector to irradiate the detector in a very small area (circle of diameter 1.4 mm) in a particular position. Fig. 2.13 represents the results of the spatial non uniformity of response test for the front face (area 25 mm  $\times$  25 mm) of a typical CsI(Tl) detector. The number in each segment is the peak positions of the  $\alpha$ -spectra in terms of ADC channel number when the source has been kept within that segment during the test. With respect to the mean peak position (776), the variation is  $\sim \pm 0.49\%$  which is less than the specified value ( $< 1\%$ ). Total of 96 CsI(Tl) detectors for 24 telescopes have been procured. All detectors have been characterised in the same way as mentioned above.

## 2.3 Development of event reconstruction technique

In this section the general features of the data analysis tools that have been developed will be discussed. For the analysis, the standard analysis platform (ROOT) has been used. The whole analysis process for such an array involving multiple detector is quite complex and is generally executed in several steps; the major steps being

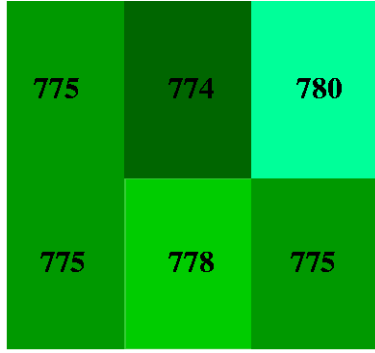


**Figure 2.13:** Non-uniformity in the light output. Numbers are the peak position of the  $\alpha$ -spectrum in terms of channel number.

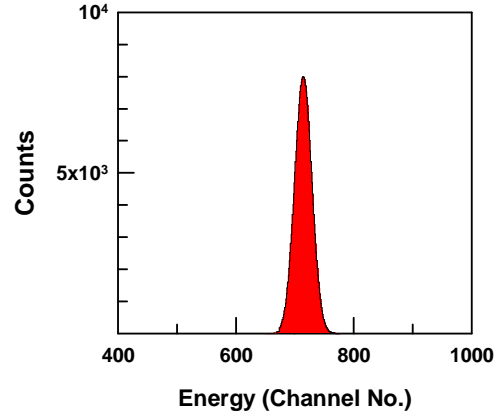


**Figure 2.14:** Spectrum of  $\alpha$ -particle emitted from  $^{241}\text{Am}$  measured using a CsI(Tl) detector.

sampling/selection of events of interest, reconstruction of the selected events to extract complete information about the ejectiles, comparison with the simulation data, etc. The data reduction algorithm has been developed in ROOT platform to extract the details of the detected particle in each event [angular position ( $\theta$ ,  $\Phi$ ), energy, types of particle, number of coincidence particles, etc.]. The main building blocks of the present analysis package are described in different sub-sections below.

### 2.3.1 Event selection

First step of the data reduction technique is to identify valid events. The programme identifies all valid events by selecting those events above a pre-set experimental threshold (depending upon the noise in the experiment) and then stores all these events with full information. In the second step, energy calibration of each channel of the telescope is done. The angular positions ( $\theta$ ,  $\Phi$ ) of the emitted particles have been defined by the corresponding positions identified in the DSSD detector of the telescopes. The position identification technique in DSSD has been described below.

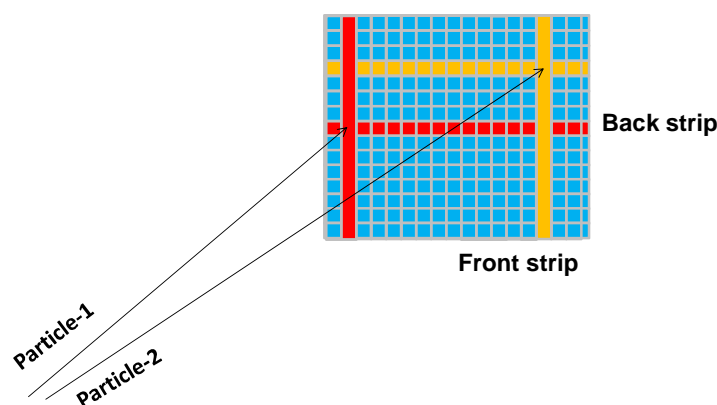


**Figure 2.15:** Schematic diagram for hit position generation using DSSD. Two particles are incident (as shown by two arrows) on the DSSD and their positions are defined by the corresponding front and back strips (shown in different colours).

### 2.3.2 Position identification in DSSD

The position identification in DSSD detector is very complicated and very challenging for high multiplicity events as we will see for the present experiment in next chapter. For single particle incident on the detector, it is very simple to identify the position as only one front and one back strip will have the signal; hence their intersection defines the position of the particle. For more than one particle hits in one event, identification problem starts showing up, multiple (more than one) front and back strips are likely to fire, as shown in Fig. 2.15. The identification of the hit position requires matching the front strip signals with the corresponding back one. To identify X-Y positions (front and back strip number, respectively) for the particles incident on the strip detector, an algorithm has been developed in ROOT platform. The Program works in event-by-event mode. For each event, first it reads data for all elements of the detector; then for each case, it checks for valid hit (signal is above preset threshold as stated before) and then stores all valid hits in the form of a 2-dimensional (X-Y) array. In the next stage, by comparing the energy (or channel number) difference between each forward (X) - backward (Y) pair, the program identifies all genuine X-Y pairs corresponding to the particles that hit the detector. The result is illustrated in Fig. 2.16,

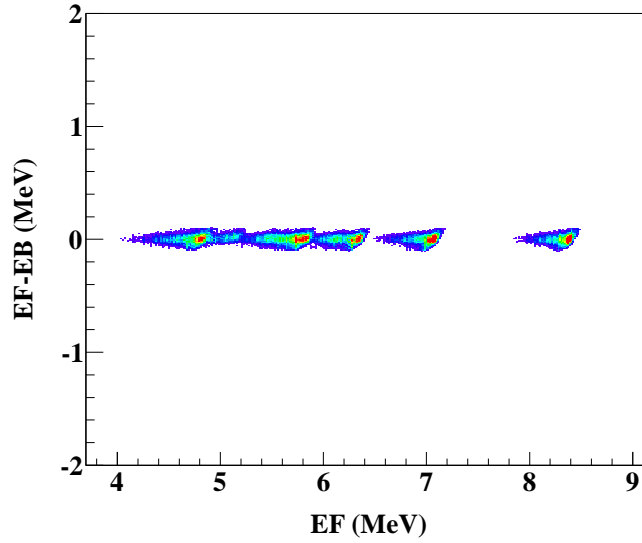


**Figure 2.16:** Two-dimensional scattered plot of position identification threshold given in DSSD for  $^{229}\text{Th}$ - $\alpha$  source. Five different blocks of energies (as shown) correspond to the five different groups of energies of the source.

where EF, EB correspond to the energies registered in X and Y strips. Genuine event is defined by the condition  $\text{EF}-\text{EB}=0$  (within experimental uncertainties). So from this program front and back strip numbers of each particle can be determined, which define the position of the particle. Though it looks simple, but in reality it is very difficult and more complex to extract positions for the coincident particles of nearly same energy. For multiple-hits, it has been observed that for a single particle there will be multiple positions within the experimental uncertainty (in EF-EB). So a minimization routine has been used to get the expected position of different particles. Using  $^{229}\text{Th}$ - $\alpha$ -source at a certain distance from the DSSD, position has been determined using the position identification algorithm as shown in Fig. 2.17. After the position (X, Y) identification in DSSD, the corresponding position has been converted into the angular position ( $\theta$ ,  $\Phi$ ) using the perpendicular distance from the point of origin (0, 0) (experimental origin point is the target position) and each strip width (3 mm).

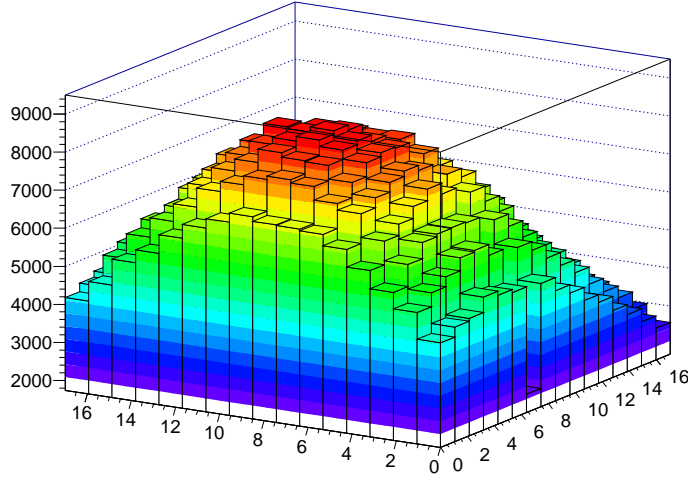


**Figure 2.17:** Three-dimensional scattered plot of position identification in DSSD using the same data as in Fig. 2.16.

### 2.3.3 Particle Identification by $\Delta E - E$ method

After position identification in DSSD, event selection has been performed (multi-particle coincidence or single particle events). In the next step, particle identification in the telescope was done by  $\Delta E - E$  method as described below.

The energy loss of charged particle passing through matter is given by Bethe Bloch formula [64]

$$-\frac{dE}{dx} = \frac{4\pi e^4 z^2}{m_0 v^2} NB \quad (2.1)$$

where

$$B = Z \left[ \ln \frac{2m_0 v^2}{I} - \ln \left( 1 - \frac{v^2}{c^2} \right) - \frac{v^2}{c^2} \right] \quad (2.2)$$

$E(= \frac{1}{2}Mv^2)$ ,  $v$ ,  $ze$ ,  $M$  are the energy, velocity, charge and mass of the incident particle and  $N$ ,  $Z$  are the number density and atomic number of the absorber (here detector material) and  $m_0$ ,  $e$  are the mass, charge of electron, respectively. The parameter,  $I$ , represents the average excitation and ionization potential of the absorber and normally treated as an experimentally determined parameter for each element. For non-relativistic particle ( $v \ll c$ ), the second and third terms of  $B$  are negligibly small and

whole  $B$  varies very slowly with the energy of the incident particle. So, the equation 2.1 reduces to

$$-\frac{dE}{dx} \propto \frac{Mz^2}{E} \quad (2.3)$$

In the case of a detector telescope which consists of one thin detector followed by a thick detector, the energy loss of the particle in this thin detector ( $\Delta E$ ) is usually small compared to the total energy ( $E$ ). Under such condition, equation 2.3 becomes

$$\Delta E \cdot E = f(A, z) \quad (2.4)$$

which is the equation of a rectangular hyperbola. From the equation, it has been seen that the particles of different mass or charge generate different rectangular hyperbola in the scatter plot of  $\Delta E$ - $E$ . After the particle identification, the program will store, event wise, all the information needed for physics extraction.

Another program package, as a part of the event reconstruction technique, has been developed in ROOT platform to study the resonance particle spectroscopy of different particle unbound states using multi-particle in coincidence from this type of array. It uses many body kinematics for reconstruction of source excitation energy spectrum from the detected multi-particles in coincidence and identification the different particle unbound states of the corresponding source. The excitation energy,  $E_x$ , of source has been reconstructed from the detected multi-particles (n-particle) in coincidence using the equation given by

$$E_x = \sum_{i=1}^n E_i - \frac{(P_1 + P_2 + P_3 + \dots + P_n)^2}{2M_{source}} + E_{th} \quad (2.5)$$

where, 'n' is the number of particle detected in coincidence,  $E_i$  and  $P_i$  for  $i=1, 2, 3, \dots, n$  are the energy and momentum of the n-particles in laboratory, respectively,  $M_{source}$  is the mass of the source, and  $E_{th}$  is the multi-particle breakup threshold. The use of the above event reconstruction technique will be discussed in the performance test of prototype telescope in next section.

## 2.4 In beam performance test of a prototype telescope

Main motivation behind the development of the array was to study the thermodynamical properties (*i.e.*, temperature, specific heat, etc.) of the hot nucleus produced in intermediate energy nuclear collisions. The measurement of temperature is crucial to characterise the equation of state of finite nuclear matter and to look for possible phase transition in the system. Since several methods such as slope thermometry, excited state thermometry and double-isotope thermometry, are being widely used to determine the temperature of the hot nucleus, it was decided that a prototype telescope should be developed first to measure the temperature in different ways using in-beam experiments. The in-beam test will also help in testing other characteristics of the prototype detectors and readout electronics, *i.e.*, energy resolution, noise, etc. At the same time, analysis software packages will also get tested in course of the data analysis.

The prototype telescope has been designed for testing before final procurement of all the telescope elements. It was developed from the standard Si-strip detectors as available in catalogue of M/s Micron semiconductor Pvt. Ltd., UK [62] and also the standard CsI(Tl) detectors from the manufacturer M/s Scionix Holland Bv, The Netherland [63]. The telescope consisted of a  $65 \mu\text{m}$   $\Delta\text{E}$  single-sided silicon strip detector (SSSD),  $300 \mu\text{m}$   $\text{E}/\Delta\text{E}$  double-sided silicon strip detector (DSSD) and backed by four CsI(Tl) crystals (thickness  $\sim 4 \text{ cm}$  and area  $2 \text{ cm} \times 2 \text{ cm}$ ). In beam test of telescope has been performed as described below.

### 2.4.1 Experimental details

The experiment has been performed at the Variable Energy Cyclotron Centre, Kolkata, India, using  $145 \text{ MeV } ^{20}\text{Ne}$  beam on a  $^{12}\text{C}$  target (self supported, thickness  $\sim 550 \mu\text{g}/\text{cm}^2$ ). Different fragments have been detected using the prototype 3-element telescope. The telescope was placed at a distance  $20 \text{ cm}$  from the target. The angular range in the laboratory covered by the telescope was from  $27^\circ$  to  $40^\circ$ . Typical angular

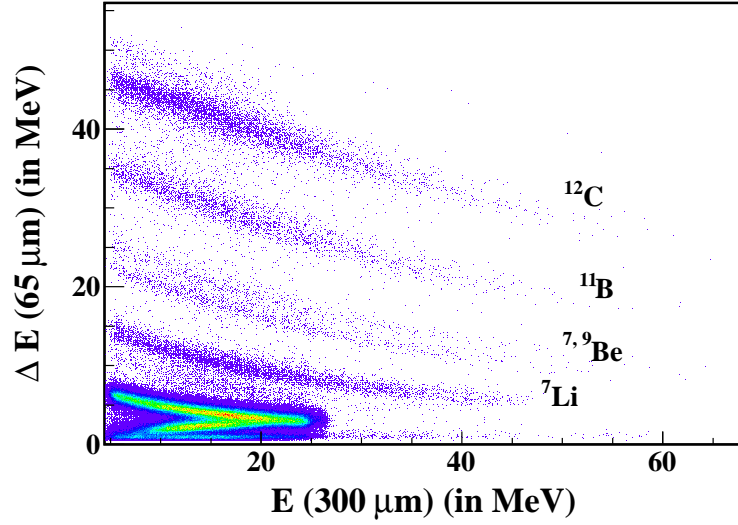


**Figure 2.18:** Two dimensional spectrum between  $\Delta E$ , 65  $\mu\text{m}$  strip, versus  $E$ , 300  $\mu\text{m}$  strip. Charged particles are emitted in the reaction 145 MeV  $^{20}\text{Ne}$  on  $^{12}\text{C}$  obtained by the prototype telescope.

resolution of each Strip is  $\pm 0.4^\circ$ . All Strips and the CsI(Tl) detectors were read out individually using standard readout electronics. A VME-based online data acquisition system, indigenously developed at VECC, was used for collection of data on event-by-event basis. The silicon detectors were calibrated using elastically-scattered  $^{20}\text{Ne}$  ion from  $^{197}\text{Au}$  target, a precision pulser and a  $^{229}\text{Th}$   $\alpha$ -source. Energy calibrations of the CsI(Tl) detectors were done using the two-dimensional spectra between the 300  $\mu\text{m}$  Si-Strip and the CsI(Tl) detectors [57]. Event reconstruction from the hit patterns in orthogonal directions of the DSSD provided two-dimensional position information of the detected particle. Typical two dimensional spectra obtained in this experiment have been shown in Fig. 2.18 and Fig. 2.19. Good isotopic distribution have been obtained for  $Z = 1$  and  $Z = 2$  particles as shown in Fig. 2.19. In this case  $\Delta E$  detector has a poor resolution ( $> 2\%$  (110 keV) in 5 MeV  $\alpha$ ), hence isotopic identification of different fragments could not be obtained as shown in Fig. 2.18.

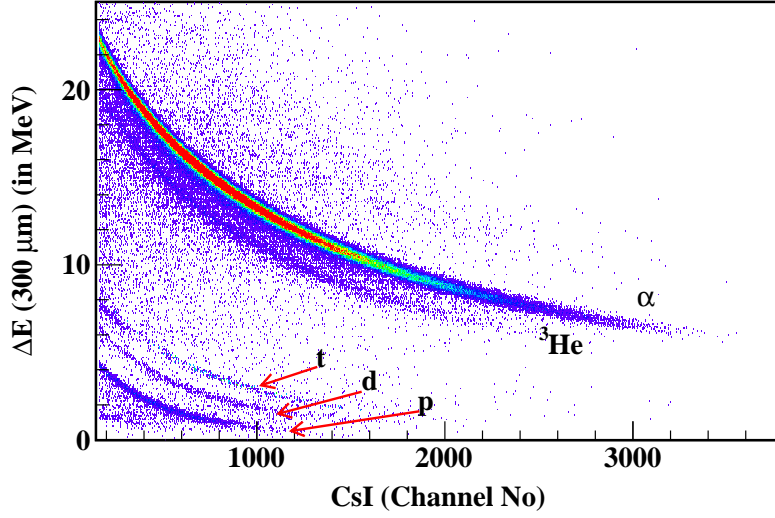


**Figure 2.19:** Two dimensional spectrum between 300  $\mu\text{m}$  strip versus CsI(Tl) detector. Light charged particles emitted in the reaction  $145\text{MeV } ^{20}\text{Ne}$  on  $^{12}\text{C}$  obtained by the prototype telescope.

## 2.4.2 Performance Testing of event reconstruction technique

Event reconstruction technique code has been tested in this experiment to obtain information about the particle unstable state by identifying the coincidence events. Different two particle coincidences ( $\alpha$ - $\alpha$  and  $d$ - $\alpha$ ) have been measured and the reconstructed particle-particle correlation spectra from the relative momentum distribution for different particle unstable states as described below. The two particle angle-averaged correlation function [65, 66],  $1 + R(q)$ , is defined experimentally by the following equation:

$$\sum Y_{12}(p_1, p_2) = C_{12}[1 + R(q)] \sum Y_1(p_1)Y_2(p_2) \quad (2.6)$$

where  $p_1, p_2$  are the laboratory momenta of the coincident pair of particles with masses  $m_1$  and  $m_2$ ,  $q (= \mu |(\frac{p_2}{m_2} - \frac{p_1}{m_1})|)$  is the relative momentum of the correlated pair and  $C_{12}$  is a normalization constant which is determined by the requirement that  $R(q) = 0$  for large  $q$ . The sum on both sides of equation 2.6 are taken over all detectors and particle energy combinations satisfying a specific gating condition.  $Y_1$  and  $Y_2$  are the single-particle

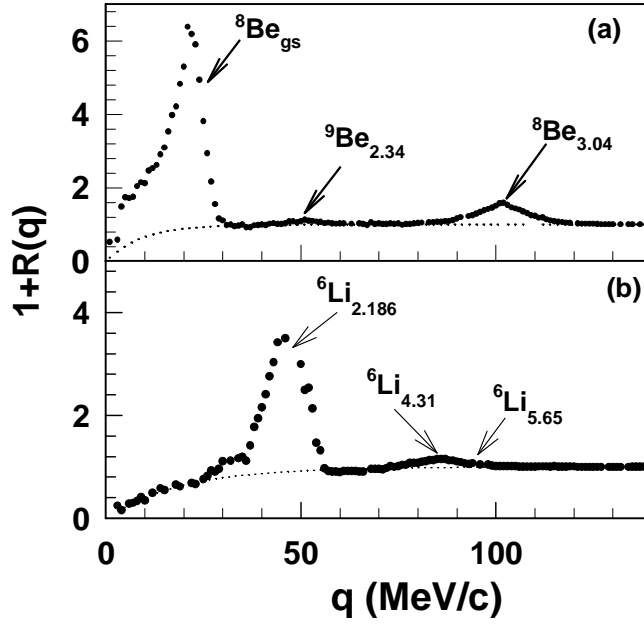


**Figure 2.20:** (a)  $\alpha$ - $\alpha$  and (b)  $d$ - $\alpha$  correlation functions plotted as a function of the relative momentum,  $q$ , for the reaction  $^{20}\text{Ne} + ^{12}\text{C}$  at 145 MeV. Filled circles are the experimental data and the dotted line is the background (see text).

yields for particle 1 and 2 respectively and  $Y_{12}(p_1, p_2)$  is the two-particle coincidence yield.

Experimentally, the product of single particle yields  $Y_1(p_1)Y_2(p_2)$  has been approximated as ‘uncorrelated’ two particle yields,  $Y_{12}^{unc}(p_1, p_2)$ , and was constructed by the ‘event-mixing technique’ [67, 68]. The two-particle correlation functions have been calculated as

$$\sum Y_{12}(p_1, p_2) = C_{12}[1 + R(q)] \sum Y_{12}^{unc}(p_1, p_2) \quad (2.7)$$

The  $\alpha$ - $\alpha$  correlation function obtained in the reaction  $^{20}\text{Ne} + ^{12}\text{C}$  is shown in Fig. 2.20(a). The background from the total coincidence yield which does not proceed through the decay of particle-unstable nuclei is shown in dotted line in the Fig. 2.20(a) [69]. The peaks at  $q = 20$  MeV/c and 100 MeV/c correspond to decays of the particle-unstable ground state of  $^8\text{Be}$  ( $J^\pi = 0^+$ ) with decay width of 6.8 eV and the 3.04 MeV

excited state of  ${}^8\text{Be}$  ( $J^\pi = 2^+$ ) with decay width of 1.5 MeV, respectively. Both of these states decay only by  $\alpha$  particle emission. In addition, the peak at  $q = 50$  MeV/c is due to the decay of the 2.43 MeV state in  ${}^9\text{Be}$ .

The d- $\alpha$  correlation function obtained in this experiment is shown in Fig. 2.20(b). The measured correlation function exhibits two maxima corresponding to the  $J^\pi = 3^+$  unstable excited state of  ${}^6\text{Li}$  at 2.186 MeV with decay width of 24 keV and the  $J^\pi = 2^+$  at 4.31 MeV excited state of  ${}^6\text{Li}$  with decay width 1.3 MeV, respectively. A third peak, corresponding to 5.65 MeV excited state of  ${}^6\text{Li}$  with decay width of 1.9 MeV is also observed in the correlation function, which is in close proximity with the second peak.

### 2.4.3 Physics extraction from the prototype telescope testing

Using the above particle unstable state formations and isotopic identification of light particles, nuclear temperature have been estimated by using three different thermometric techniques (Slope thermometry, excited state thermometry and double isotope thermometry) at this moderate excitation energy. Temperature of excited composite  ${}^{32}\text{S}^*$  formed in the nuclear reaction  ${}^{20}\text{Ne} + {}^{12}\text{C}$  have been estimated using these thermometric techniques [70].

**Temperature from slope thermometry:** This method is based on the concept of a canonical ensemble. The particles evaporated from the hot system are taken to be Maxwellian in shape [71, 72] and the value of the temperature can be extracted from the slopes of the kinetic energy spectra of light charged particles [73, 74, 75, 76, 77]. Experimentally obtained proton and  $\alpha$ -particle spectra in the center of mass are shown in Fig. 2.21 and Fig. 2.22, respectively.

In order to extract temperature using the slope thermometer, the spectra have been fitted with a function  $\sim f(E_{c.m})\exp(-E_{c.m}/T)$ , shown by the solid line in the Figs. 2.21

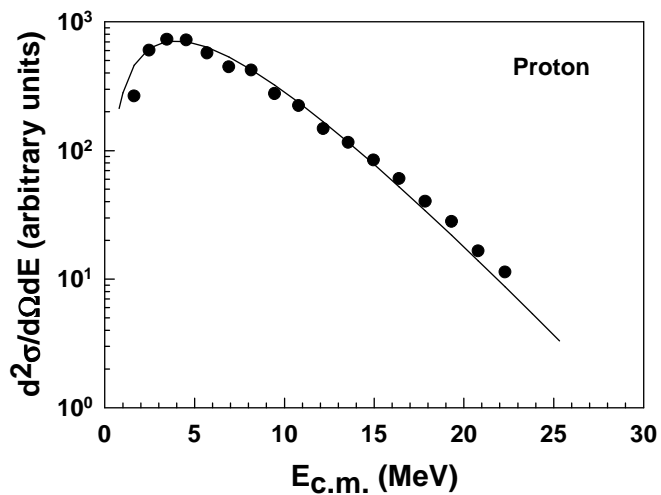


*Figure 2.21:* Typical energy spectrum of protons in the c.m, for the reaction  $^{20}\text{Ne} + ^{12}\text{C}$ . Filled circles are the experimental data and the solid line represents the fitted curve to extract the slope.

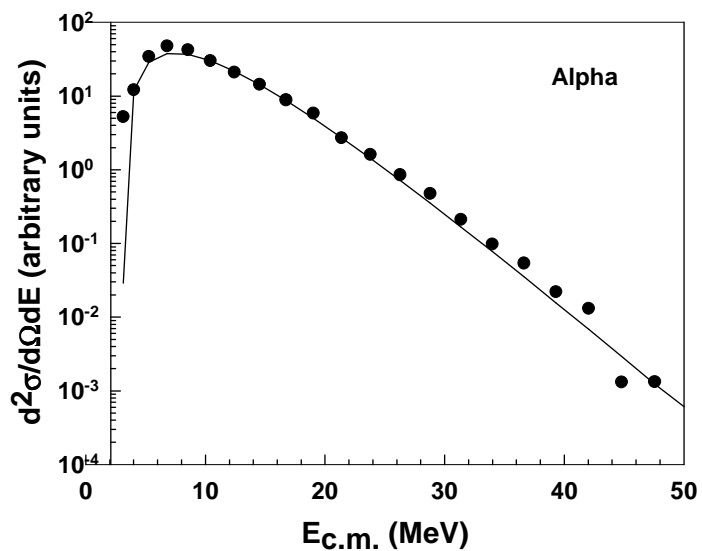


*Figure 2.22:* Same as Fig. 2.21 for  $\alpha$  particles.

and 2.22. The temperatures extracted from the slopes of proton and  $\alpha$  spectra are  $T=2.6 \pm 0.3$  MeV and  $T=2.9 \pm 0.5$  MeV, respectively.

**Temperature from excited-state thermometry:** By knowing the phase space of the decay configuration, the “emission temperature” can be determined from the relative abundances of different particle species, or more directly from the relative populations of states in a given nucleus [78, 79, 80, 81]. The ratio,  $R_p$ , of the populations of two states (if no feeding by particle decay takes place) is related to the temperature ( $T$ ) through the relation;

$$R_p = \frac{(2j_u + 1)}{(2j_l + 1)} \exp(-E_{diff}/T) \quad (2.8)$$

where,  $j_u$  and  $j_l$  are the spins of the upper and lower states respectively and  $E_{diff}$  is the energy difference between these two states.

In order to extract the information of the population of different particle-unstable states, we have measured the coincidence yield (sum of all coincident pair of hits between any two front side strips of DSSD) detected from the decay of particle-unstable nuclei and extracted the two-particle correlations function [65, 66], as described in previous subsection.

Nuclear temperatures have been extracted both from  ${}^8\text{Be}$  and  ${}^6\text{Li}$  decays using the  $\alpha$ - $\alpha$  correlation (Fig. 2.20(a)) and d- $\alpha$  correlation spectra (Fig. 2.20(b)), respectively. The populations of the particle-unstable states were extracted by integrating the experimental yields over the range of  $q$  dominated by the corresponding resonance. The temperature has been extracted using equation 2.8 from the ratio of yields of  ${}^8\text{Be}_{g.s.}/{}^8\text{Be}_{3,04}$  and is found to be  $T=2.2 \pm 0.5$  MeV. Similarly, the temperature has been extracted from the ratio of yields of  ${}^6\text{Li}_{2,186}/{}^6\text{Li}_{4,31}$  and is found to be  $T=2.6 \pm 0.4$  MeV.

**Temperature from double-isotope thermometry:** This method evaluates the temperature of equilibrated nuclear regions from which light fragments are emitted using the yields of different light nuclides. In this scheme, originally proposed by Albergo et

al. [82] based on grand canonical ensemble, the isotope yield for a system in chemical and thermal equilibrium can be related to temperature  $T_{iso}$  via the expression

$$T_{iso} = \frac{B}{\ln(aR)} \quad (2.9)$$

where ‘ $R$ ’ is the ground state fragment yield ratio, ‘ $B$ ’ is the binding energy parameter, and ‘ $a$ ’ is the statistical weights of the ground state nuclear spins. Expression for  $B$ ,  $a$  and  $R$  are

$$B = BE(A_i, Z_i) - BE(A_i + \Delta A, Z_i + \Delta Z) - BE(A_j, Z_j) + BE(A_j + \Delta A, Z_j + \Delta Z) \quad (2.10)$$

$$a = \frac{[2S(A_j, Z_j) + 1]/[2S(A_j + \Delta A, Z_j + \Delta Z) + 1]}{[2S(A_i, Z_i) + 1]/[2S(A_i + \Delta A, Z_i + \Delta Z) + 1]} \times \left( \frac{[A_j/(A_j + \Delta A)]}{[A_i/(A_i + \Delta A)]} \right)^\gamma \quad (2.11)$$

$$R = \frac{[Y(A_i, Z_i)/Y(A_i + \Delta A, Z_i + \Delta Z)]}{[Y(A_j, Z_j)/Y(A_j + \Delta A, Z_j + \Delta Z)]} \quad (2.12)$$

Here,  $BE(A_i, Z_i)$ ,  $S(A_i, Z_i)$  and  $Y(A_i, Z_i)$  are the known binding energy, ground-state spin and the total yield of the fragment with mass  $A_i$  and charge  $Z_i$ , respectively. The value of  $\Delta A$  and  $\Delta Z$  are chosen to be same for both  $i^{th}$  and  $j^{th}$  fragment pairs [82]. The value of the exponent  $\gamma$  is 1 or 1.5 depending on the assumption of surface or volume emission, respectively. In order to remove the coulomb effects in determining the temperature using double-isotope thermometer, we have taken system with  $\Delta Z=0$  and  $\Delta A=1$ , which is the most reliable thermometer [83]. The temperature has been calculated, assuming  $\gamma$  to be 1 (surface emission), using equation 2.9 and from the isotopic yields of p, d, t,  $^3\text{He}$  and  $\alpha$ . The temperature of hot composite  $^{32}\text{S}^*$  was estimated to be  $2.6 \pm 0.2$  MeV from the double isotopic yields of (p, d), ( $^3\text{He}$ ,  $\alpha$ ) and  $2.4 \pm 0.3$  MeV from the yields of (d, t), ( $^3\text{He}$ ,  $\alpha$ ), respectively.

Thus, temperatures of excited composite  $^{32}\text{S}^*$  formed in the nuclear reaction  $^{20}\text{Ne} + ^{12}\text{C}$  have been estimated using different thermometric techniques. The experiment was performed in a single run to minimize the contributions of systematic errors. The

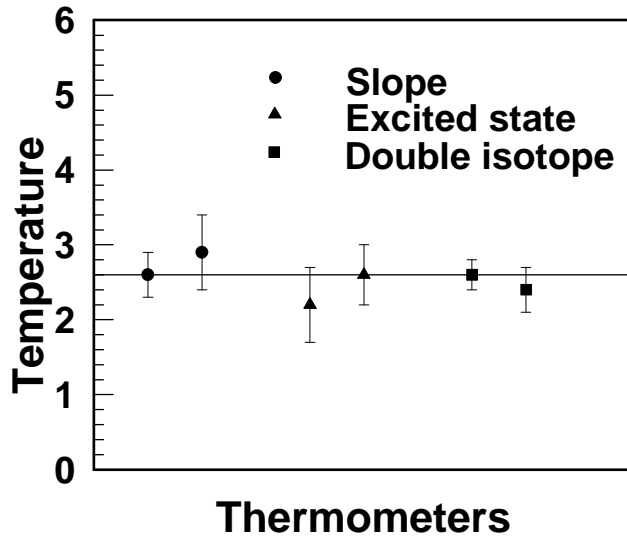


**Figure 2.23:** Comparison of temperatures obtained from different “thermometers”. The solid line is the weighted average.

estimated temperatures are shown in Fig. 2.23 and their weighted average value ( $2.6 \pm 0.1$ ) is shown by solid line. From Fig. 2.23 it is evident that temperatures estimated by different techniques are consistent within the limits of experimental uncertainties for the present system [70].

#### 2.4.4 Performance test of final telescopes

The experiment was performed at the BARC-TIFR 14UD Pelletron Accelerator Laboratory, Mumbai, using 77 MeV  $^{12}\text{C}$  ion and 75 MeV  $^{13}\text{C}$  beams on a  $^{12}\text{C}$  target (self supported, thickness  $\sim 90 \mu\text{g}/\text{cm}^2$ ). Different fragments have been detected using one final prototype of the final 3-element telescope. The telescope consisted of a  $\sim 50 \mu\text{m}$   $\Delta E$  single-sided silicon strip detector (16 channels),  $\sim 500 \mu\text{m}$   $\Delta E/E$  double-sided silicon strip detector (16 X 16 channels) and backed by four CsI(Tl) detectors (thickness  $\sim 6$  cm). Angular coverage of telescope was from  $18^\circ$  to  $32^\circ$ . Typical angular resolution of each strip was  $\sim \pm 0.45^\circ$ . All strips and the CsI(Tl) detectors were read out individually using standard readout electronics (procured from M/s Mesytec, GmbH). Particle identification spectra have been obtained in this experiment have been

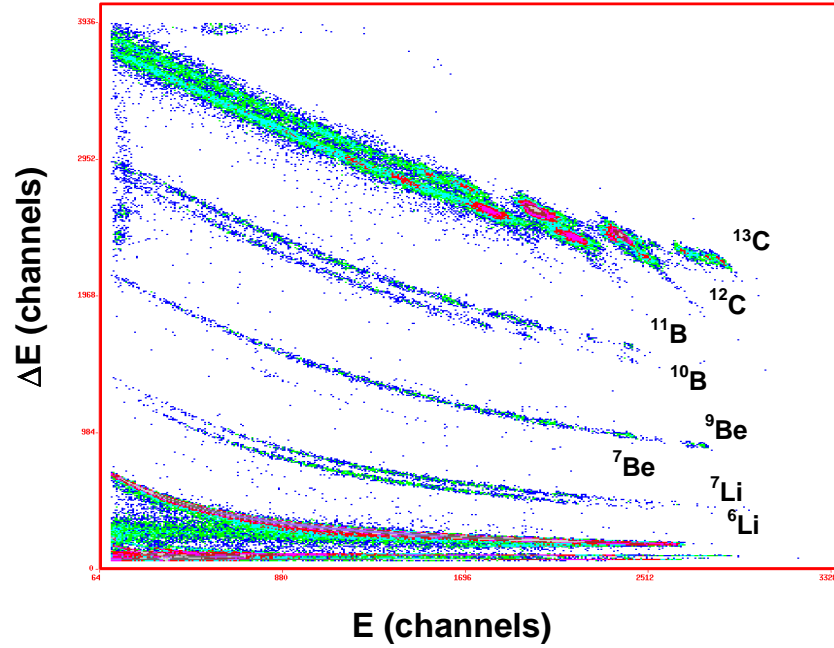


**Figure 2.24:** Particle identification spectra obtained in  $^{13}\text{C} + ^{12}\text{C}$  reaction using the final telescope.

shown in Fig. 2.24. It is clear from Fig. 2.24 that very good isotopic identification of the fragments have been obtained upto  $Z=6$ .

For the present study, event reconstruction technique has also been tested, all detected  $2\alpha$  and  $3\alpha$  events have been extracted from the inclusive event-by-event data to reconstruct the excitation energy spectra of the respective decays. The  $2\alpha$  events originate mainly from (i) decay of particle unbound  $^8\text{Be}$  states and (ii) decay of particle unbound excited states of  $^{12}\text{C}$  ( $^{13}\text{C}$ )  $\rightarrow 3\alpha$  (+n) emission, either directly or through the sequential process  $^{12}\text{C}$  ( $^{13}\text{C}$ )  $\rightarrow ^8\text{Be}$  ( $^9\text{Be}$ ) +  $\alpha \rightarrow 3\alpha$  (+n). The decay of  $^8\text{Be}$  was identified by reconstructing the  $^8\text{Be}$  excitation energy spectrum for all events in which two alpha particles hit two separate strips within the detector. Fig. 2.25 shows the plot of reconstructed excitation energy spectra of all events of two coincident alpha particles in these two reactions (normalize cross sections along the Y-axis of Fig. 2.25). The peaks at excitation energy ( $E_x$ ) = 0 MeV correspond to decays of the particle-unstable ground state of  $^8\text{Be}$  ( $J^p = 0^+$ ) formed in both the reactions; it is seen that the yield is more in the case of  $^{12}\text{C} + ^{12}\text{C}$  reaction. The pronounced bump at excitation energy 0.51

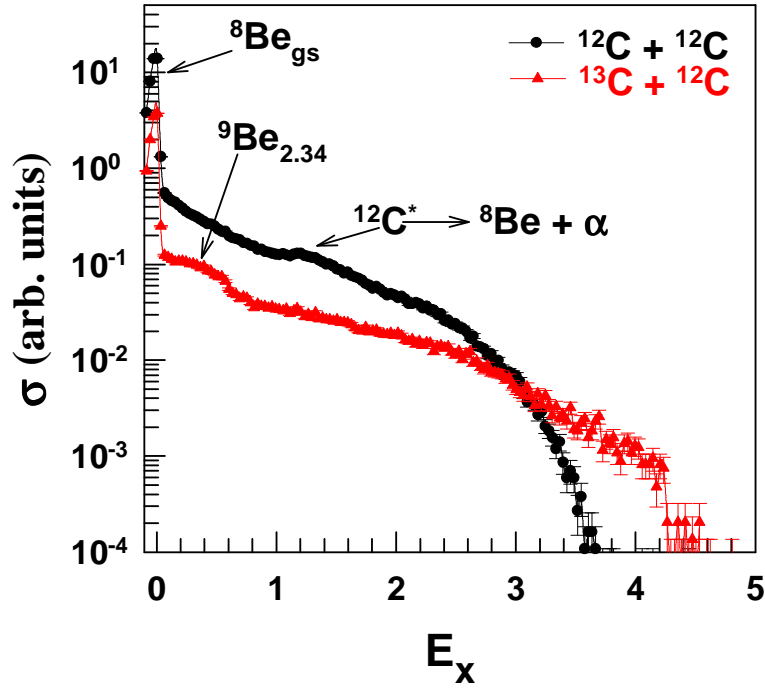


**Figure 2.25:** Excitation energy of  ${}^8\text{Be}$  reconstructed from  $2\alpha$  coincidence in both  ${}^{12}\text{C} + {}^{12}\text{C}$  (solid circle) and  ${}^{13}\text{C} + {}^{12}\text{C}$  (solid triangle) reactions. Normalized cross sections along the Y-axis.

MeV observed in the reaction  ${}^{13}\text{C} + {}^{12}\text{C}$  is due to the decay of the 2.43 MeV state in  ${}^9\text{Be}$ , which is not at all visible for  ${}^{12}\text{C} + {}^{12}\text{C}$  reaction. The broad peak observed at  $E_x = 1.41$  MeV, is due to the sequential breakup channel of  ${}^{12}\text{C}$  and is more pronounced for  ${}^{12}\text{C} + {}^{12}\text{C}$  reaction.

The reconstructed excitation energy spectra of  ${}^{12}\text{C}$  obtained for observed  $3\alpha$  events have been shown in Fig. 2.26 for the reactions ( ${}^{12}\text{C} + {}^{12}\text{C}$  and  ${}^{13}\text{C} + {}^{12}\text{C}$ ). The peak at  $E_x = 7.65$  MeV corresponds to second  $0^+$  level in  ${}^{12}\text{C}$ , known as the Hoyle state. The broad peak near  $E_x = 9.64$  MeV corresponds to  $3^-$  level in  ${}^{12}\text{C}$ . It is clear from Fig. 2.26 that the relative yields of both these states are more in case of  ${}^{12}\text{C} + {}^{12}\text{C}$  reaction, which might be due to the fact that both target and projectile are alpha cluster nuclei [84].

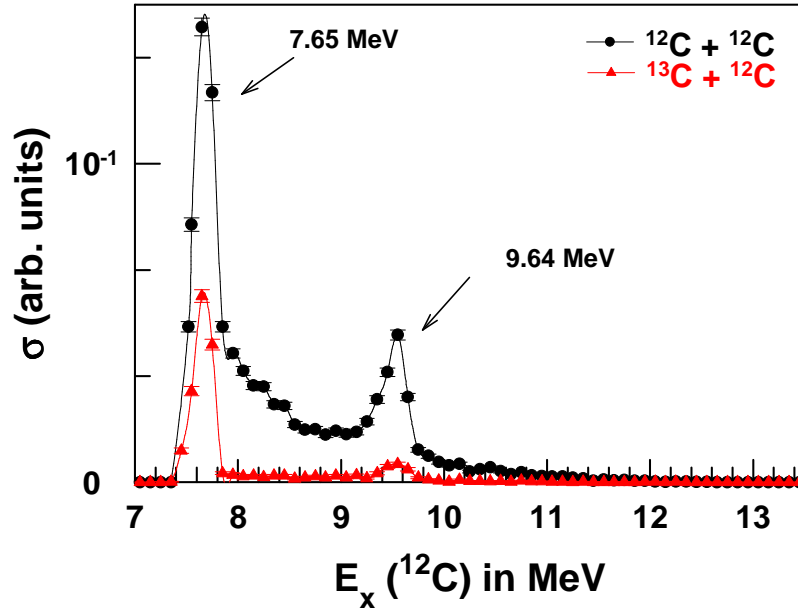


**Figure 2.26:** Excitation energy of  $^{12}\text{C}$  reconstructed from  $3\alpha$  coincidence in both  $^{12}\text{C} + ^{12}\text{C}$  (solid circle) and  $^{13}\text{C} + ^{12}\text{C}$  (solid triangle) reactions. Normalized cross sections along the Y-axis.

## 2.5 Design and development of mechanical structure of detector array

The mechanical structure of the array consists of two parts; (1) housing of individual telescope and (2) support structure which holds all the telescopes in a particular configuration as per specification. In this section, the details of mechanical design of each telescope as well as the support structure of the array have been discussed.

### 2.5.1 Single telescope housing

To encapsulate the detectors, in a telescopic mode, a special housing has been designed and fabricated as shown in Fig. 2.27. The fabrication of the mechanical housing of all telescopes were done using a special pure ultra high vacuum grade Aluminum (6061-T6) for smooth fitting of all the elements. The housing was designed and fabri-

cated so as to contribute as small as possible to the dead area of the detector telescope. The entire detector telescope assembly was housed in two separable aluminium boxes and can be reassembling with the help of screws. Two separate slot have been designed for the two Si-strip detectors as shown in Fig. 2.27 (left). The Si-strip detectors have been fixed rigidly in the housing with the help of three holes on the housing frame through which screws were inserted to the threaded hole on the strip frame. To keep the four CsI(Tl) detectors rigidly behind the strip detector (DSSD), the inner volume of the housing has been given a shape similar to the overall shape of four CsI(Tl) detector assembly, *i.e.*, truncated pyramid. The assembly of 4 CsI(Tl) detectors has been held in proper position with the help of a back support plate connected to a long threaded rod as shown in Fig. 2.27 (left). By rotating the rod slowly, the detectors can be placed in proper position. In the inner sides of the housing there are slots of depth 0.8 mm and width 44 mm to take out the kapton of the strip detectors. The outer sides of the housings have been shaped in such a way that when all telescope would be fitted in the form of array, the front surface would form a part of a sphere of radius 20 cm. To attach all housings in the form of a array, a deep slot was kept in the outer side of the walls of the housings, as shown in the side of Fig. 2.27 (left). The complete assembly of a housing with all the detectors (top plate opened) is shown in Fig. 2.27 (right).

## 2.5.2 Support structure of detector array

To put the telescopes in a form of array, a support structure has been designed and fabricated. The telescopes have been put in 5 columns with five telescopes in each except in the middle column; one telescope has been removed from middle of this column for the exit of beam. Shapes of the housings are such that, all the front faces together will form the surface of an imaginary sphere of radius 20 cm. The whole array will be kept on two parallel rails inside a large reaction chamber SHARC [85]. To align the whole array with the beam line axis, arrangement has been kept to

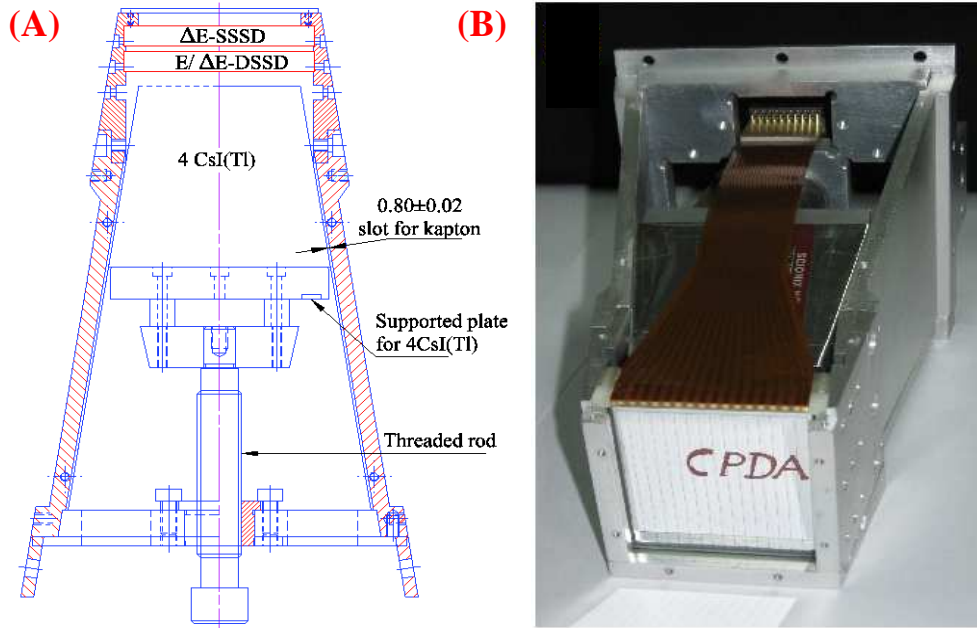


**Figure 2.27:** (A) Design of a telescope, and (B) photograph of the telescope with strip detectors and CsI(Tl) detectors.

move it vertically and horizontally. Complete assembly of all telescopes along with the detectors has been shown in Fig. 2.28.

### 2.5.3 Readout electronics and data acquisition system

In this subsection, a general description of the electronics and the data acquisition system will be described. A schematic diagram of the readout electronics for a single strip or channel is shown in Fig. 2.29 and for the typical full electronics for 24 telescopes as shown in Fig. 2.30. The electronic signals from the strip is fed to the pre-amplifier, the output of which is a fast rising differential signal of few millivolts with a long tail of the order of  $50 \mu\text{s}$  or more. The pre-amplifier out is differential. Differential signal of preamplifier has been chosen in order to eliminate the interfering noise, which cancels out due to positive and negative signals of the same signal in differential mode, when the amplifier subtracts the differential reference from the normal signal. The output of the pre-amplifier is then fed to the amplifier for further

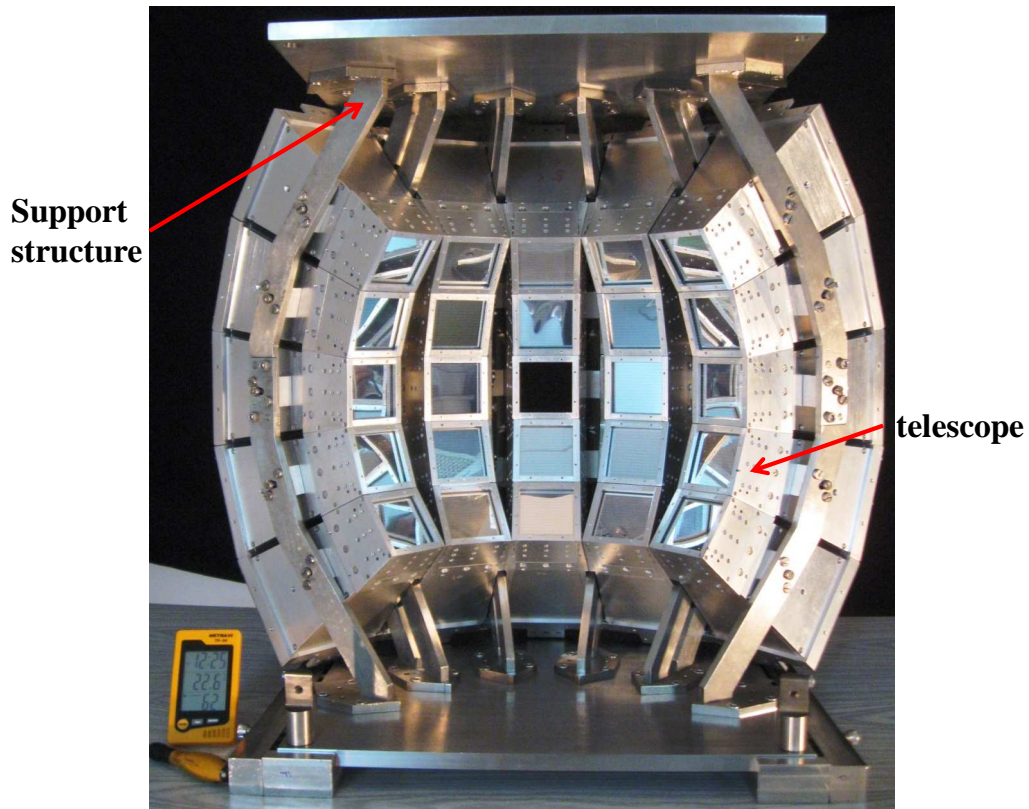


*Figure 2.28: Complete high resolution charged particle detector array with support structure.*

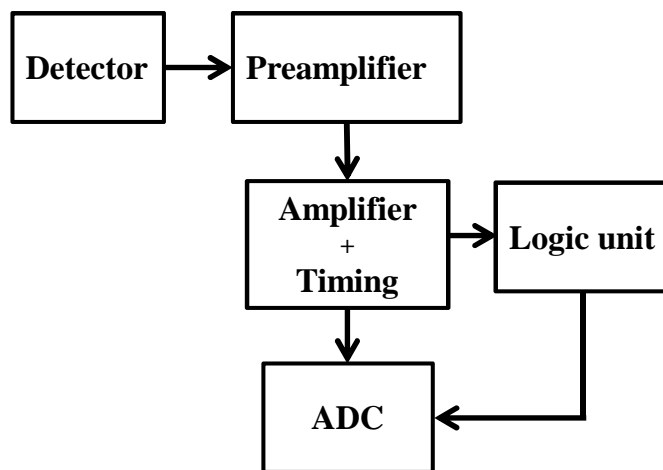


*Figure 2.29: Block diagram of electronics used for individual channel.*

amplification and shaping. The output of the amplifier is a Gaussian shaped pulse of height  $\sim$  a few volts and a width of  $1 \mu\text{s}$ , which is directly fed to the analog to digital converter (ADC) (maximum of 8 volts, range of ADC) and stored using the data acquisition system. The schematic given above is for a single channel electronics but each Si-strip detector has 16 channels per side, so we have used custom made 16 channels pre-amplifier (MPR-16, differential output) and 16 channels amplifier (MSCF-16, differential input) manufactured by M/s Mesytec Pvt. Ltd, Germany as per our specification. The MSCF 16 channel amplifier has in built TFA (Timing-Filter-Amplifier) - CFD (Constant Fraction Discriminator), for timing and threshold applications. In addition to the energy signal, these amplifiers also generate one OR-logic output of all 16 channels, which has been used for master trigger generation after some logic operation. Then these amplifier signals are fed to 32 channel ADC (Model CAEN V778) for further processing with the help of a Versa-Module Eurocard (VME) data acquisition system (DAQ) developed in-house. For the all CsI(Tl) detectors, we have used custom made 16 channel shaper with timing filter amplifier and constant fraction discriminator (MSCF-16, unipolar header input). Full electronics setup (all parameters of amplifier and the detector bias voltage) of the array as well as the VME-DAQ are remotely controllable via the ethernet.

#### **2.5.4 Status of the high resolution array**

Performance test of all elements of the detector array have been completed. The complete high resolution detector array with electronics is shown in Fig. 2.31. The complete detector array with all the elements as well as the electronics have been tested in offline with  $\alpha$ -source and also using a precision pulsar at 10K rates for continuously 72 hours. Now the array (full or part of it) is being used for physics experiment.

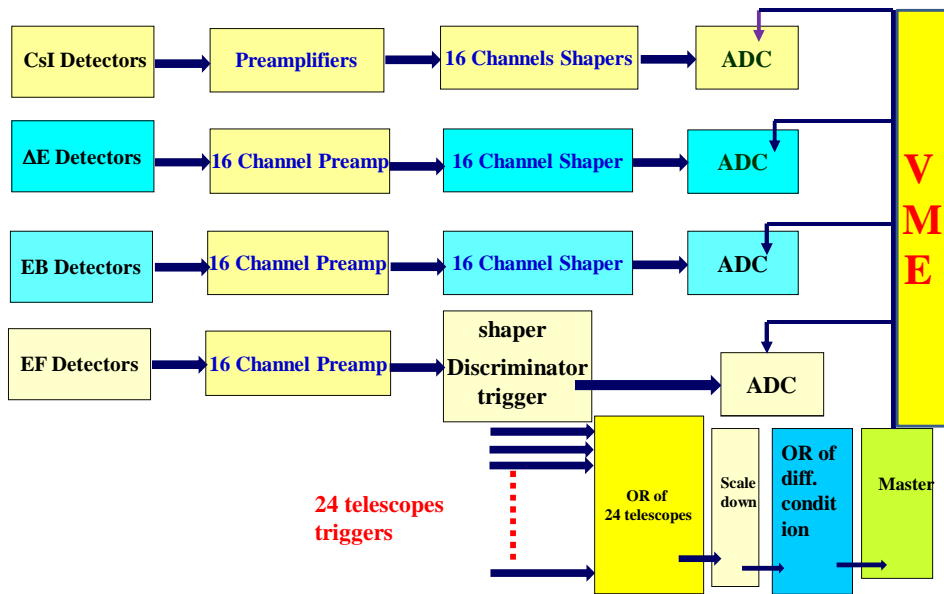


Figure 2.30: Block diagram of electronics for 24 telescopes.



Figure 2.31: Detector array with complete electronics and data acquisition system (DAQ).

# Chapter 3

## Study of decay mechanism of the Hoyle state

### 3.1 Introduction

The main objective of this experiment was to study the decay mechanism, *i.e.*, sequential *versus* direct decay, of the  $^{12}\text{C}$  states above the three- $\alpha$  breakup threshold. In the present thesis, the decay mechanism of the Hoyle state of  $^{12}\text{C}$  ( $0_2^+$ ,  $E_x \sim 7.654$  MeV) in particular has been studied in details. The breakup process is believed to carry the signature of the structure of final state of the nucleus. In particular, the direct three body breakup of the Hoyle state has evoked a lot of interest in recent times as it is considered the key to solve several unsolved questions on the nucleosynthesis process as well as exotic structure of the state. In order to achieve the goal, a high resolution, high statistics, complete kinematic measurement of the Hoyle state decay, has been performed. Different states of  $^{12}\text{C}$  were excited through inelastic scattering of 60 MeV  $^4\text{He}$  on  $^{12}\text{C}$  target. The system  $^4\text{He} + ^{12}\text{C}$  was chosen for this purpose for its specific advantage regarding the detection of complete events, as it has only a few open reaction channels compared to other heavy ion induced reactions.

This chapter consists of several sections, organized in the following manner. The details of the experiment (the accelerator, the experimental setups and the measurement tools used for the particle detection) have been described in section 3.2. The details of the data analysis procedure has been described in section 3.3. In sections 3.4 and 3.5, the techniques used for estimation of decay mechanism of the Hoyle state have been described in great details. Finally in the section 3.6, results and discussions have been presented.

## 3.2 Experiment for study of the Hoyle state

### 3.2.1 Accelerator used: Variable energy cyclotron

The experiment has been performed at the Variable Energy Cyclotron Centre (VECC), Kolkata. The Variable energy cyclotron, also known as K130 cyclotron, is a sector-focused, isochronous cyclotron with three spiral sectors [86]. The room temperature main magnet of diameter of 224 cm, produce a maximum magnetic field of 2.1 T in the pole gap. Details of the machine parameters are given in Table 3.1. It is able to deliver accelerated light ion as well as heavy ion beams with the help of Penning Ionisation Gauge (PIG) and Electron Cyclotron Resonance (ECR) ion sources, respectively. As per design specification, it can accelerate charged particles upto the energy of  $130 (Q^2/A)$  MeV, where,  $Q$  and  $A$  are the charge state and the atomic mass of the accelerated particle, respectively.

Fig. 3.1 shows the picture of the cyclotron with the switching magnet and different beam lines. Details of the beam lines layout have been shown in Fig. 3.2. The  $0^0$  beam line (shown as Ch# 1 in Fig. 3.2) is used for high current or irradiation type experiments. The general purpose scattering chamber has been placed in the second beam line (Ch# 2 in Fig. 3.2) for charged particle experiments. Experiments with  $\gamma$ -detectors as well as charged particle detector are performed in the third beam line (Ch#

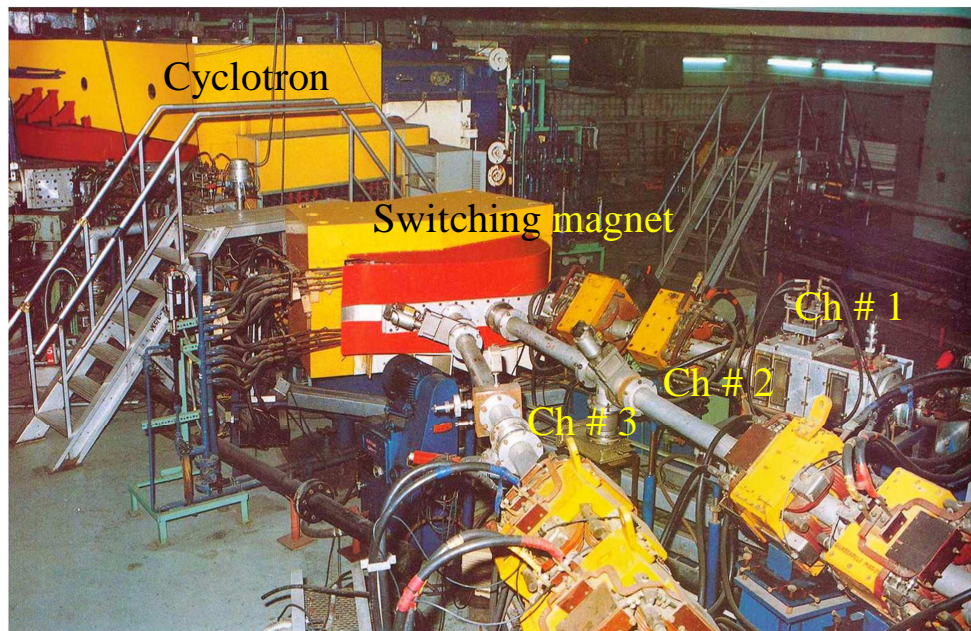


*Figure 3.1: K130 Variable energy cyclotron with switching magnet and various beam lines.*

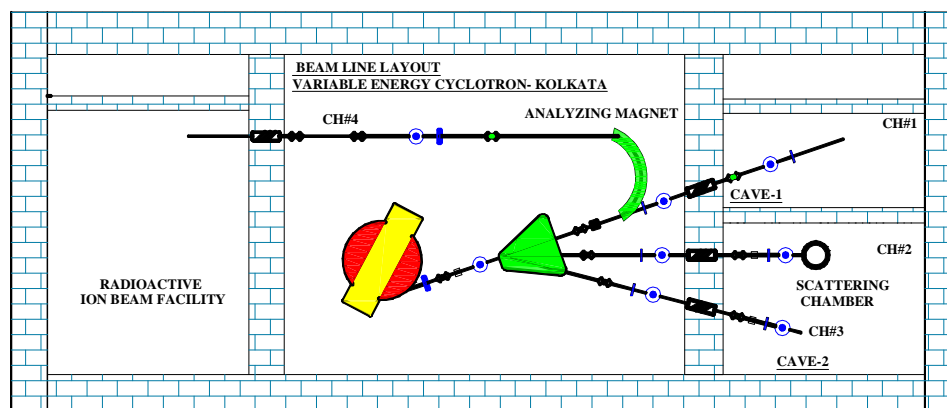


*Figure 3.2: Layout of different beam lines of K130-cyclotron.*

**Table 3.1:** Technical specifications of K130 cyclotron.

<b>Cyclotron</b>	
Cyclotron type	:Azimuthally Varying Field (AVF)
<b>Magnet</b>	
Shape of magnet	: H-shaped electromagnet
Pole diameter	: 224 cm
Average pole gap	: 24.5 cm
Average magnetic field	: 17.1 kG (max. of 2.1 T)
Main coil power	: 490 kW
Trim coil power	: 433 kW
Valley coil power	: 27 kW
<b>R. F. System</b>	
Frequency range	: 5.5 - 16.5 MHz
Dee Voltage	: 70 kV (max)
Energy gain	: 140 keV /turn (max)
Oscillator power output	: 300 kW (max)
<b>Ion Source</b>	
Type	: Hot cathode PIG, ECR
Filament current	: 500 A (max)
Arc current	: 0- 2 A
Arc voltage	: 10 - 600 V
<b>Deflector</b>	
Type	: Electrostatic 120 kV (max)
<b>Vacuum</b>	
Operating pressure	: $10^{-6}$ Torr
<b>Beam</b>	
Energy	: Proton 6 - 30 MeV : Deuteron 12 - 65 MeV : Alpha 25 - 130 MeV : Heavy ion 7-11 MeV/A
Internal beam current	: 100 $\mu$ A
External beam current	: 20 $\mu$ A
Extraction radius	: 99 cm
Resolution	: 0.5% (FWHM)
Beam pulse width for particles	: 4 ns

3), where the present experiment has also been performed. The fourth beam line (Ch# 4) has been dedicated to the radioactive ion beam (RIB) facility as shown in Fig. 3.2.

### 3.2.2 Experimental setup

The experiment has been performed using 60 MeV  $^4\text{He}$  ion beam from the K130 cyclotron on  $^{12}\text{C}$  target (self supported, thickness  $\sim 90 \mu\text{g}/\text{cm}^2$ ). The experimental setup inside the scattering chamber is shown in Fig. 3.3. Two Si-strip detectors were placed at a distance  $\sim 80$  mm down stream from the target and one Si-strip telescope was placed in the backward direction at a distance  $\sim 60$  mm up stream from the target. Different excited states of  $^{12}\text{C}$ , Hoyle state in particular, have been populated through inelastic scattering of 60 MeV  $\alpha$  from  $^{12}\text{C}$  and the decay of the Hoyle state has been studied by exclusive complete kinematical measurement of all the out going particles (events, where all four  $\alpha$ -particles, three from the decay of  $^{12}\text{C}^*$  and the inelastically scattered one, were detected)

The Si-strip detectors used in the forward direction are double sided Si-strip detectors (DSSD) of  $500 \mu\text{m}$  thickness, which have been used to detect  $3\alpha$  decay from  $^{12}\text{C}^*$ . The telescope in backward direction consisted of a  $50 \mu\text{m}$ ,  $\Delta E$ , single-sided silicon strip detector (SSSD) followed by  $500 \mu\text{m}$  DSSD E-detector, for detecting the inelastic  $\alpha$ -particles. The two DSSD detectors and strip detector telescope were placed at kinematically correlated angles for coincident detection of inelastically scattered  $^4\text{He}$  in the backward angle telescope (covering the angular range of  $88^\circ - 132^\circ$ ) and the three  $\alpha$ -particles, originating from the decay of the Hoyle state of the recoiling  $^{12}\text{C}^*$ , at the forward angle detectors (covering the angular range  $20^\circ - 52^\circ$  and  $60^\circ - 92^\circ$ ). Schematic diagram of the setup is shown in Fig. 3.4. One horizontal collimator (of 2 mm in width) was placed in front of the backward telescope such that the detection of inelastic  $\alpha$ -particles was restricted to only a few strips (1 or 2) around the median plane. So, the corresponding coincident recoiling  $^{12}\text{C}^*$  nucleus in the forward direction was also restricted to more around the median plane; this helped to enhance the per-

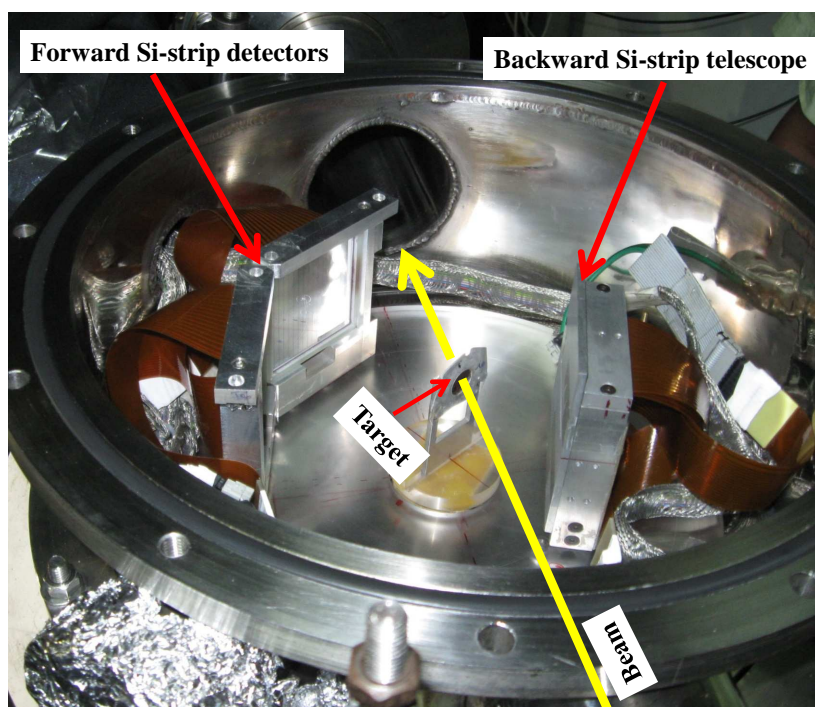


**Figure 3.3:** *Experimental setup used in the experiment inside the scattering chamber of third beam line.*

centage of completely detected events (in which all three decaying  $\alpha$ -particles remain confined within the span of the forward detectors and get detected) among the whole set of coincident events. Typical beam current used for the experiment was  $\sim 2.5$  pA.

### 3.2.3 Readout electronics and data acquisition system

The readout electronics setup for strip detector has already been discussed in last chapter and the same setup for each strip detector has been used. The block diagram of current experimental electronics setup is as shown in Fig. 3.5 and in reality as shown in Fig. 3.6. The MSCF 16-channel amplifier has in built TFA (Timing-Filter-Amplifier) - CFD (Constant Fraction Discriminator), which eliminates noise by checking that the input signal is above some preset threshold level. In addition to the energy signal, this amplifier also generate one OR-logic output of all 16 channels, which has been used for master trigger generation after some logic operation. The main master trigger was

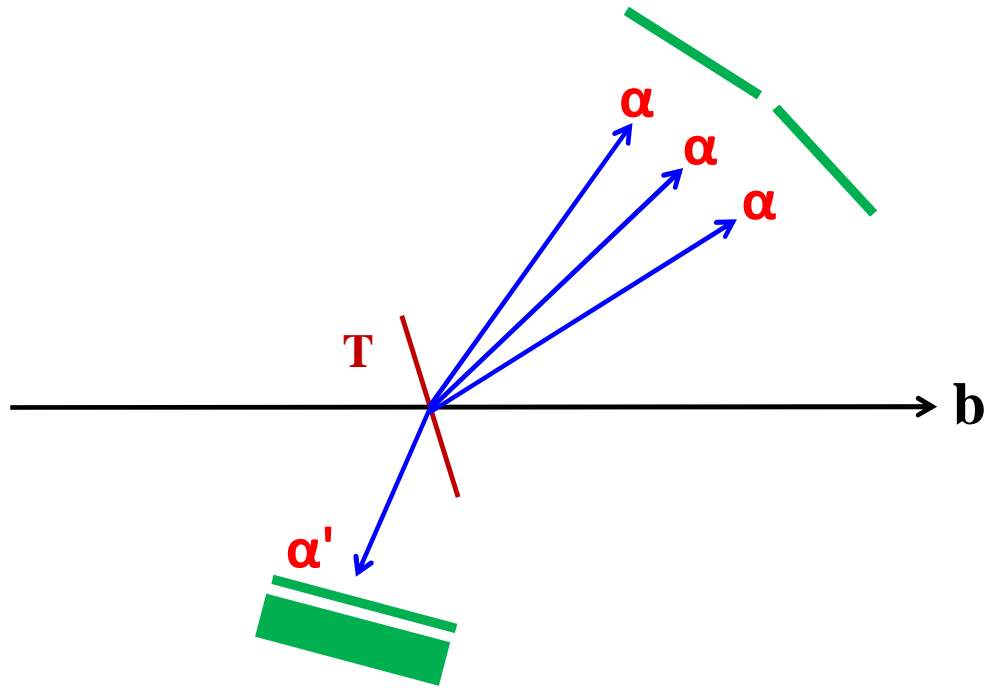


*Figure 3.4: Schematic of the experimental setup as used in the experiment.*

coincidence (logic AND) between two forward detectors and the backward telescope. All amplifier outputs of the energy signals of the strips were fed to the 32 channels Analog-to-Digital -Converters (ADC's). A VME - based on-line data acquisition system was used for the collection of data on event-by-event basis. Rejection of unwanted (mixed) events has been done in hardware by properly synchronising the operations of all ADCs with the master gate vetoed with the ADC BUSY signals to disable all ADCs till conversion of a valid event was completed. Finally, the true events of interest have been extracted by using the analysis procedure described in the next section in details.

### **3.3 Data Analysis procedure**

In this section the procedures, which have been developed and used for data analysis will be discussed in details. All the analysis procedures, described here, have been developed using the C++ based ROOT platform.

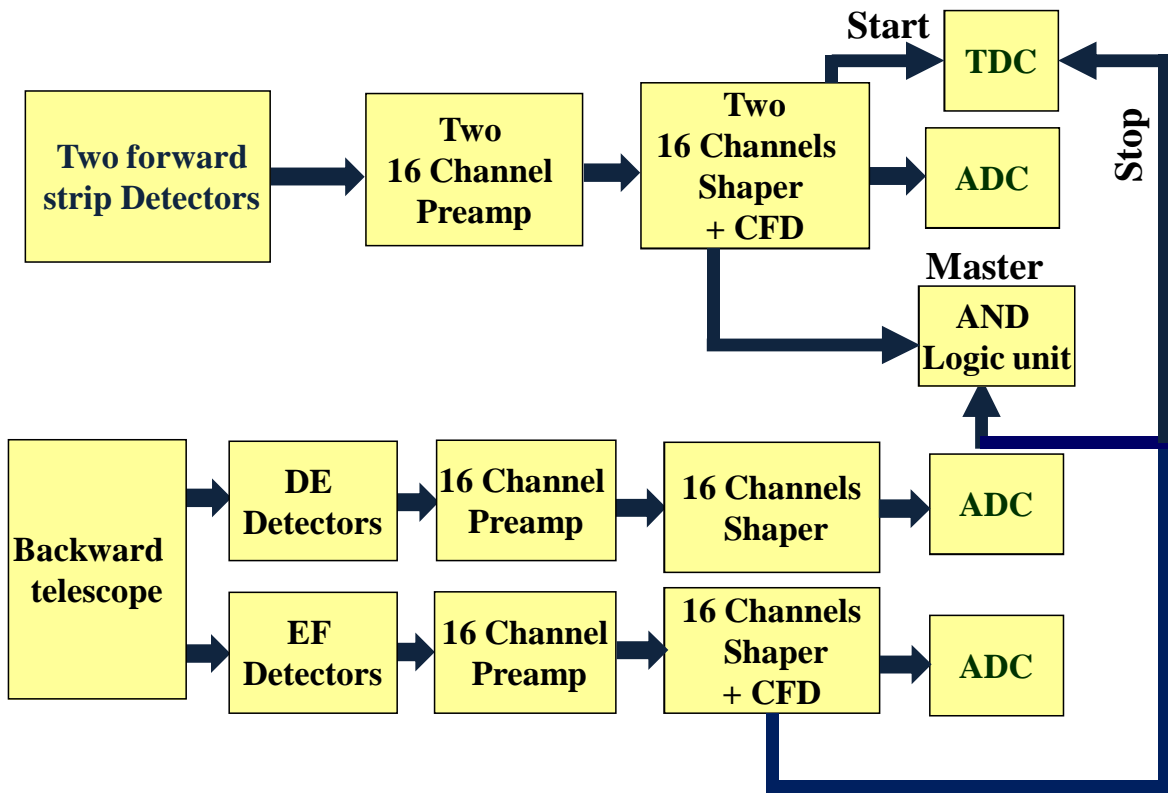
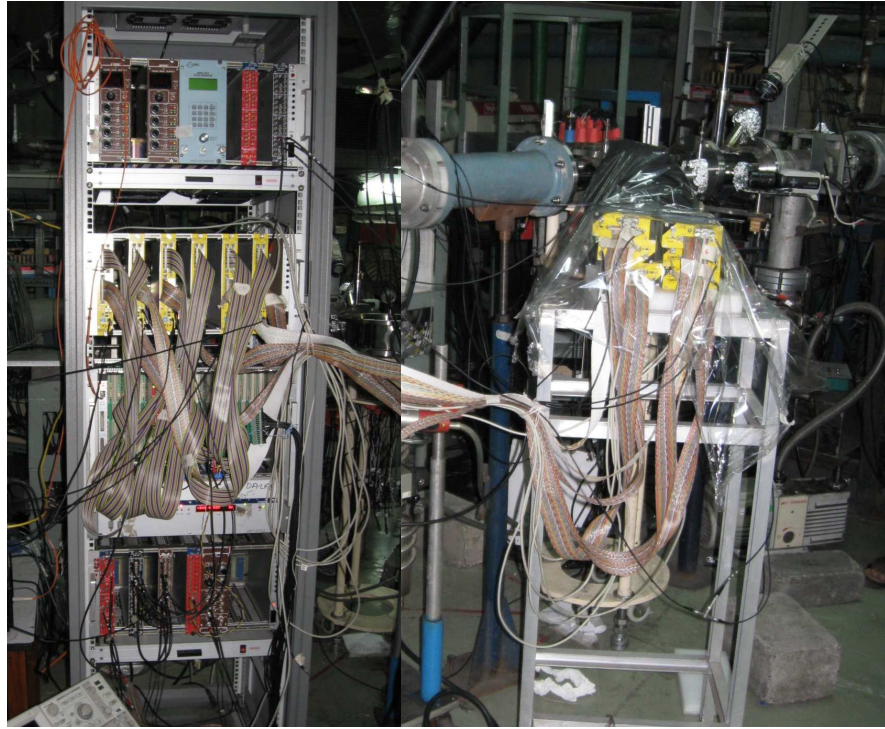


Figure 3.5: Block diagram of electronic setup.



*Figure 3.6: Electronic setup used in the experiment.*

### **3.3.1 Energy calibrations**

Energy calibration of the detector is the first step of the data analysis procedure. The present experiment involved a total of 112 channels (three DSSD, each of 32 strips and one SSSD with 16 strips); each channel or strip has been calibrated separately. The energy calibrations were performed twice, once before the actual experiment started, and finally after the experiment was over.

To perform the energy calibration of the strips,  $^{229}\text{Th}$ - $\alpha$  source has been used. The source has five groups of  $\alpha$  energies (4.79, 5.82, 6.34, 7.07 and 8.38 MeV), the spectrum of which is shown in Fig. 3.7 for a particular strip. It is cleared from Fig. 3.7 that, there is no significant degradation in the energy resolution of the detector before the actual experiment started (black histogram) and after the experiment was over (red histogram). Since the silicon detector behaves linearly with the energy of the charged particle, calibration was performed by doing linear fit between the reference energies

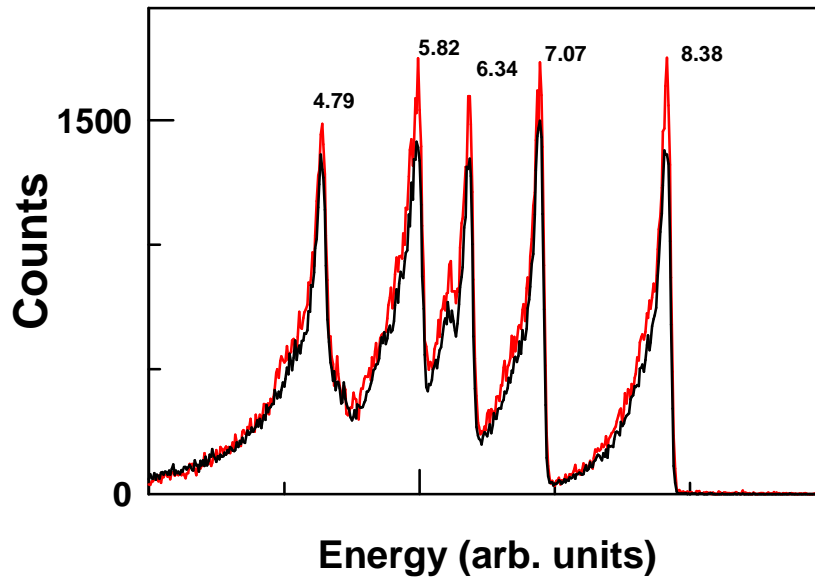


**Figure 3.7:** Spectrum of  $^{229}\text{Th}$ - $\alpha$  source in Si-strip detector. The energy calibration before experiment started is shown in black histogram and the same after experiment was over is shown in red histogram.

of source and channel number corresponding to the positions of the centroid of the peaks in each strip. In the case of thin detector  $\Delta E$  of the backward telescope, the interested range of energy was upto 10 MeV, hence, only  $^{229}\text{Th}$  source peaks have been used for calibration and the corresponding linear fitting for a single strip is shown in Fig. 3.8. But in the case of thick E-detector of backward telescope as well as the forward detectors (two DSSDs), the interested energy is upto 30 MeV, hence calibration of each strip has been performed using  $^{229}\text{Th}$  source energies, elastic and inelastic scattering of  $\alpha$  on  $^{12}\text{C}$  (ground state and 4.4 MeV state of  $^{12}\text{C}$ ). The linear fitting for a typical single strip of E (DSSD) detector is shown in Fig. 3.9. After the energy calibration completed, in the next step of data analysis, position of different particles in DSSD have been identified as described in the following subsection.

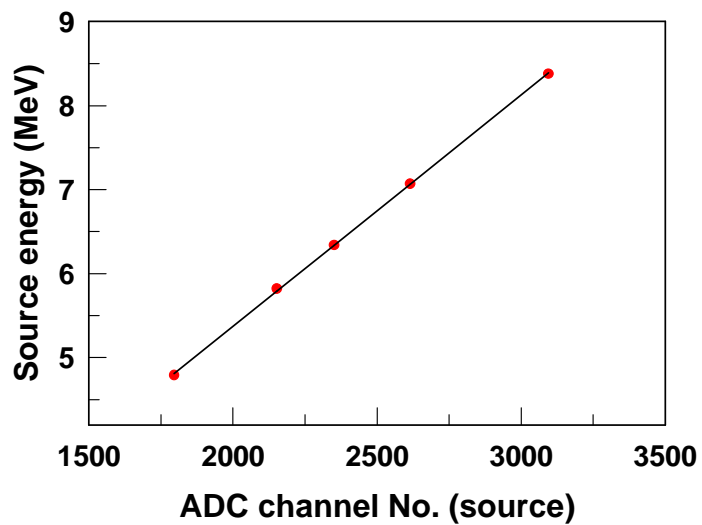


*Figure 3.8:* Calibration curve for a typical strip of  $50\mu\text{m}$ ,  $\Delta E$ -detector of the backward telescope.

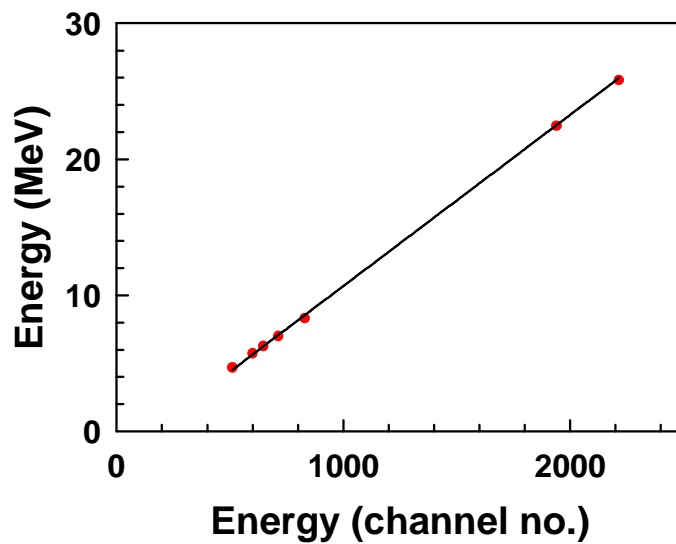


*Figure 3.9:* Calibration curve for a typical strip of  $500\mu\text{m}$ ,  $E$ -detector.

### 3.3.2 Position identification in DSSD

In the present experiment, forward detectors and backward telescope were placed at a distance 80 mm and 60 mm from the target, respectively; hence, the average angular resolution was  $2^\circ$  for forward detectors and  $3^\circ$  for the backward telescope. The angular positions ( $\theta$ ,  $\Phi$ ) of the incident particle on the detector has been defined by the corresponding position in the DSSD detector for both the forward detectors as well as in the backward telescope.

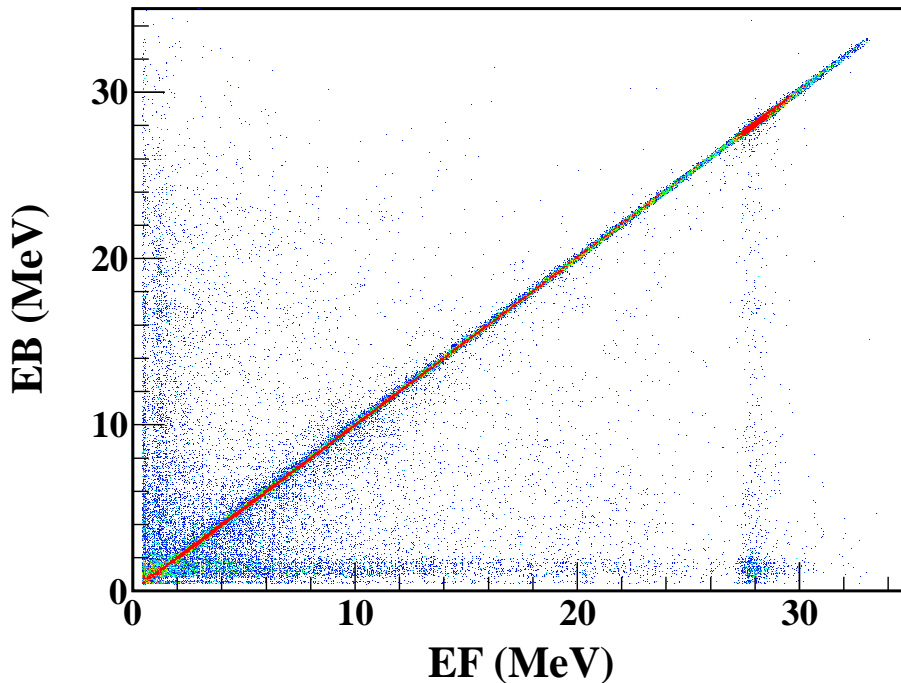


**Figure 3.10:** Two-dimensional scattered plot between energy obtained in front strip (EF) versus back strip (EB) in DSSD.

The position identification procedure has been described in the previous chapter in the event reconstruction technique section. The energy of the particles obtained in front strip (EF) and back strip (EB) has been plotted in Fig. 3.10. The straight line form in Fig. 3.10, basically define the position for the corresponding inter-cross strip (front-back strip). In this case the genuine positions in DSSD have been identified within

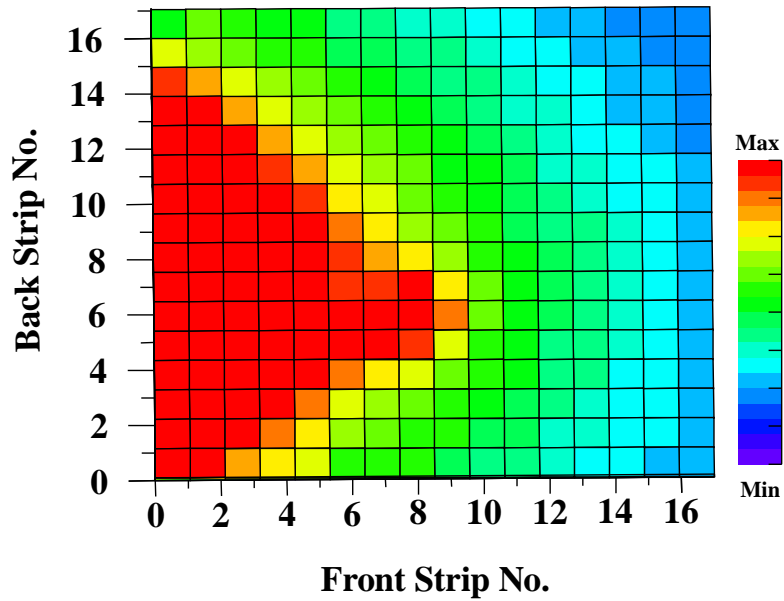


*Figure 3.11: Position identification in DSSD.*

the threshold of less than 50 keV (maximum variation between front and back strip). A typical spectrum for position identification in forward DSSD detector is shown in Fig. 3.11.

### 3.3.3 Particle Identification technique

Particle identification in the backward telescope has been done by  $\Delta E - E$  method, as mentioned in previous chapter. A typical  $\Delta E - E$  two dimensional spectrum of the particles emitted in the reaction  $\alpha$  (60 MeV) +  $^{12}\text{C}$  and detected using the telescope is shown in Fig. 3.12. From the Fig. 3.12, it is seen that good isotopic identification has been obtained for particle of charge  $Z = 1$  and  $Z = 2$ .

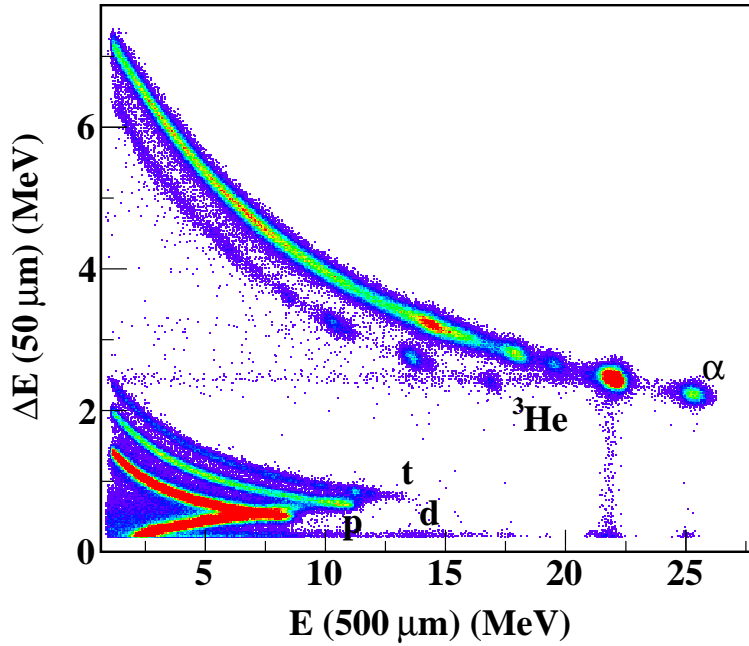


**Figure 3.12:** Two-dimensional scattered plot between  $\Delta E - E$  for the backward telescope strip at  $105^0$ .

### 3.3.4 Target thickness measurement

Target thickness ( $^{12}\text{C}$ ) has been measured using a  $^{229}\text{Th}-\alpha$  source, which has well separated five groups of known energies, and a single surface barrier detector with the standard electronic setup. First, the energy spectrum of  $\alpha$ -source has been measured after placing the target foil in between the detector and the source. Then, in the next step, the same measurement has been repeated without the target. The energy loss in the target has been calculated from the ADC channel shift in the  $\alpha$  energy spectra with and without target. Now from the known energy peaks of the  $\alpha$ -particles, ADC channel number has been calibrated and the corresponding energy loss in the target was calculated. The stopping power ( $dE/dx$ ) of  $\alpha$ -particle in the target ( $^{12}\text{C}$ ) material at the respective peak energies have been obtained from the code SRIM 2008 [87]. The average thickness of the target has been estimated by taking the average of the

ratios of energy loss in the target and stopping power corresponding to different  $\alpha$  peak energies. The thickness of the  $^{12}\text{C}$  target has been estimated and found to be  $\sim 90 \mu\text{g}/\text{cm}^2$ .

### 3.3.5 Energy loss corrections

After the target thickness measurement, the energy of the emitted particle has been corrected for energy loss in target as well as detector dead area. The emitted particle after collision must pass through the target foil and the dead layers of the detector before being detected in detector volume. Hence energy correction should be performed to get accurate energy of the particles. The energy correction has been done in different steps on event by event basis during data analysis. The energy loss of particle depends on the effective thicknesses (of the target and the detector dead layer), which in turn depends upon the emitted angle and the energy of the emitted particles. The energy losses in different materials (of the target and the detector dead layer) have been calculated using the code SRIM 2008 [87]. After incorporating all these corrections, the correct energy of the particles is given by

$$E_c = E_{det} + \Delta E_t + \Delta E_d \quad (3.1)$$

where,  $E_c$  is the corrected energy of the particle,  $E_{det}$  is the measured energy in the detector,  $\Delta E_t$  is the energy loss in target foil and  $\Delta E_d$  is the energy loss in dead layers of the detector.

As the target has a finite thickness, the target elements may be considered to be distributed in multiple layers. The interaction between target and projectile may then be assumed to occur at any of the layers distributed over the whole thickness of the target. Therefore, it is very difficult to correct the energy of the particle by considering the accurate point of interaction of the emitted particle. For simplicity, during target energy loss correction, it has been assumed that the reaction occurs uniformly over the whole thickness of the target. So for the energy correction of the projectile as well

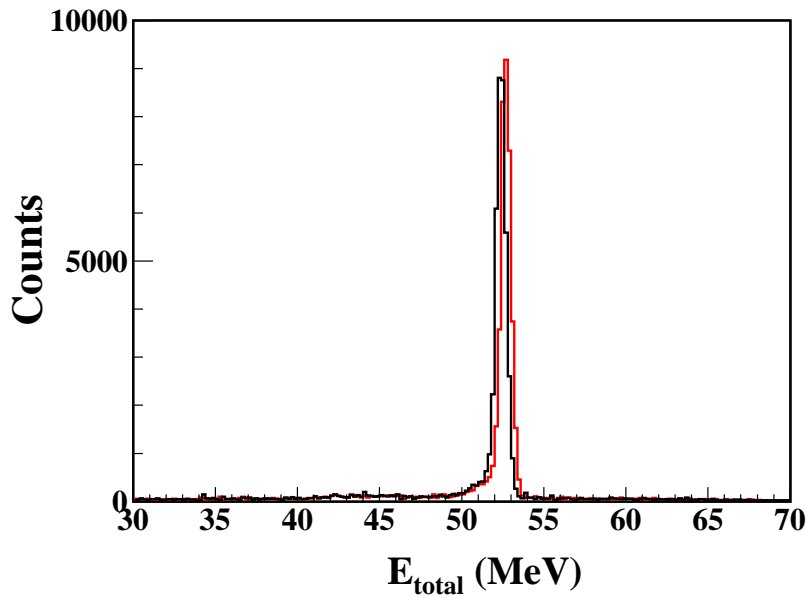


**Figure 3.13:** The effect of energy loss correction in total energy spectrum of four  $\alpha$ . The total energy spectrum, where no corrections have been taken into account, only the measured sum energies of four  $\alpha$ 's is shown in black line and the other one (red line) is the corresponding spectrum after incorporated all energy corrections.

as for emitted particles, it has been assumed that the reaction (target and projectile interaction) takes place at half thickness (middle) of the target (average point of interaction). During the energy loss correction for the detected particles in dead layer of the detectors, the thickness of the dead layer has been considered as mentioned by the manufacturer [62]. After incorporating all the corrections, the effect of the energy loss correction in the total energy spectrum of four  $\alpha$  particles in the exit channels is shown in Fig. 3.13. The black and red lines in Fig. 3.13 show the measured sum energies of four  $\alpha$ -particles without and with all energy loss corrections, respectively.

### 3.3.6 Event reconstruction

The aim of the experiment was to study the decay of the (unbound) excited states of  $^{12}\text{C}$  by exclusive complete kinematical measurement of all outgoing particles; only

completely detected events (events where all four  $\alpha$  particles, three from the decay of  $^{12}\text{C}^*$ , as well as the inelastically scattered one were detected separately) have been used for the present analysis to remove any ambiguity about the origin of the detected particles [88]. In this regard, a program has been developed for identification of kinematically complete events. For each event, in the first step, it identifies the  $\alpha$ -particle in backward telescope by the above mentioned particle identification method; for each detected  $\alpha$  in the same event, it then tried to look for three hits in the forward detectors as a pre condition that the event may be stored as an interesting event for further processing. In the next stage, all these stored events were processed to extract physics information as mentioned below.

### 3.3.7 Kinematical cuts for filtering of events

The processed data set of the four particles (three in the forward detectors and one in the backward telescope) event has been further processed using different kinematical filters to extract the genuine kinematically complete  $4\alpha$  events. In the first step, excitation energy,  $E_x$ , of recoiling  $^{12}\text{C}^*$  has been reconstructed from the three detected particles in the forward detectors (assuming three as  $\alpha$ -particles) using the equation 2.5 for three particles as given by

$$E_x = \sum_{i=1}^3 E_i - \frac{(P_1 + P_2 + P_3)^2}{2M_{^{12}\text{C}}} + E_{th} \quad (3.2)$$

here,  $E_i$  and  $P_i$  for  $i = 1, 2, 3$ , are the energies and momenta of the three  $\alpha$ -particles,  $M_{^{12}\text{C}}$  is the mass of the  $^{12}\text{C}$ , and  $E_{th}$  is the  $3\alpha$  breakup threshold (7.27 MeV) of  $^{12}\text{C}$ . In the next step, the same excitation energy of the recoiling  $^{12}\text{C}^*$  has been obtained from the inelastic  $\alpha$  (detected in backward telescope in coincidence with the  $3\alpha$ ) from the known binary kinematics. Then, two-dimensional plot has been generated between excitation energy of the recoiling  $^{12}\text{C}^*$  reconstructed from invariant mass of  $3\alpha$  detected in forward detectors and the same obtained from the inelastically scattered  $\alpha$  detected in backward telescope, which is shown in Fig. 3.14 (a), without imposing any condition. Then, in the next step, events have been filtered out with the TDC time gate.

As the ADC acceptance window was  $2.0 \mu\text{s}$ , which is relatively large compared to the response time of Si-strip detector ( $\sim 100 \text{ ns}$ ), restriction imposed on the event acceptance window with a narrow time gate of the TDC of the order of detector response time would greatly reduce the random coincidences, particularly the coincidences with the elastic beam like particles. In this case, the TDC time width was found to be 18 ns (FWHM) as shown in Fig. 3.15. The effect of TDC-time cuts is shown in Fig. 3.14(b).

In the next step, in order to further reduce the random coincidences, we have taken advantage of the complete kinematic measurement by making cuts on both total measured energy and momenta using energy and momentum conservation laws. For each valid event, the initial projectile and the final emitted particles must satisfy the following equations

$$P_{beam} = P_1 + P_2 + P_3 + P_4 \quad (3.3)$$

$$E_{beam} + Q = E_1 + E_2 + E_3 + E_4 \quad (3.4)$$

here,  $(E_{beam}, P_{beam})$ , and  $(E_i, P_i)$  (for  $i = 1, 2, 3, 4$ ) are the energies and momenta of the beam and the four emitted  $\alpha$  particles, respectively. The exit channel total energy and momentum spectra (summed energy/momentum of 4-particle exit channel) for the reaction are shown in Fig. 3.16 and Fig. 3.17, respectively. Vertical lines (red) shown in Fig. 3.16 and Fig. 3.17 are the cuts used to remove the random coincidence events. Fig. 3.14(c) demonstrates the effect of simultaneous energy and momentum cuts. From the Fig. 3.14 (b) and Fig. 3.14 (c), it is clear that time cut is not as effective as the energy-momentum cut. Time cut in TDC mostly removes the random coincidences related to beam like particles, whereas the energy and momentum conservation conditions are crucial to pick up the  $4\alpha$  decay channels from the detected four particle events. Therefore, the true events have been extracted by filtering the raw data with simultaneous cuts on the TDC time gate as well as energy and momentum gates satisfying the above equations (3.3 and 3.4), [89], which has been shown in Fig. 3.14(d). In total, nearly  $\sim 20,000$  completely detected events within the Hoyle state (cut in two-

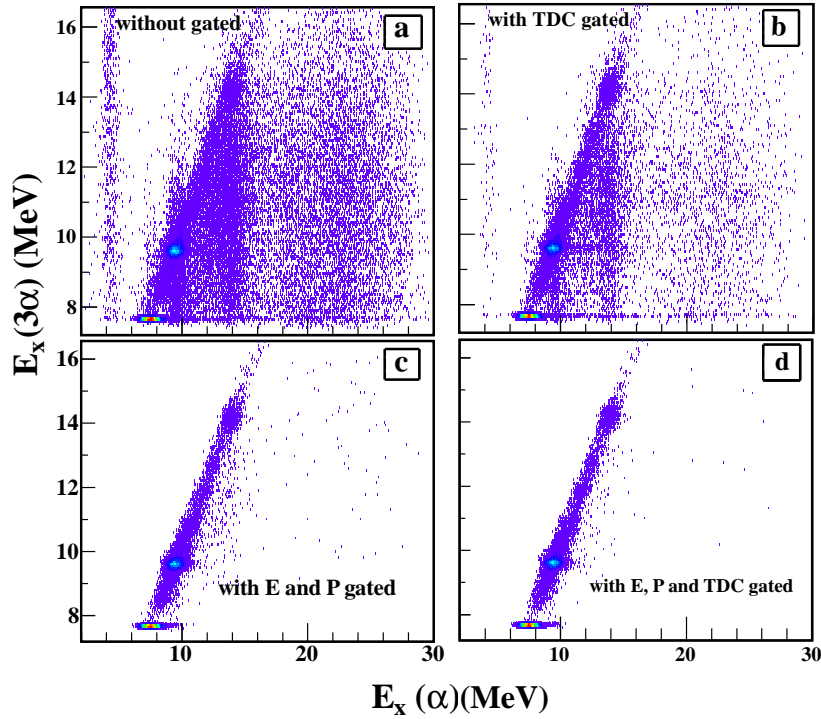


**Figure 3.14:** (a, b, c, d) Illustration of the use of different gates in filtering the data. The excitation energy of the recoiling  $^{12}\text{C}$  obtained from the inelastic  $\alpha$  has been plotted against the excitation energy reconstructed from the three decay  $\alpha$  particles (see text for details).

dimension on the Hoyle state in Fig. 3.14(d)) were collected in the present experiment; these have been analyzed further to extract the structure of the Hoyle state.

### 3.3.8 Monte Carlo simulation

Monte Carlo Simulation, which is an indispensable tool to study the multi-particle correlation, has been done in details by taking care of complete experimental effect and compared with the experimental data. In the present experiment, while studying the  $^{12}\text{C}$  the Hoyle state breakup, we were in particular, interested in the breakup events that proceed as direct  $3\alpha$  decay (not the two step sequential decay) as they are more interesting from the structure as well as astrophysics point of views. In order to study the decay mechanism of the Hoyle state, an event-by-event Monte Carlo simulation

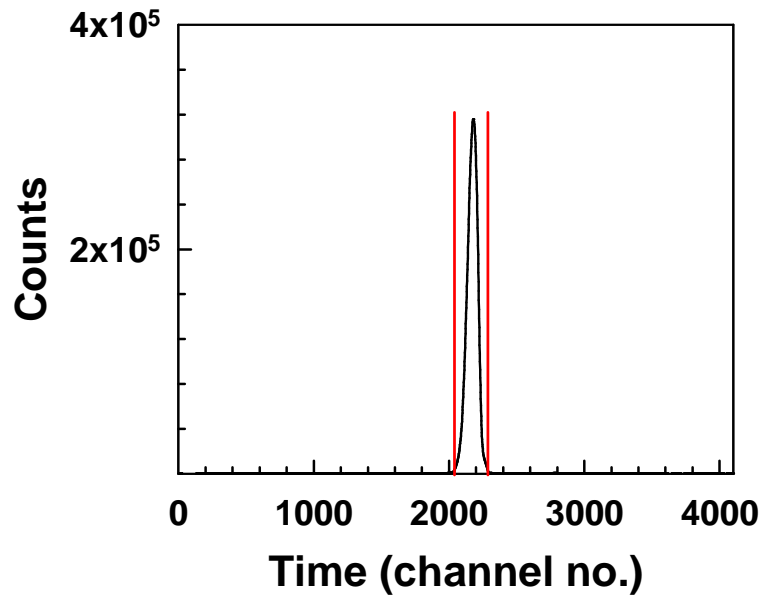


Figure 3.15: TDC time gate (see text).

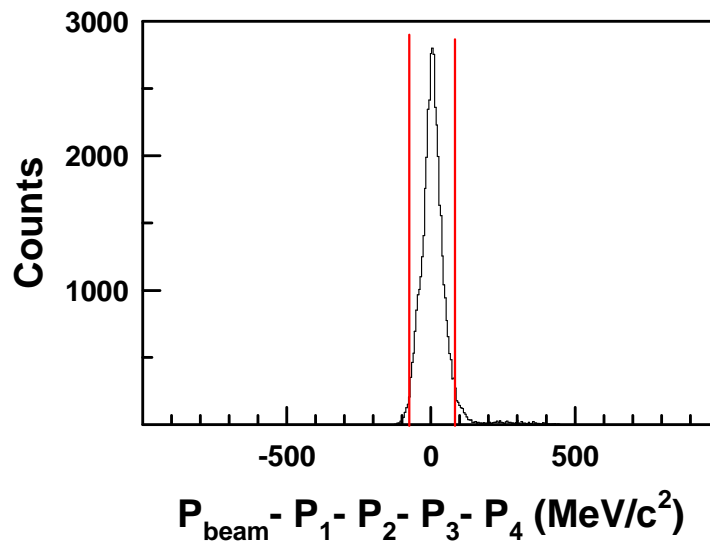
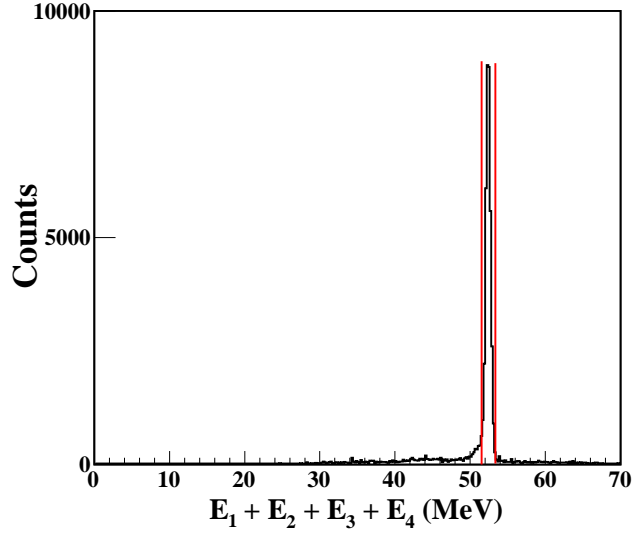


Figure 3.16: Momentum conservation gate (see text).



*Figure 3.17: Total energy gate (see text).*

has been performed to take into account the geometrical efficiencies of the setup. Simulation has been done in ROOT platform using CERN library. The reaction events have been generated by N-Body Monte Carlo Event Generator (GENBOD) function (W515 from CERMLIB) using the Raubold and Lynch method [90]. The complete simulation package has been developed in ROOT platform in several steps. In the first step, inelastic scattering of 60 MeV  $\alpha$ -particle on  $^{12}\text{C}$  corresponding to the Hoyle state has been generated. In the next step, the three  $\alpha$  decay of  $^{12}\text{C}$  have been generated in its own frame and finally boosted along the direction of  $^{12}\text{C}$  in lab. The energies and linear momenta of the decay particles for each event in the rest frame of the decaying nucleus have been generated in such way that the total energy ( $E_{total}$ ) of the three particles is equal to

$$E_{total} = E_x - E_{th}, \quad (3.5)$$

where,  $E_x$  is the excitation energy, for Hoyle state ( $E_x = 7.65$  MeV), and  $E_{th}$  is the threshold for the three body decays; the value of  $E_{th}$  is 7.36 MeV for sequential decay (SD:  $^{12}\text{C}^* \rightarrow {}^8\text{Be} + \alpha \rightarrow 3\alpha$ ), and 7.27 MeV for direct decay (DD:  $^{12}\text{C}^* \rightarrow 3\alpha$ ). In case of SD, the energy of  $\alpha$ -particle emitted in the first step carries  $\frac{2}{3}$  of the total energy

available in center of mass and the rest is carried by  ${}^8\text{Be}$ , which decays into two  $\alpha$ -particles in the next step. The center of mass energies of the two  $\alpha$ -particles originating from  ${}^8\text{Be}$  decay depend on the orientation of the second step breakup relative to the first. As the Hoyle state and its intermediate and final decay states ( ${}^8\text{Be}, \alpha$ ), all have spin 0, the particles have been generated isotropically in the respective rest frame (in case of  ${}^8\text{Be} + \alpha$  decay the rest frame is  ${}^{12}\text{C}$  and for the decay of  ${}^8\text{Be} \rightarrow \alpha + \alpha$ , the rest frame is  ${}^8\text{Be}$ ). In addition to the sequential decay, three direct  $3\alpha$  decay modes have been taken into account (DDE, representing the decay mode where equal energy sharing occurs among three  $\alpha$ -particles, DDL, representing the decay of a linear chain like configuration, leading to one  $\alpha$ -particle at rest and the other two moving with equal but opposite velocities, and  $\text{DD}\Phi$ , characterizing uniform sampling of phase space by the decay products, all in the  ${}^{12}\text{C}$  frame). The complete experimental geometry of the forward and the backward detectors have been incorporated and only those events were accepted for the comparison with experimental data for which the directions of linear momenta of the three- $\alpha$  decay particles were within the active geometrical coverage of forward two detectors and the inelastically scattered  $\alpha$ -particle was also within the active acceptance of backward detector telescope. In addition, we have considered all other experimental effects, such as, beam resolution, detector threshold, dead area of detector, angular and energy resolutions of the strip detectors, event rejection due to multiple hit in single strip, etc. All these states (the Hoyle state, ground state of  ${}^8\text{Be}$ ) have intrinsic widths, which have been taken to be Breit-Wigner shapes in the simulation. For the present experimental setup, it has been found that the geometrical detection efficiencies for all these types of decay are nearly same (SD efficiency = 0.82 %, DDE efficiency = 0.85 %, DDL efficiency = 0.90 %, and  $\text{DD}\Phi$  efficiency = 0.80 %, for the Hoyle state) for this reaction. All the  $\alpha$ -particles have been generated in laboratory frame and the accepted particles which fulfill the above conditions have been taken for the comparison with the experimental data. The simulation events were treated in the same way as the analysis procedure was performed for the experimental data so that the comparison would be fruitful.

In order to investigate the decay pattern of the Hoyle state, Dalitz plot has been extensively used in the present analysis. Dalitz plot is an ideal tool for visual representation of phase space of a three body decay. It was first introduced by R. Dalitz [91] for the representation of  $\tau$  Meson decay in high energy particle physics. The details of the Dalitz plot technique will be described in the following subsection.

### 3.3.9 Dalitz Plot technique

Dalitz plot provides an excellent tool for studying the dynamics of three-body decays. The kinematics of three body decays can be completely described by two variables. Let us consider a parent nucleus decays into three final particles of names 1, 2, 3 with kinetic energies  $T_1$ ,  $T_2$  and  $T_3$ , respectively. For a definite total energy,  $E$ , in center of mass of the three particles, all the final states have a continuous distribution of configurations, each specified in such a way that the energy  $E$  is shared among the three particles. This energy sharing may be represented uniquely by a point,  $P(X, Y)$ , within the equilateral triangle,  $ABC$ , (as shown in Fig. 3.18) such that the perpendicular distances to its three sides are equal in magnitude to the kinetic energies of the particles  $T_1$ ,  $T_2$  and  $T_3$ . The most important property of this representation is that the area occupied within this triangle by any set of configuration is directly proportional to its volume in phase space. Not all points  $P$  within the triangle  $ABC$  correspond to a physical configuration, since the energies of particles 1, 2, 3 must be consistent with zero total momentum. With non-relativistic kinematics and with equal masses  $m$  for particles 1, 2, 3, the only allowed configurations are those corresponding to points  $P$  lying within the circle inscribed by the triangle, as shown in Fig. 3.18 and the equation of circle is given by

$$X^2 + Y^2 = \left(\frac{H}{3}\right)^2, \quad (3.6)$$

where,  $H$ , is the height of triangle and  $H = T_1 + T_2 + T_3$ . and, the centroid of the triangle is the origin of the coordinate axis. The point  $P$  inside the circle can be described by

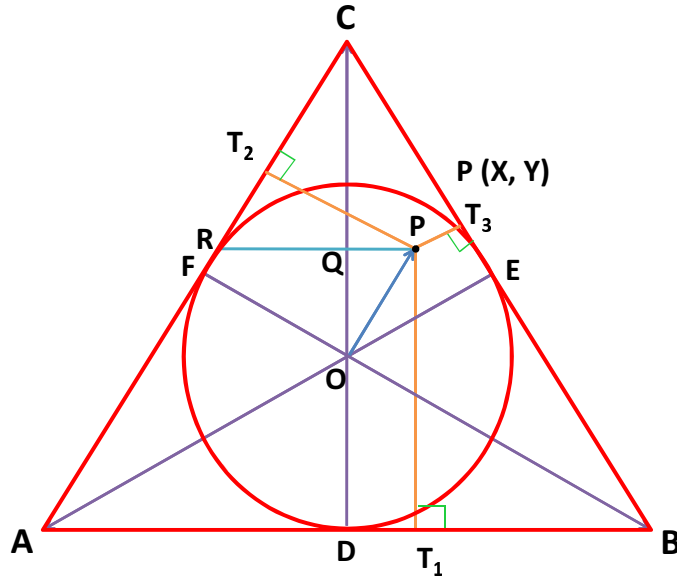


**Figure 3.18:** Schematic diagram of Dalitz plot.

the coordinates (X, Y) and are given by

$$X = QP = RP - RQ = \frac{2}{\sqrt{3}}T_2 - \frac{(T_2 + T_3)}{\sqrt{3}} = \frac{(T_2 - T_3)}{\sqrt{3}}, \quad (3.7)$$

$$Y = OQ = T_1 - \frac{H}{3} = \frac{(2T_1 - T_2 - T_3)}{3}, \quad (3.8)$$

Uniqueness about the Dalitz's plot is that if there is any intermediate state involved in the three body decay, it will impose a constrain on the kinetic energies of the corresponding two-particle decay from the intermediate state and all points defined by (X, Y) will follow a restricted locus; this corresponds to the decay which is known as sequential decay (SD). On the other hand, if the decay occurs without any intermediate state of particle, *i.e.* the decay occur directly (known as direct decay (DD)), then none of the energies are constrained. In this case, it can be shown that the data points will be distributed uniformly over the area of a circle with radius  $\frac{H}{3}$  as shown in Fig. 3.18.

Using the laws of conservation of momentum and the equation of relative energies of any two of the three  $\alpha$ -particles ( $E_{rel}(ij) = \frac{1}{2}\mu(V_i - V_j)^2$ ), one can deduce a relation

as

$$E_{rel}(12) + E_{rel}(23) + E_{rel}(31) = \frac{3(E_x - E_{th})}{2}, \quad (3.9)$$

here, the relative energy indices 1, 2 and 3 refer to the particles emitted with highest, second highest and lowest energies, respectively,  $E_{th}$  is the threshold for the three body decay,  $E_{rel}(ij)$  is the relative energy between  $i^{th}$  and  $j^{th}$  particle

From the above equations ( 3.6 to 3.9), one can obtain as

$$X = \frac{\sqrt{3}(E_{rel}(23) - E_{rel}(12))}{2}, \quad (3.10)$$

$$Y = \frac{(2E_{rel}(31) - E_{rel}(23) - E_{rel}(12))}{2}, \quad (3.11)$$

and radius,

$$R = \frac{3(E_x - E_{th})}{4}, \quad (3.12)$$

These parameters  $X = \sqrt{3}[E_{rel}(12) - E_{rel}(23)]/2$  and  $Y = [2E_{rel}(31) - E_{rel}(12) - E_{rel}(23)]/2$  are called Dalitz parameters.

In order to compare the simulation with experimental data, the relative energies between the three  $\alpha$ -particles have been calculated using the measured energies of the particles and the simulation data. Fig. 3.19 shows the comparison between the simulation data with experiment in terms of relative energies and the excitation energy of  $^{12}\text{C}$ . From the Fig. 3.19 , it is clear that the experimental effect has been taken care in simulation very carefully. The simulations of different types of decays and the corresponding Dalitz plot presentations are displayed in Fig. 3.20. It is seen that different types of decay have their characteristic features in the Dalitz plot. This clearly illustrates the importance of Dalitz plot in deciphering the contribution of different types of Hoyle decay. The experimental Dalitz plot for the Hoyle state constructed from the fully detected ( $4\alpha$ ) events of the present experiment has been shown in Fig. 3.21. The triangular locus in Fig. 3.21 indicates that the decay is mostly sequential in nature (sequential :  $^{12}\text{C}^* \rightarrow ^8\text{Be} + \alpha \rightarrow \alpha + \alpha + \alpha$ ). Very few events are observed to be

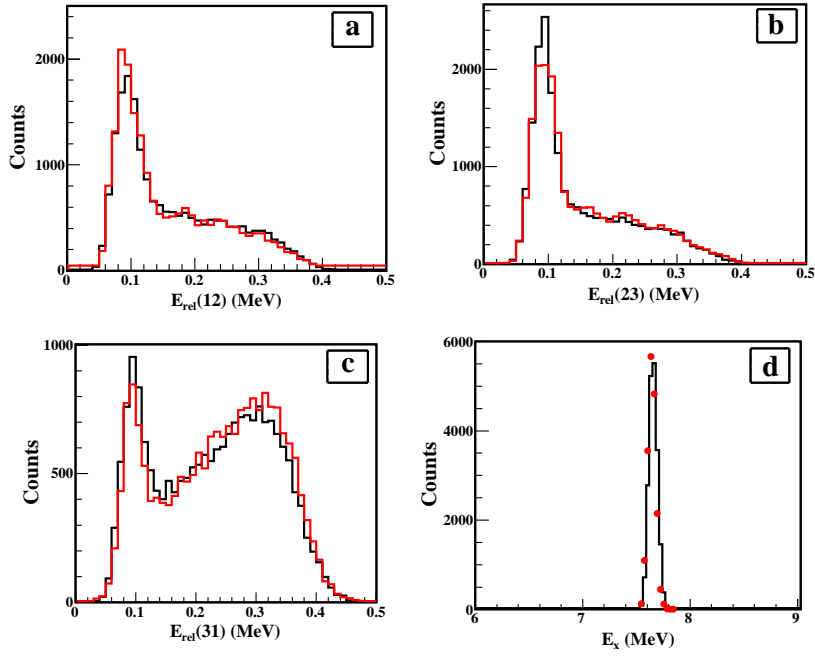


**Figure 3.19:** Relative energy spectra for the Hoyle state decay three  $\alpha$ -particles. The histograms in (a), (b), (c) and solid circles in (d) are the experimental data (red line/solid circle) and the  $k$

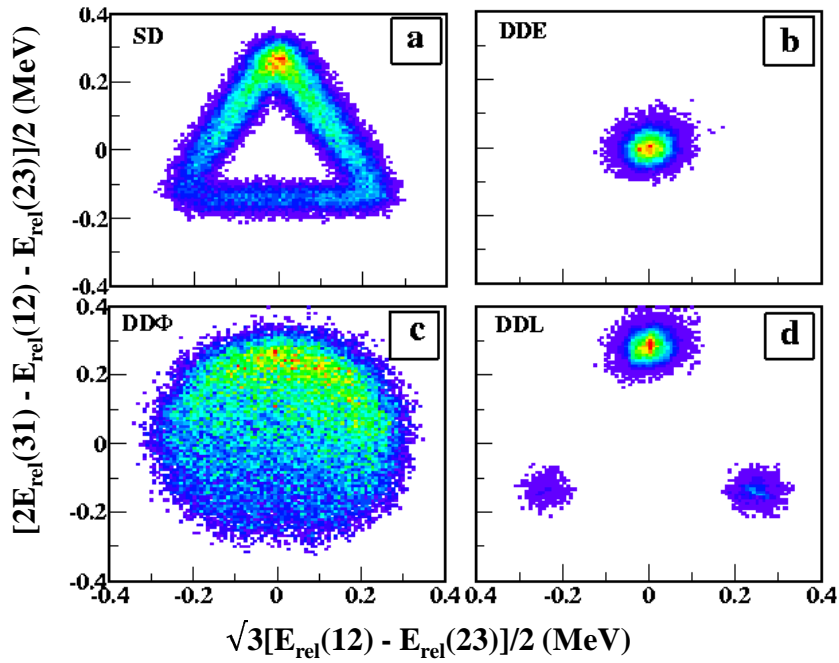


**Figure 3.20:** Monte Carlo simulation for different types of the Hoyle state decay; (a) SD, (b) DDE, (c) DD $\Phi$ , (d) DDL (see text for details).

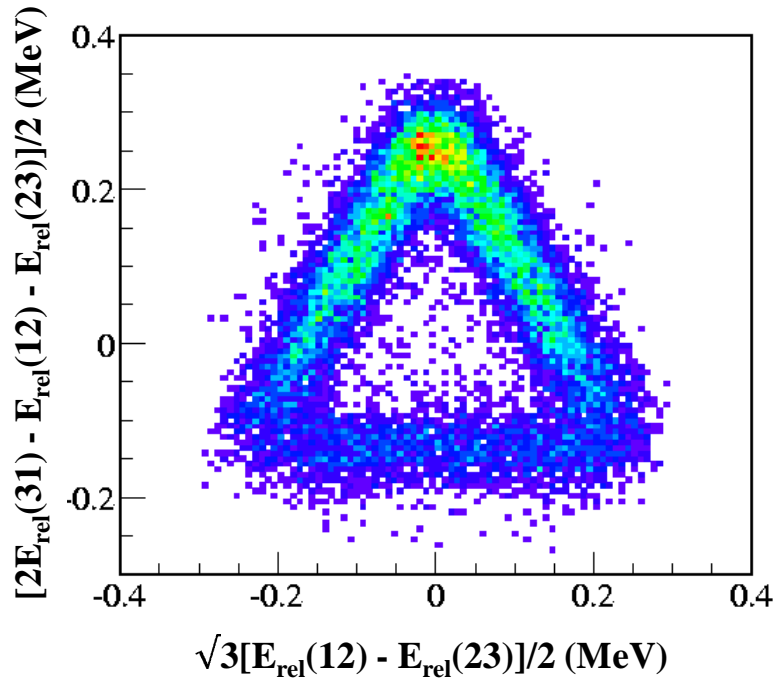


**Figure 3.21:** Experimental Dalitz plot for fully detected Hoyle events for the reaction  $\alpha + {}^{12}\text{C}$ .

distributed over the circle or in the central region of the triangle - indicating that the contribution from direct break up is very small. One can directly estimate the contribution of these direct decay mechanism by integrating the area define by the circle of radius R, but however, there are detector effects which must be taken into account while evaluating the yields [37].

### 3.4 Techniques used for estimation of decay mechanism

In order to determine the contributions of different decay modes (of the Hoyle state), three different distributions (*i.e.*, the distributions of relative energy in  ${}^8\text{Be}$ -like pairs, root mean square deviation of energy, and radial projection of the symmetric Dalitz plot) obtained from the experimental data have been simultaneously fitted with

those calculated from the simulation data [92, 93]. All the three distributions have been discussed below;

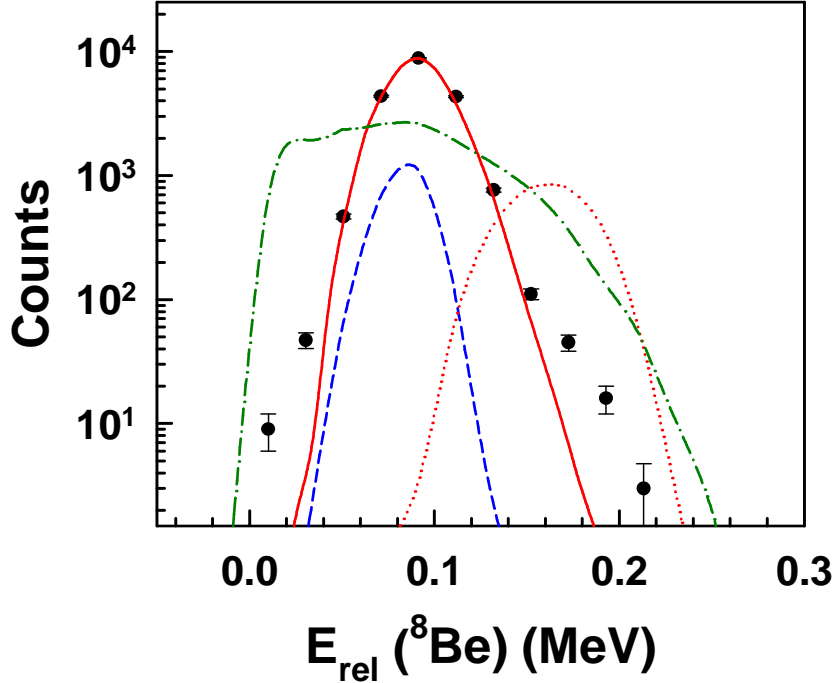


**Figure 3.22:** Schematic representation of the contributions of SD, DDE, DDL and DD $\Phi$  processes as a function of the relative energy of  ${}^8\text{Be}$  like pairs (see text). Solid circles are experimental data and solid line (red), dotted line (red), dash line (blue), dash-dot line (green) curves are simulation results for SD, DDE, DDL and DD $\Phi$ , respectively.

### 3.4.1 The relative energy distribution of ${}^8\text{Be}$ like pairs

This is the distribution of the lowest relative energy between any two  $\alpha$ -particles in each  $3\alpha$  decay event of the Hoyle state [37, 52]. So, all SD events decaying through the  ${}^8\text{Be}$  ground state will contribute to the peak at a relative energy of  $\sim 92$  keV, the breakup energy of  ${}^8\text{Be}_{g.s.}$ . On the other hand, for DDE mode of decay, it should peak at  $E_{rel} \approx 188$  keV. The relative energy distribution of the  ${}^8\text{Be}$  like pairs in the experimental data (filled circles) is displayed in Fig. 3.22 along with those obtained from simulation events for SD [solid line (red)], DDE [dotted line (red)], DDL [dash line (blue)] and

DDΦ [dash-dot line (green)] processes in the same format ( ${}^8\text{Be}$  like pairs) to show the nature of distribution for different types of decays. It is seen that the experimental distribution is dominated by the peak at around 92 keV signifying strong dominance of the SD process though a small distortion in the distribution near the tail region and indicating small but finite contributions of the direct processes in the Hoyle state decay.

### 3.4.2 The distribution of root mean square energy deviation:

The root mean square energy deviation,  $E_{rms}$ , has been defined as [51, 52],

$$E_{rms} = \sqrt{\langle E_\alpha^2 \rangle - \langle E_\alpha \rangle^2} \quad (3.13)$$

where,  $E_\alpha$  are the energies of the  $\alpha$ -particles from the decay of the Hoyle state, and the average is over the energies of the three  $\alpha$ -particles of each event. So,  $E_{rms}$  is the root mean square energy deviation of the energies of the  $\alpha$ -particles of each Hoyle state decay event in the rest frame. Fig. 3.23 displays the distribution of  $E_{rms}$  for the fully

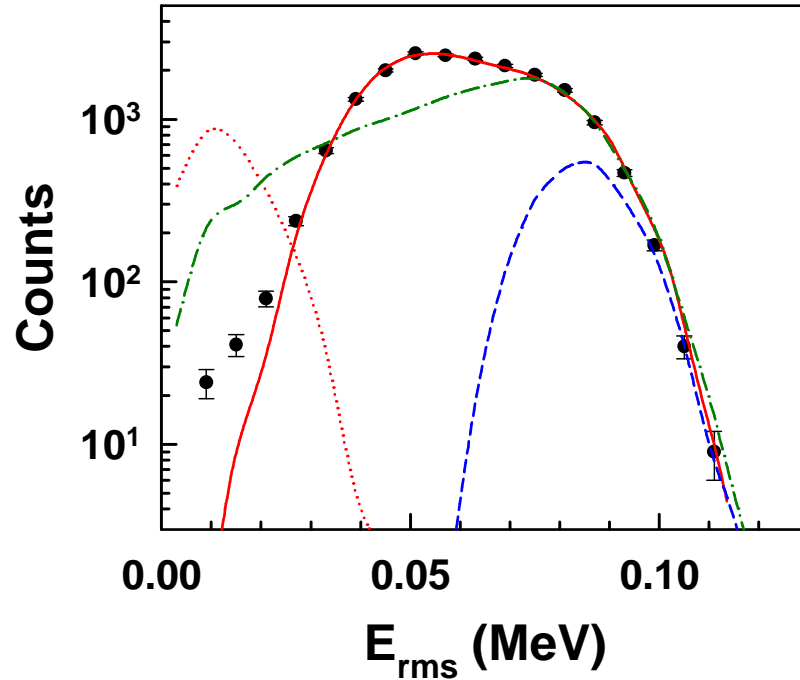


**Figure 3.23:** The distribution of root mean square energy deviation, symbols/lines are same as in Fig. 3.22.

detected events along with the simulation events, same as in Fig. 3.22. It is clear from equation 3.13 that, in this case DDE should contribute prominently in the neighborhood of  $E_{rms} \simeq 0$  in the distribution, subject to finite broadening due to the total instrumental resolution. From the shape of the curve in Fig. 3.23, it is again evident that there is some small but finite contributions from direct processes such as DDE.

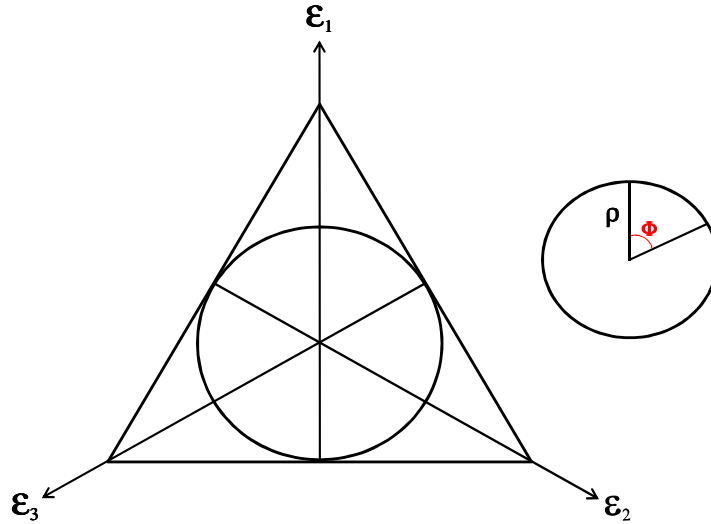


**Figure 3.24:** The Dalitz plot and associated projections,  $\rho$  and  $\Phi$ , here  $\varepsilon_i$  denotes the normalized energy of the  $i^{\text{th}}$   $\alpha$ -particle.

### 3.4.3 The distribution of radial projection of the Dalitz plot:

Two-dimensional Dalitz plots are not very suitable for visual comparison of experimental and theoretical distributions in details. For this purpose, one-dimensional projections like the radial ( $\rho$ ) and angular ( $\Phi$ ) projections shown in Fig. 3.24 are much more useful. Two dimensional symmetric Dalitz plot using simulation data for different types of decays are shown in Fig. 3.25 and the experimental two dimensional symmetric Dalitz plot is shown in Fig. 3.26 . The experimental data in their original form were used directly for generating the plot and no event-by-event kinematic fitting procedure [53] were required.

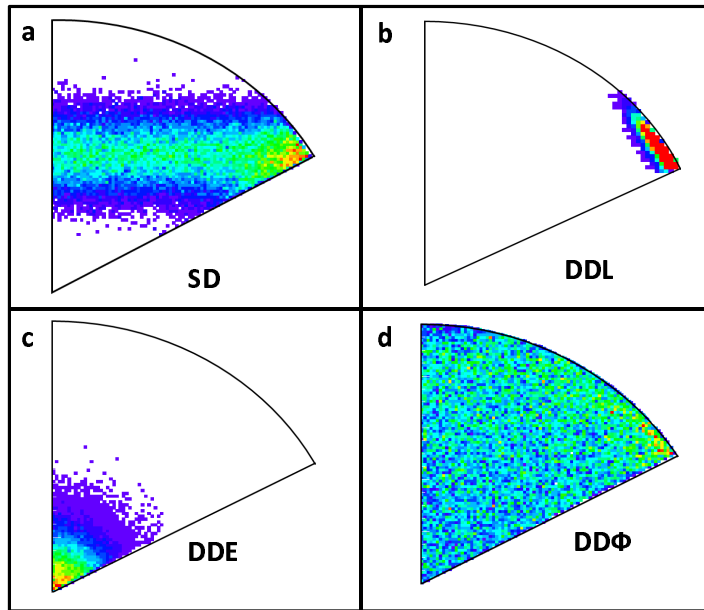


*Figure 3.25: Symmetric Dalitz plots for (a) SD, (b) DDL, (c) DDE (d) DD $\Phi$ .*

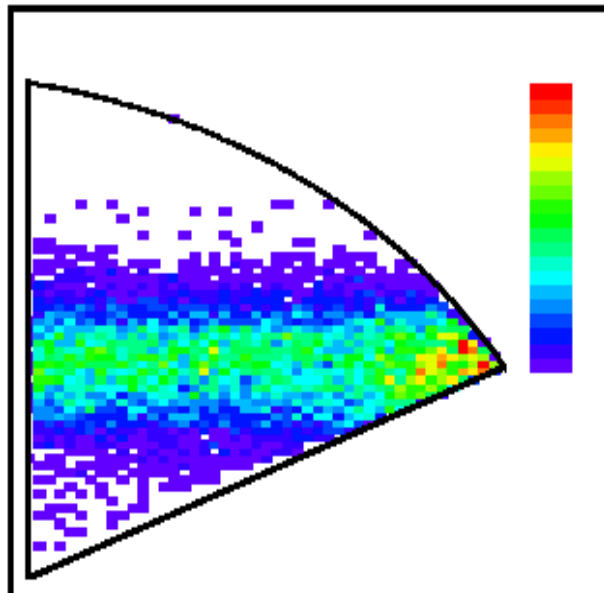


*Figure 3.26: Measured Dalitz plot distribution without any kinematic fitting.*

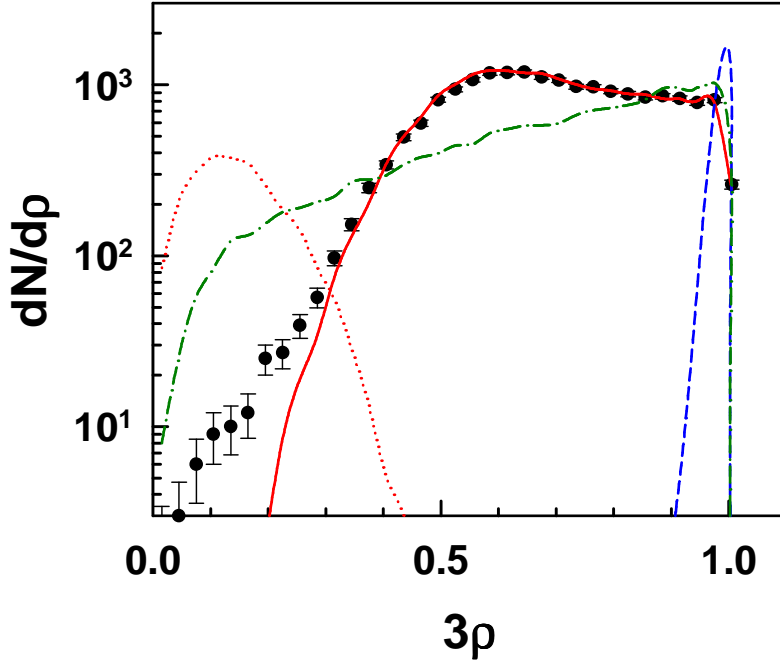


**Figure 3.27:** The distribution of the radial projection of the symmetric Dalitz plot, symbols/lines are same as in Fig. 3.22.

One-dimensional projections of Dalitz plot [radial ( $\rho$ ) and angular ( $\Phi$ ) projections] is shown in Fig. 3.24. In the present case, as the Hoyle state has spin 0, it decay isotropically into  $3\alpha$  (also have spin 0), so the decay of the state has no directional memory as well as it obeys the energy-momentum conservation laws, knowledge of two alpha-particle energies fully specifies the kinematics of the decay. It has recently been shown that the technique of radial projection of the Dalitz plot is very useful to gain deeper insight into the decay mechanism [53]. The radial coordinate of the symmetric Dalitz plot,  $\rho$  is given by

$$(3\rho)^2 = (3\varepsilon_i - 1)^2 + 3(\varepsilon_i + 2\varepsilon_j - 1)^2 \quad (3.14)$$

where,  $\varepsilon_{i,j,k} = E_{i,j,k}/(E_i + E_j + E_k)$  are the normalized  $\alpha$ -particle energies in the  $^{12}\text{C}$  frame and  $E_i > E_j > E_k$ . The radial projection of the Dalitz plot using the present data of  $\sim 2 \times 10^4$  fully detected ( $4\alpha$ ) Hoyle decay events is shown Fig. 3.27 along with the simulation of different types of decays. It is also evident from Fig. 3.27 that the whole

spectrum of one dimensional projection of symmetric Dalitz plot cannot be reproduced with only sequential decay component (SD), some fraction of direct decay component (DD) is needed along with SD to explained the whole spectrum.

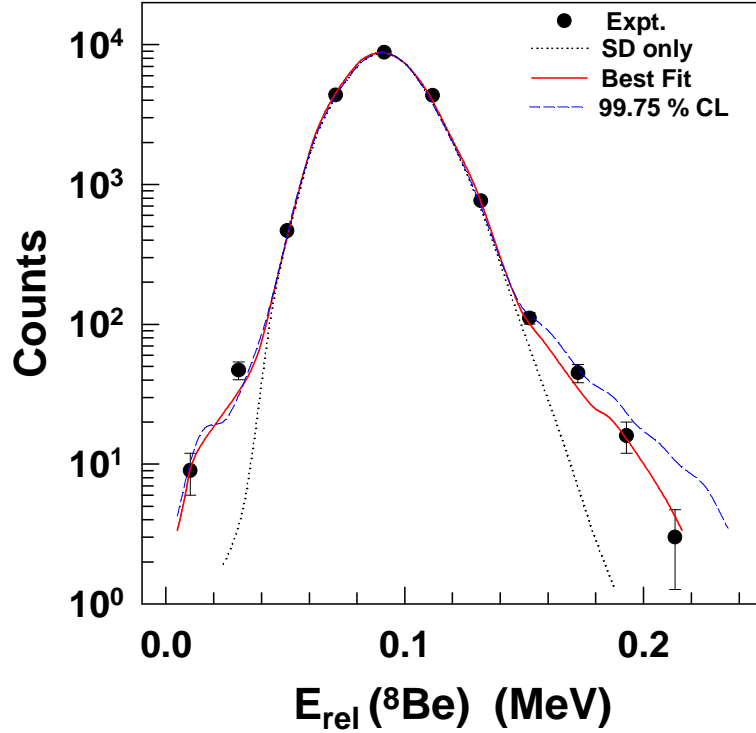


**Figure 3.28:** The distribution of <sup>8</sup>Be like pairs of each event of the Hoyle state decay of <sup>12</sup>C\* (filled circle). Filled circles correspond to the experimental data and the lines correspond to various simulation results; only sequential decay (dotted line), total decay (including SD, DDE, DDL and DDΦ)- best fit (red line), total decay - with 99.75 % upper confidence limit (blue dash line)(see text).

### 3.5 Estimation of decay components of the Hoyle state

Estimation of different types of decay mechanisms have been obtained by simultaneous optimization of three different distributions (as mentioned above) from the experimental data with those generated from the Monte Carlo simulation event set [92]. The experimental results have been compared with those obtained using simulated data

sets containing contributions of different decay processes in varied proportions. The simulated event sets have been validated by taking care of all experimental effects as mentioned earlier; 5, 00, 000 valid events for sequential decay and 50,000 valid events each for all (three) types of direct decay have been generated within the detector geometrical efficiencies. For each fitting procedure, a mixed event set consisting of various decay processes has been chosen randomly in varied proportions from the event sets corresponding to the individual decay processes and then fitted with  $\chi^2$  minimization technique simultaneously for the distributions of energy of  $^8\text{Be}$  like pairs, root mean square energy deviation, and the radial projection of symmetric Dalitz plot, with the normalization fixed by equal area under the graph. The above fitting procedure has been repeated for 2,00,000 times using different, randomly selected mixed event sets to obtain the dispersion of the best-fit parameters. From this analysis, the best-fit values for different direct decay processes of the Hoyle state have been extracted to be  $0.60 \pm 0.09$  % for  $\text{DD}\Phi$ ,  $0.30 \pm 0.1$  % for  $\text{DDE}$ , and  $0.01 \pm 0.03$  % for  $\text{DDL}$ ; the corresponding  $\chi^2$  (per degree of freedom) values are 0.987 in Fig. 3.28, 0.99 in Fig. 3.29, and 0.83 in Fig. 3.30. It is evident that both  $\text{DD}\Phi$  and  $\text{DDE}$  branching ratios are significantly larger than zero; in the case of  $\text{DDL}$ , the best-fit value was associated with larger (than the value) uncertainty and therefore the upper limit of the corresponding branching ratio has been extracted to be 0.1 % at 99.75 % CL [92].

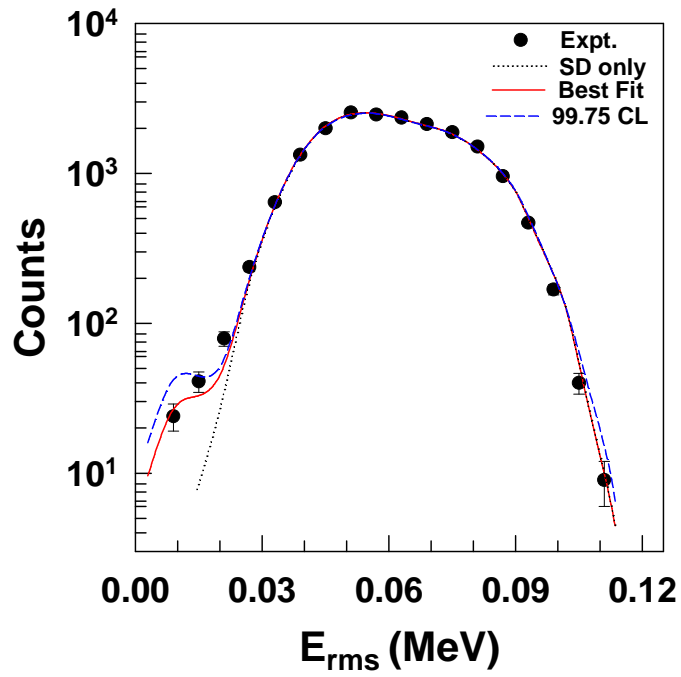


*Figure 3.29: The distribution of root mean square energy deviation of the  $\alpha$ -particles from the Hoyle state decay events. The symbols are explained in Fig. 3.28.*

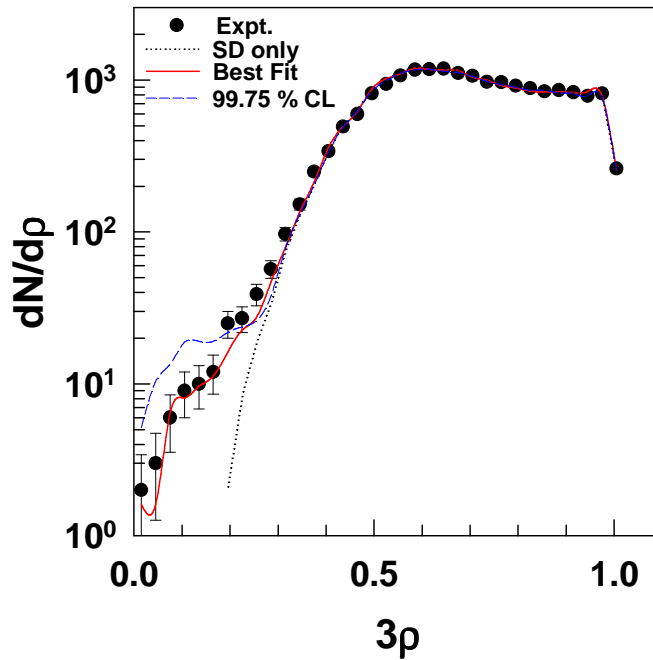


*Figure 3.30: The distribution of the radial projection of the symmetric Dalitz plot of each event of the Hoyle state decay in the  $^{12}\text{C}$  frame (filled circle). The symbols are explained in Fig. 3.28.*

## 3.6 Results and discussions

Thus, it can be said that the total direct decay branching ratio as obtained in the present study is 0.91 (14) %, out of which DDE contributes 0.3(1) %; this further implied that, according to [51], 0.3(1) % of the Hoyle decay events are candidates for nuclear Bose-Einstein condensates (BEC). The presently determined nonzero branching ratios for  $DD\Phi$  and DDE, as well as the estimated upper limit at 99.75 % CL for DDL mode, are widely different from those reported in [51] (see Table 3.2 for comparison); they are, however, in general consistent with the upper limits of different direct decay branching ratios reported in [37, 52, 53].

It is pertinent, at this point, to mention that deciphering the link between the observed energy distributions of the decay  $\alpha$ -particles and the structure of the Hoyle state may not be quite straightforward because of the influence of tunneling through the barrier on the former [53]; moreover, the importance of correlation between the observation of a particular direct decay mode and the existence of a particular structure (*e.g.*, DDE and *vis-à-vis* nuclear BEC) is also sometimes debated in theory [94]. All these problems notwithstanding, precise, high-statistics measurement of the energy distribution of the decay particles and its representation in various forms (relative energy distribution of  ${}^8\text{Be}$ -like pairs, distribution of root-mean-square energy deviation, and Dalitz plot distribution) to extract precisely the branching ratios of various decay modes, combined with the predictions of advanced decay models (for example, [95, 96]), are expected to provide unambiguous information about the structure models. In this context, the present results assume significance with the determination of nonzero branching ratios for various direct decay modes, which, though in general agreement with the recently determined upper limits [52, 53], are nearly an order of magnitude less than those reported in [51] and thus clearly contradict that measurement. In this context, the current measurement, at highest statistics till date, assumes significance and the determination of nonzero branching ratios for various direct decay

modes may help in arriving at a consensus, so far as experimental determinations and estimations are concerned [92, 93].

**Table 3.2:** Comparison of different experimental estimates of direct decay modes of the Hoyle state.

Experiment	Total events	DDE (%)	DDL (%)	DD $\Phi$ (%)	Total (%)	CL (%)
Ref. [37]	$\sim 2000^a$	-	-	-	$< 4$	99.5
Ref. [51]	$\sim 1000^b$	$7.5 \pm 4.0^c$	$9.5 \pm 4.0^c$	-	$17.0 \pm 5.0^c$	
Ref. [52]	$\sim 4000^b$	$< 0.45$	-	$1.3 \pm 0.9$ ( $< 3.9$ )	$< 3.9$	99.75
Ref. [53]	$\sim 5000^a$	$< 0.09$	$< 0.09$	$< 0.5$	$< 0.5$	95
Ref. [92]	$\sim 20000^a$	$0.3 \pm 0.1^c$	$< 0.1^c$	$0.60 \pm 0.09^c$	$0.91 \pm 0.14^c$	99.75

<sup>a</sup>fully detected events only.

<sup>b</sup> $3\alpha$  reconstructed events.

<sup>c</sup>total error from statistical,  $\chi^2$ , and background.



## Chapter 4

### Summary and Conclusions

In summary, in order to study the properties of hot nucleus formed in heavy ion reactions, a high resolution, low threshold, high granular charged particle detector array has been designed and developed as a part of the present thesis work and the details of which (mechanical design, fabrication, test, etc.) have been presented in this thesis. The array consists of 24 telescopes, each telescope is made up of three elements; first element is a  $50\ \mu\text{m}$ ,  $\Delta E$ , Single-sided Silicon Strip Detector (SSSD : 16 strips, each of dimension  $50\ \text{mm} \times 3\ \text{mm}$ ), second element is a  $500/1000\ \mu\text{m}$ ,  $E/\Delta E$ , Double-sided Silicon Strip Detectors (DSSD : 16 strips (each  $50\ \text{mm} \times 3\ \text{mm}$ ) per side in mutually orthogonal directions) and third element is CsI(Tl) detector (4 nos.), each of thickness 6 cm. The array elements has been chosen to provide good isotopic identification of fragments ( $Z \leq 10$ ) by the  $\Delta E$ -E technique with good angular resolution over a wide dynamic range in energy. The complete mechanical structure is such that the array, after complete assembly, form a surface of a sphere of radius 20 cm. To minimize the dead area and allow close-packing of the telescopes in the array, a compact frame for the Silicon strip detectors has been developed. Details characteristics of different elements of the telescope have been studied offline as well as in beam. The event reconstruction technique has been developed in ROOT platform for the analysis of the experimental data from this high granular multi-telescopes array. Performance test of the event reconstruction technique has been done in two experiments  $^{20}\text{Ne} + ^{12}\text{C}$  and

$^{12,13}\text{C} + ^{12}\text{C}$  reactions and study of particle unstable state of different unstable particle has been presented. The complete detector array with all the elements as well as the electronics have been tested in offline with  $\alpha$ -source and precision pulsar (with high count rates; 10k rates). Now the array (full or part of it) is being used for physics experiment.

In the second part of the thesis work, a high statistics and high resolution complete kinematical measurement has been performed to study the decay mechanism of the Hoyle state. The experiment has been performed at the Variable Energy Cyclotron Centre, Kolkata, using 60 MeV  $^4\text{He}$  ion beam from the K130 cyclotron on  $^{12}\text{C}$  target. The  $\alpha$ -particles emitted in the decay of the Hoyle state have been detected using two 500  $\mu\text{m}$  double-sided silicon strip detectors (in forward direction) in coincidence with the inelastically scattered projectile ( $\alpha$ -particle) using one strip detector telescope in backward direction. Only completely detected events (events where all four  $\alpha$  particles, three from the decay of  $^{12}\text{C}^*$ , as well as the inelastically scattered one were detected separately) have been used for the present analysis to remove any ambiguity about the origin of the detected particles. The genuine Hoyle events have been extracted by filtering the raw data with proper cuts on the TDC time signal as well as total energy - momentum gates. Total of  $2 \times 10^4$  events have been observed within the Hoyle state after all conditions imposed. Three different distributions have been used for estimation of decay components of the Hoyle state. First one is the relative energy distribution of  $^8\text{Be}$ -like pairs, where the sequential decay events are expected to be peak around the ground state of  $^8\text{Be}$ , *i.e.*, around 92 keV. There was evidence for non-sequential decays in this distribution in the form of small wings on the tails of the main peak of ground state of  $^8\text{Be}$ . Second one is the distribution of root mean square energy deviation (rms), where the events of direct decay with equal energies are likely to show up around the zero rms value within the experimental setup resolution, which was actually seen. Third one is the radial projection of symmetric Dalitz plot, which has been known to be very useful for the study of decay pattern in case of spin zero particle. Simultaneous optimization of all these three different distributions derived from the

experimental data with those generated from a simulated event set has been performed to arrive at a consistent estimate of the contributions of various direct decay modes. The optimization procedure was further repeated numerous times with different sets of simulated data sampled randomly from a much larger pool of simulated events to extract the distribution of the best-fit values and determine the contribution for each mode; if the contribution for some mode was not found to be statistically significant, the upper limit of the contribution has been extracted at 99.75 % confidence limit (CL). Simultaneous optimization of three different distributions using  $\chi^2$  minimization technique has led to the determination of non-zero branching ratios for direct decay in phase space (DD $\Phi$  :  $0.60 \pm 0.09$  %), and direct decay with equal energy (DDE :  $0.30 \pm 0.1$  %). The present study has also led to the estimation of upper limit for direct decay of linear chain (DDL : 0.1 %) at 99.75 % confidence level. The presently determined branching ratios are clearly at variance with those reported earlier by Raduta *et al.*[51], but are consistent with other recently estimated upper limits of the same [52, 53].

Interestingly, another recent study published after the present work has, however indicated that the upper limit of direct decay could be even smaller, down to ( $< 0.2\%$  at 95 % CL) [97].

Regarding the link between the experimental observations discussed above and the structure of the Hoyle state, the signatures may be distorted due to the influence of barrier tunneling; in addition, the link between the observation of a particular direct decay mode and the existence of a particular structure (*e.g.*, DDE and *vis-à-vis* nuclear BEC) is also not quite straightforward [94]. However, high-statistics and high resolution measurement of completely detected events to extract precisely the branching ratios of various decay modes, combined with the refinement of decay models (for example,[95, 96]), are expected to provide better and more unambiguous information about the structure. As the consensus on the non zero branching ratios for various direct modes is yet to be achieved, the topic is still very live and interesting; more detailed experiments are likely to be performed in future to reach a definite conclusion on this issue.



# Bibliography

- [1] M. Freer, *Reports on Progress in Physics* **70**, 2149 (2007).
- [2] W. von Oertzen, M. Freer, Y. Kanada-Eñyo .
- [3] C. Beck, Y. Abe, N. Aissaoui, B. Djerroud, F. Haas, *Phys. Rev. C* **49**, 2618 (1994).
- [4] M. Freer, *Nature* **487**, 309 (2012).
- [5] J. P. Ebran, E. Khan, T. Nikšić, D. Vretenar, *Nature* **487**, 341 (2012).
- [6] P. Papka, C. Beck, *Cluster in Nuclei, Vol. 2, C. Beck (Ed.): Lecture Notes in Physics* **848**, 299 (2012).
- [7] W. von Oertzen, *Cluster in Nuclei, Vol. 1, C. Beck (Ed.): Lecture Notes in Physics* **818**, 102 (2010).
- [8] T. Yamada, *et al.*, *Cluster in Nuclei, Vol. 2, C. Beck (Ed.): Lecture Notes in Physics* **848**, 229 (2012).
- [9] L. R. Hafstad, E. Teller, *Phys. Rev.* **54**, 681 (1938).
- [10] K. Ikeda, N. Takigawa, H. Horiuchi, *Prog. Theor. Phys. Suppl.* **464**, 464 (1968).
- [11] M. Freer, H. O. U. Fynbo, *Progress in Particle and Nuclear Physics* **78**, 1 (2014).
- [12] H. A. Bethe, *Phys. Rev.* **55**, 434 (1939).
- [13] E. J. Opik, *Proc. Roy. Irish Acad.* **A54**, 49 (1951).
- [14] E. E. Salpeter, *Astrophys. J.* **155**, 326 (1952).
- [15] F. Hoyle, *Astrophys. J. Suppl. Ser.* **1**, 121 (1954).
- [16] D. N. F. Dunbar, R. E. Pixley, W. A. Wenzel, W. Whaling, *Phys. Rev.* **92**, 649 (1953).
- [17] C. W. Cook, W. A. Fowler, C. C. Lauritsen, T. Lauritsen, *Phys. Rev.* **107**, 508 (1957).

- [18] H. O. U. Fynbo, *et al.*, *Nature* **433**, 136 (2005).
- [19] M. Freer, *Pramana* **83**, 643 (2014).
- [20] M. Livio, D. Hollowell, A. Weiss, J. W. Truran, *Nature* **340**, 281 (1989).
- [21] E. Epelbaum, H. Krebs, D. Lee, U.-G. Meißner, *Phys. Rev. Lett.* **106**, 192501 (2011).
- [22] E. Epelbaum, H. Krebs, T. Lähde, D. Lee, U.-G. Meißner, *Phys. Rev. Lett.* **109**, 252501 (2012).
- [23] P. Navrátil, J. Vary, B. Barrett, *Phys. Rev. Lett.* **84**, 5728 (2000).
- [24] A. C. Dreyfuss, K. D. Launey, T. Dytrych, J. P. Draayer, C. Bahri, *Physics Letters B* **727**, 511 (2013).
- [25] M. Chernykh, H. Feldmeier, T. Neff, P. von Neumann-Cosel, A. Richter, *Phys. Rev. Lett.* **98**, 032501 (2007).
- [26] H. Morinaga, *Phys. Rev.* **101**, 254 (1956).
- [27] S. I. Fedotov, O. I. Kartavtsev, V. I. Kochkin, A. V. Malykh, *Phys. Rev. C* **70**, 014006 (2004).
- [28] A. S. Umar, J. A. Maruhn, N. Itagaki, V. E. Oberacker, *Phys. Rev. Lett.* **104**, 212503 (2010).
- [29] D. J. Marin-Lambarri, *et al.*, *Phys. Rev. Lett.* **113**, 012502 (2014).
- [30] M. Kamimura, *Nuclear Physics A* **351**, 456 (1981).
- [31] A. N. Danilov, T. L. Belyaeva, A. S. Demyanova, S. A. Goncharov, A. A. Ogloblin, *Phys. Rev. C* **80**, 054603 (2009).
- [32] E. Uegaki, S. Okabe, Y. Abe, H. Tanaka, *Prog. Theor. Phys.* **57**, 1262 (1977) .
- [33] H. Horiuchi, *Prog. Theor. Phys.* **51**, 1266 (1974); **53**, 447 (1975) .
- [34] A. Tohsaki, H. Horiuchi, P. Schuck, G. Röpke, *Phys. Rev. Lett.* **87**, 192501 (2001).
- [35] Y. Funaki, A. Tohsaki, H. Horiuchi, P. Schuck, G. Röpke, *Phys. Rev. C* **67**, 051306 (2003).
- [36] A. Okamoto, *et al.*, *Phys. Rev. C* **81**, 054604 (2010).
- [37] M. Freer, *et al.*, *Phys. Rev. C* **49**, R1751 (1994).
- [38] W. Zimmerman, *et al.*, *Phys. Rev. Lett.* **110**, 152502 (2013).
- [39] K. Ogata, M. Kan, M. Kamimura, *Prog. Theor. Phys.* **122**, 1055 (2009) .

- [40] R. de Diego, E. Garrido, D. V. Fedorov, A. S. Jensen, *Physics Letters B* **695**, 324 (2011).
- [41] C. Angulo, *et al.*, *Nuclear Physics A* **656**, 3 (1999).
- [42] F. Herwig, S. Austin, J. Lattanzio, *Phys. Rev. C* **73**, 025802 (2006).
- [43] C. Tur, A. Heger, S. M. Austin, *Astrophys. J.* **718**, 357 (2010).
- [44] C. Tur, A. Heger, S. M. Austin, *Astrophys. J.* **671**, 821 (2007).
- [45] O. S. Kirsebom, *Journal of Physics: Conference Series* **436**, 012072 (2013).
- [46] M. Chernykh, H. Feldmeier, T. Neff, P. von Neumann-Cosel, A. Richter, *Phys. Rev. Lett.* **105**, 022501 (2010).
- [47] M. Itoh, *et al.*, *Phys. Rev. C* **84**, 054308 (2011).
- [48] M. Freer, *et al.*, *Phys. Rev. C* **86**, 034320 (2012).
- [49] N. B. Nguyen, F. M. Nunes, I. J. Thompson, E. F. Brown, *Phys. Rev. Lett.* **109**, 141101 (2012).
- [50] R. G. Markham, S. M. Austin, M. A. M. Shahabuddin, *Nuclear Physics A* **270**, 489 (1976).
- [51] A. R. Raduta, *et al.*, *Physics Letters B* **705**, 65 (2011).
- [52] J. Manfredi, *et al.*, *Phys. Rev. C* **85**, 037603 (2012).
- [53] O. S. Kirsebom, *et al.*, *Phys. Rev. Lett.* **108**, 202501 (2012).
- [54] R. T. De Souza, N. L. Neindre, A. Pagano, K. H. Schmidt, *European Physical Journal A* **30**, 275 (2006).
- [55] J. Pouthas, *et al.*, *Nucl. Instrum. Methods A* **357**, 418 (1995).
- [56] S. Aiello, *et al.*, *Nuclear Physics A* **583**, 461 (1995).
- [57] B. Davin, *et al.*, *Nucl. Instrum. Methods A* **473**, 302 (2001).
- [58] M. S. Wallace, *et al.*, *Nucl. Instrum. Methods A* **583**, 302 (2007).
- [59] D. Lacroix, A. Van Lauwe, D. Durand, *Phys. Rev. C* **69**, 054604 (2004).
- [60] D. Gupta, *et al.*, *Proc. of International Workshop on multifragmentation and related topics, Caen(France)* **95**, 321 (2007).
- [61] D. Gupta, *et al.*, *Proc. of DAE- BRNS symposium on Nucl. Phys.* **53**, 701 (2008).
- [62] *Micronsemiconductor limited, Royal buildings, Marlborough road, Lancing, Sussex, BN 158UN, England .*

- [63] *Scionix Holand BV, P. O. Box 143, 3980 CC Bunnix, The Netherland .*
- [64] *Text book: Radiation Detection and Measurement by Glenn E Knoll .*
- [65] S. E. Koonin, *Physics Letters B* **70**, 43 (1977).
- [66] J. Pochodzalla, *et al.*, *Phys. Rev. Lett.* **55**, 177 (1985).
- [67] G. Verde, A. Chbihi, R. Ghetti, J. Helgesson, *GANIL Rep. P 06 05 .*
- [68] G. I. Kopylov, *Physics Letters B* **50**, 472 (1974).
- [69] T. K. Nayak, *et al.*, *Phys. Rev. C* **45**, 132 (1992).
- [70] T. K. Rana, *et al.*, *Phys. Rev. C* **78**, 027602 (2008).
- [71] W. A. Friedman, W. G. Lynch, *Phys. Rev. C* **28**, 16 (1983).
- [72] W. A. Friedman, W. G. Lynch, *Phys. Rev. C* **28**, 950 (1983).
- [73] D. J. Morrissey, *et al.*, *Physics Letters B* **148**, 423 (1984).
- [74] G. D. Westfall, *et al.*, *Physics Letters B* **116**, 118 (1982).
- [75] B. V. Jacak, *et al.*, *Phys. Rev. Lett.* **51**, 1846 (1983).
- [76] A. S. Goldhaber, *Phys. Rev. C* **17**, 2243 (1978).
- [77] R. Wada, *et al.*, *Phys. Rev. C* **39**, 497 (1989).
- [78] J. Pochodzalla, *et al.*, *Phys. Rev. C* **35**, 1695 (1987).
- [79] H. Xi, *et al.*, *Nuclear Physics A* **552**, 281 (1993).
- [80] H. M. Xu, *et al.*, *Phys. Rev. C* **40**, 186 (1989).
- [81] C. Schwarz, *et al.*, *Phys. Rev. C* **48**, 676 (1993).
- [82] S. Albergo, S. Costa, E. Costanzo, A. Rubbino, *Nuovo Cimento* **89**, 1 (1985).
- [83] M. B. Tsang, W. G. Lynch, H. Xi, W. A. Friedman, *Phys. Rev. Lett.* **78**, 3836 (1997).
- [84] T. K. Rana, *et al.*, *International Journal of Modern Physics E* **20**, 789 (2011).
- [85] S. Kundu, *et al.*, *J. Phys. Conf. Ser.* **390**, 012075 (2012).
- [86] A. S. Divatia, *Eighth International Conference on Cyclotron and their application, Bloomington, Indiana (1978).*
- [87] J. F. Ziegler, *SRIM 2008*, <http://www.srim.org/SRIM/SRIM%2008.pdf> .

- [88] O. S. Kirsebom, *Ph. D. thesis, Aarhus University* (2010).
- [89] M. Alcorta, *et al.*, *Nucl. Instrum. Methods A* **605**, 318 (2009).
- [90] F. James, *CERN 68-15* (1968).
- [91] R. Dalitz, *Philos. Mag.* **44**, 1068 (1953).
- [92] T. K. Rana, *et al.*, *Phys. Rev. C* **88**, 021601 (R) (2013).
- [93] S. Bhattacharya, *et al.*, *Pramana* **83**, 673 (2014).
- [94] T. Yamada, P. Schuck, *Phys. Rev. C* **69**, 024309 (2004).
- [95] R. Álvarez Rodríguez, A. Jensen, D. Fedorov, H. O. U. Fynbo, E. Garrido, *Phys. Rev. Lett.* **99**, 072503 (2007).
- [96] R. Álvarez Rodríguez, A. Jensen, E. Garrido, D. Fedorov, H. O. U. Fynbo, *Phys. Rev. C* **77**, 064305 (2008).
- [97] M. Itoh, *et al.*, *Phys. Rev. Lett.* **113**, 102501 (2014).